



ATLAS Note



Draft version 5.0

1

2 Search for flavor-changing neutral currents tHq 3 interactions with $H \rightarrow \tau^+\tau^-$ in proton-proton 4 collisions at $\sqrt{s} = 13$ TeV

5

The ATLAS Collaboration

6

21st April 2021

7

A search is presented for flavor-changing neutral currents tHq interactions with $H \rightarrow \tau^+\tau^-$ using a data set collected with the ATLAS detector at the LHC, corresponding to an integrated luminosity of 140 fb^{-1} of proton-proton collisions at a center-of-mass energy of 13 TeV. The search is performed in the decay chain $t\bar{t} \rightarrow Wb + Hq$ or $qg \rightarrow tH \rightarrow Wb + H$ ($q = c/u$), where the W boson decays inclusively and H decays to $\tau^+\tau^-$. Upper limits at 95 % confidence level for the corresponding $t \rightarrow cH$ and $t \rightarrow uH$ decay branching ratios are measured to be XXX and XXX , while the expected limits are $0.046^{+0.020}_{-0.012}\%$ and $0.034^{+0.014}_{-0.012}\%$, respectively.

15 **Contents**

16	1 To do list	4
17	2 On going studies	4
18	3 Change log	4
19	3.1 From V1 to V2	4
20	3.2 From V2 to V3	5
21	3.3 From V3 to V3.1	5
22	3.4 From V3.1 to V4.0	5
23	3.5 From V4.0 to V5.0	5
24	4 Introduction	6
25	5 Analysis outline	7
26	5.1 Signal regions	7
27	5.2 Analysis strategy for leptonic channels	8
28	5.3 Analysis strategy for in Hadronic channels	10
29	5.4 Statistical strategy	12
30	5.5 Blinding strategy	12
31	6 Detector, data set and Monte Carlo simulation	12
32	6.1 ATLAS detector	12
33	6.2 Data set	13
34	6.3 Signal and background simulation	14
35	7 Object reconstruction	16
36	7.1 Jets	16
37	7.2 b-tagging	17
38	7.3 Light leptons	17
39	7.4 Hadronic tau decays	17
40	7.5 Missing transverse energy	18
41	7.6 Tight lepton isolation: <code>PromptLeptonImprovedVeto(PLIV)</code>	18
42	7.7 Overlap removal	19
43	8 Signal regions	21
44	8.1 Trigger	21
45	8.2 Cuts	22
46	9 Reconstruction of event topology	24

Not reviewed, for internal circulation only

47	10 Background estimation	45
48	10.1 Fake tau estimation in leptonic channels	48
49	10.2 QCD fake background in $t_h\tau_{\text{lep}}\tau_{\text{had}}$ and $t_l\tau_{\text{had}}$ regions	55
50	10.3 Fake tau estimate in hadronic channels	61
51	11 MVA analysis	69
52	12 Systematic uncertainties	77
53	12.1 Luminosity	77
54	12.2 Detector-related uncertainties	77
55	12.3 Uncertainties on fake background estimations	78
56	12.4 Theoretical uncertainties on the background	79
57	12.5 Uncertainties on the signal modelling	80
58	13 Fit model and signal extraction	81
59	14 Results	88
60	Appendix	91
61	A Sample DSID list	91
62	B Derivation and framework level cuts	92
63	C BDT Optimisation steps	100

⁶⁴ 1 To do list

- ⁶⁵ Add signal samples used by FCNC $H \rightarrow multilepton$ group (Their AOD files are deleted, still not available).
- ⁶⁶
- ⁶⁷ Generate signal PS (and ME?) systematics samples.

⁶⁸ 2 On going studies

- ⁶⁹ Investigate the constraints of $t\bar{t}$ matrix element and parton shower systematics.
- ⁷⁰ For parton shower systematics, use AFII PowhegPythia instead of FullSim. Switch to 7.1 Herwig sample.
- ⁷¹
- ⁷² Double check production and decay mode signal cross section.

⁷³ 3 Change log

⁷⁴ 3.1 From V1 to V2

- ⁷⁵ Leptonic channels: 80fb-1 \rightarrow 140fb-1
- ⁷⁶ BDT tau ID \rightarrow RNN tau ID
- ⁷⁷ Updates to PFlow jets with DL1r b-tagging.
- ⁷⁸ Optimised event selection.
- ⁷⁹ Changed fake estimation method.
- ⁸⁰ Added signal regions $l\tau$ 1j and $l\tau$ 2j.

⁸¹ **3.2 From V2 to V3**

- ⁸² Added to do list and change log.
- ⁸³ Added Analysis outline section and moved signal region definition here.
- ⁸⁴ Added yield tables for CRs.
- ⁸⁵ Added plots for the variables defined.
- ⁸⁶ Added closure test for ABCD method.
- ⁸⁷ BDT optimisation.

⁸⁸ **3.3 From V3 to V3.1**

- ⁸⁹ Made the note more readable by introducing new names for SR and CR.
- ⁹⁰ ...

⁹¹ **3.4 From V3.1 to V4.0**

- ⁹² Updated with full systematics.
- ⁹³ Improved figures, clarified a few statements.
- ⁹⁴ Bug fix:
 - ⁹⁵ 1. Add the missing Double fake contribution in $t_l\tau_{had}\tau_{had}$ region into the fit.
 - ⁹⁶ 2. Require b-veto for the subleading tau in $t_l\tau_{had}\tau_{had}$ region

⁹⁷ **3.5 From V4.0 to V5.0**

- ⁹⁸ Added PS and ME systematics for ttbar sample.
- ⁹⁹ Using recommended blinding strategy.

100 4 Introduction

101 Since the discovery of the Higgs boson in 2012, great efforts are made to study its properties. As the
 102 mass of the Higgs boson is about 125 GeV [1], it is kinematically allowed that a top quark decays to
 103 a Higgs boson and an up-type quark via the flavour-changing neutral current (FCNC). In the Standard
 104 Model (SM), the FCNC interaction is forbidden at tree level and suppressed at higher orders due to the
 105 Glashow-Iliopoulos-Maiani (GIM) mechanism [2]. The $t \rightarrow u/c + H$ branching fraction in the SM is
 106 calculated to be around 10^{-15} [3]. It would be enhanced in many models beyond the SM (BSM). Examples
 107 are the quark-singlet model [4, 5], the two-Higgs doublet model with or without the flavour violation [6,
 108 7], the minimal supersymmetric standard model (MSSM) [8], supersymmetry with R-parity violation [9],
 109 the Topcolour-assisted Technicolour model [10] or models with warped extra dimensions [11], the little
 110 Higgs model with T-parity conservation [12] and the composite Higgs models [13]. Especially, the ansatz
 111 of Cheng and Sher [14] allows a branching fraction of about 10^{-3} [15]. Therefore, an observation of this
 112 decay would be a clear evidence for new physics.

113 On the other hand, if the tHq interaction exists, the single-top, Higgs associated production through this
 114 interaction should also be enhanced. The tH associated production in the SM prediction is expected to be
 115 small at LHC[16]. So the study on this process will also contribute to the FCNC interaction searches.

116 Upper 95% CL limits on $\text{BR}(t \rightarrow Hq)$ have been obtained by ATLAS based on the data from 2015 and
 117 2016, in the $H \rightarrow \gamma\gamma$ [17], $H \rightarrow WW/\tau_{\text{lep}}\tau_{\text{lep}}$ multilepton [18] and $H \rightarrow \tau\tau, H \rightarrow b\bar{b}$ [19] channels. The
 118 combined expected (observed) limits are 0.083% (0.11%) and 0.083% (0.12%) for $t \rightarrow Hc$ and $t \rightarrow Hu$
 119 decay branching ratio, respectively.

120 The $t \rightarrow Hq$ decay and $gq \rightarrow tH$ production are also searched by CMS based on the data from 2015
 121 and 2016[20] using the $H \rightarrow b\bar{b}$ decay. The branching ratio derived for $t \rightarrow Hc$ and $t \rightarrow Hu$ decay are
 122 0.47% (0.44%) and 0.47% (0.34%) as expected (observed) limits respectively.

123 The FCNC coupling is parametrised using dim-6 operators [21]. The effective Lagrangian regarding tqH
 124 interaction is:

$$\mathcal{L}_{\text{EFT}} = \frac{C_{u\phi}^{i3}}{\Lambda^2} (\phi^\dagger \phi)(\bar{q}_i t) \tilde{\phi} + \frac{C_{u\phi}^{3i}}{\Lambda^2} (\phi^\dagger \phi)(\bar{t}_i q) \tilde{\phi} \quad (1)$$

125 Where the operator notation is consistent with [21]. The coefficient $C_{u\phi}$'s can be extracted as follows
 126 according to the Madgraph calculation using TopFCNC UFO:

$$\begin{aligned} (C_{u\phi}^{i3})^2 + (C_{u\phi}^{3i})^2 &= 1946.6 \text{ BR}(t \rightarrow qH) \\ (C_{u\phi}^{13})^2 + (C_{u\phi}^{31})^2 &= \sigma(ug \rightarrow tH)/365.2 \text{ fb} \\ (C_{u\phi}^{23})^2 + (C_{u\phi}^{32})^2 &= \sigma(cg \rightarrow tH)/52.9 \text{ fb} \end{aligned} \quad (2)$$

127 To give a better impression on the numbers, we use $\text{BR}(t \rightarrow qH) = 0.2\%$ as benchmark, which is
 128 corresponding to $(C_{u\phi}^{13})^2 + (C_{u\phi}^{31})^2 = 3.89$, $\sigma(ug \rightarrow tH) = 1421.8 \text{ pb}$, $\sigma(cg \rightarrow tH) = 206.0 \text{ pb}$.

In this article, a search for the decay $t \rightarrow qH$ from one of top quarks in the $t\bar{t}$ production (TT) and single-top, Higgs associated production (ST) with $H \rightarrow \tau\tau$ and the remaining top decays into a W boson and a b quark as shown in Fig 1 using 140 fb^{-1} of proton-proton collision data at 13 TeV , taken with the ATLAS detector at the Large Hadron Collider (LHC), is presented. The final state is characterized by one top and one Higgs. In TT , there is an additional u or c as q quark forming a top resonance with Higgs.

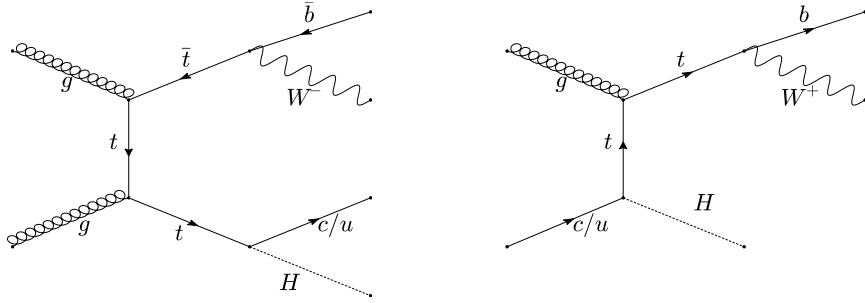


Figure 1: Diagrams of FCNC TT(left) and ST(right) process.

5 Analysis outline

In order to search for the FCNC coupling, we separate events in various signal regions (SR) defined in Sec. 5.1, each focuses on different $t \rightarrow Wb$ and $H \rightarrow \tau\tau$ decay final states in order to suppress the background. The analysis also uses various $t\bar{t}$ control regions (CR $t\bar{t}$) for calibration of tau fakes in Monte Carlo as well as data-driven fake estimations from QCD multi-jet background, and finally BDT is trained to separate the signal and background processes in each SR. The output of the SR BDT is used in a profile-likelihood fit in order to extract limits on the FCNC signal processes including all systematic uncertainties.

5.1 Signal regions

As shown in the Figure 1 in the final states containing $tt(qH)$ and tH , depending on the production modes and the decay of W boson hadronically and leptonically from the $t \rightarrow Wb$ decay referred as t_h and t_l , the signal is split into 4 kinds of final states as shown in Table 1. The $H \rightarrow \tau\tau$ decay are detected to be in either $\tau_{\text{lep}}\tau_{\text{had}}$ or $\tau_{\text{had}}\tau_{\text{had}}$ final states when the top decays hadronically (t_h) and only in $\tau_{\text{had}}\tau_{\text{had}}$ when the top decay leptonically (t_l). The decay of $H \rightarrow \tau_{\text{lep}}\tau_{\text{lep}}$ is dropped because this final state will be considered in the multi-lepton analysis. The decay of $H \rightarrow \tau_{\text{lep}}\tau_{\text{had}}$ is also dropped when top decay leptonically because in this case, the lepton fake could be important when both leptons have same-sign charge and the overlap of the fake lepton and fake taus can be difficult to estimate.

Table 1: Overview of the final states of signal events.

# of particles	alias	b-jet	jets	lepton	taus
<i>ST</i>	$W \rightarrow l\nu$	$t_l H$	1	1	1
	$W \rightarrow jj'$	$t_h H$	1	3	0
<i>TT</i>	$W \rightarrow l\nu$	$t_l t(qH)$	1	2	1
	$W \rightarrow jj'$	$t_h t(qH)$	1	4	0

Table 2: Overview of the signal regions.

Signal regions	b-jet	light flavor jets	lepton	hadronic taus	charge
$t_l \tau_{\text{had}}-2j$	1	2	1	1	$t_l \tau_{\text{had}}$ SS
$t_l \tau_{\text{had}}-1j$	1	1	1	1	$t_l \tau_{\text{had}}$ SS
$t_l \tau_{\text{had}} \tau_{\text{had}}$	1	any	1	2	$\tau_{\text{had}} \tau_{\text{had}}$ OS
$t_h \tau_{\text{had}} \tau_{\text{had}}-2j$	1	2	0	2	$\tau_{\text{had}} \tau_{\text{had}}$ OS
$t_h \tau_{\text{had}} \tau_{\text{had}}-3j$	1	≥ 3	0	2	$\tau_{\text{had}} \tau_{\text{had}}$ OS
$t_h \tau_{\text{lep}} \tau_{\text{had}}-2j$	1	2	1	1	$\tau_{\text{lep}} \tau_{\text{had}}$ OS
$t_h \tau_{\text{lep}} \tau_{\text{had}}-3j$	1	≥ 3	1	1	$\tau_{\text{lep}} \tau_{\text{had}}$ OS

150 Due to the low statistics in $t_l H$ and $t_l t(qH)$ processes, they are merged into a single region $t_l \tau_{\text{had}} \tau_{\text{had}}$
 151 where there is no light jet multiplicity requirement and the two τ_{had} are required to have opposite-sign
 152 charge. However there is a sizeable fraction of these events that one of the taus fails the reconstruction and
 153 remains as a jet or goes missing due to the low tau reconstruction efficiency. So the $t_l \tau_{\text{had}}-1j$ and $t_l \tau_{\text{had}}-2j$
 154 are also included as signal regions where the lepton from t_l and τ_{had} are required to have same-sign charge
 155 in order to reduce $t\bar{t}$ background. For the $t_h H$ and $t_h t(qH)$ channels, the two tau candidates from the
 156 $H \rightarrow \tau\tau$ decay (including both $\tau_{\text{lep}} \tau_{\text{had}}$ and $\tau_{\text{had}} \tau_{\text{had}}$) are required to have opposite-sign charge.

157 The summary for the signal regions are listed in Table 2 and their corresponding signal and background
 158 yields after fake estimation are shown in Table 3.

159 For the future convenience, $t_h \tau_{\text{lep}} \tau_{\text{had}}-2j$ and $t_h \tau_{\text{lep}} \tau_{\text{had}}-3j$ are indicated by $t_h \tau_{\text{lep}} \tau_{\text{had}}$; $t_h \tau_{\text{had}} \tau_{\text{had}}-2j$ and
 160 $t_h \tau_{\text{had}} \tau_{\text{had}}-3j$ are indicated by $t_h \tau_{\text{had}} \tau_{\text{had}}$; $t_l \tau_{\text{had}}-2j$ and $t_l \tau_{\text{had}}-1j$ are indicated by $t_l \tau_{\text{had}}$. All the of regions
 161 involving leptons from t_l or τ_{lep} are indicated by "leptonic channels", otherwise hadronic channels".

162 5.2 Analysis strategy for leptonic channels

163 The main background contributing to the leptonic channels, defined in the last section, is top pair production
 164 as shown in Figure 2. It can either contribute as reducible and irreducible background.

Table 3: The summary for the yield in the signal regions.

	$t_l \tau_{\text{had}-1j}$	$t_h \tau_{\text{lep}} \tau_{\text{had}-2j}$	$t_l \tau_{\text{had}-2j}$	$t_h \tau_{\text{lep}} \tau_{\text{had}-3j}$	$t_l \tau_{\text{had}} \tau_{\text{had}}$
Other MC	84.62 ± 6.19	3616.76 ± 36.46	83.30 ± 2.55	2054.94 ± 17.48	40.79 ± 1.05
$t\bar{t}$	280.14 ± 6.27	33758.95 ± 68.11	178.80 ± 4.97	21766.04 ± 54.57	5.10 ± 0.82
$b - \text{jets fake } \tau$	811.72 ± 10.82	1007.05 ± 11.53	1015.84 ± 11.49	924.32 ± 10.69	68.15 ± 2.91
$\text{lepton fake } \tau$	221.68 ± 16.47	1120.54 ± 30.89	87.81 ± 5.45	650.24 ± 11.32	0.88 ± 0.31
τ_W	839.60 ± 10.20	7256.82 ± 26.72	963.47 ± 10.41	6236.96 ± 24.82	4.96 ± 0.64
<i>Other Fake τ</i>	2918.71 ± 106.64	3829.90 ± 80.98	2625.87 ± 49.02	4372.94 ± 32.42	139.31 ± 6.02
QCD Fake lep	916.84 ± 53.16	821.77 ± 58.67	434.65 ± 27.74	484.10 ± 53.60	/
<i>double fake τ</i>	/	/	/	/	89.74 ± 20.11
background	6073.31 ± 121.52	51411.79 ± 133.30	5389.74 ± 58.93	36489.54 ± 89.81	348.93 ± 21.25
data	6353.00 ± 79.71	50412.00 ± 224.53	5410.00 ± 73.55	35942.00 ± 189.58	351.00 ± 18.73
$\bar{t}t \rightarrow bWcH$	57.59 ± 0.61	102.58 ± 0.97	52.80 ± 0.58	133.14 ± 1.19	66.43 ± 0.65
$cg \rightarrow tH$	2.23 ± 0.04	5.66 ± 0.08	1.38 ± 0.03	4.47 ± 0.08	5.10 ± 0.06
tcH merged	59.82 ± 0.61	108.24 ± 0.98	54.19 ± 0.58	137.61 ± 1.19	71.53 ± 0.65
$\bar{t}t \rightarrow bWuH$	59.72 ± 0.62	105.62 ± 0.96	55.47 ± 0.60	139.67 ± 1.18	69.10 ± 0.67
$ug \rightarrow tH$	11.36 ± 0.21	28.60 ± 0.40	7.51 ± 0.17	24.78 ± 0.40	24.00 ± 0.31
tuH merged	71.08 ± 0.66	134.22 ± 1.04	62.98 ± 0.62	164.45 ± 1.25	93.10 ± 0.73

	$t_h \tau_{\text{had}} \tau_{\text{had}-2j}$	$t_h \tau_{\text{had}} \tau_{\text{had}-3j}$
SM Higgs	17.29 ± 0.43	25.88 ± 0.43
Diboson	8.40 ± 0.62	10.75 ± 0.63
$Z \rightarrow \tau\tau$	485.70 ± 8.52	406.02 ± 7.64
Rare	17.84 ± 1.58	10.05 ± 1.18
$t\bar{t}$	225.85 ± 6.15	209.75 ± 5.90
$t\bar{t}V$	0.75 ± 0.08	5.46 ± 0.24
<i>only $\tau_{\text{sub real}}$</i>	64.23 ± 3.58	84.46 ± 3.82
Fake	277.11 ± 8.95	332.77 ± 9.61
background	1097.17 ± 14.37	1085.13 ± 14.22
data	1033.00 ± 32.14	1052.00 ± 32.43
$\bar{t}t \rightarrow bWcH$	28.13 ± 0.61	80.14 ± 1.04
$cg \rightarrow tH$	3.35 ± 0.07	4.30 ± 0.08
tcH merged	31.48 ± 0.61	84.44 ± 1.04
$\bar{t}t \rightarrow bWuH$	28.37 ± 0.62	83.75 ± 1.10
$ug \rightarrow tH$	17.29 ± 0.34	21.63 ± 0.40
tuH merged	45.66 ± 0.71	105.38 ± 1.17

Not reviewed, for internal circulation only

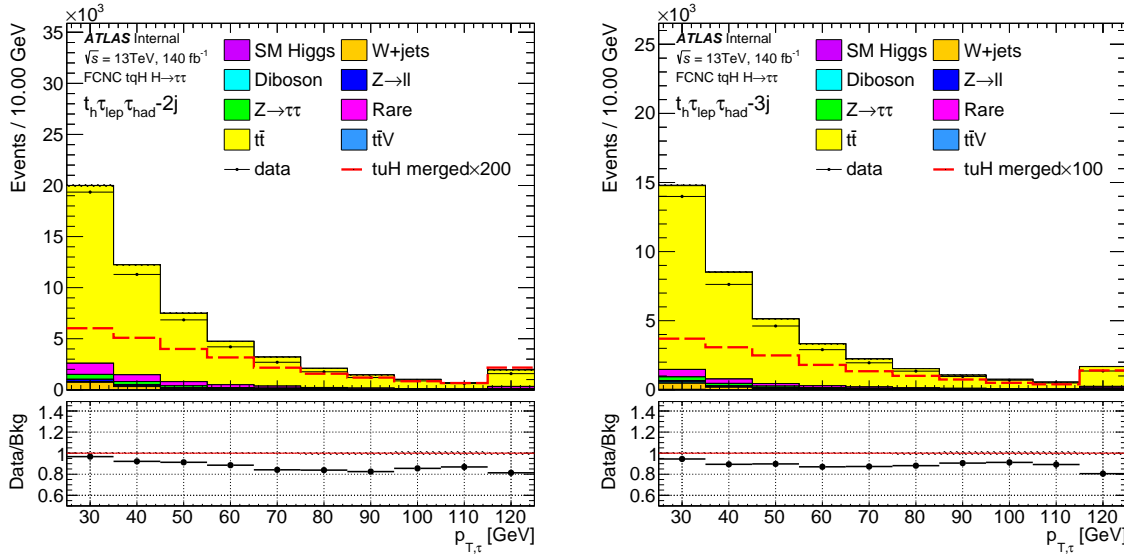


Figure 2: The distributions of τ p_T in $t_h \tau_{\text{lep}} \tau_{\text{had}} - 2j$ (left) and $t_h \tau_{\text{lep}} \tau_{\text{had}} - 3j$ (right) signal regions.

165 As irreducible background, when both tops decay leptonically to a l and a τ , and one of the b -jets from
 166 top decay fails the b-tagging, the event ends up in the $t_h \tau_{\text{lep}} \tau_{\text{had}}$ regions. This irreducible background is
 167 modelled directly by Monte Carlo.

168 For reducible background, when the top pair decays dileptonically, to a l and a τ_{had} , and one of the b -jets from
 169 top decay fails the b-tagging, if the b -jet or one of other jets is reconstructed as a τ_{had} , the event
 170 could end up in the $t_l \tau_{\text{had}} \tau_{\text{had}}$ regions if two τ_{had} have opposite-sign charge. When the top pair decays
 171 semi-leptonically, and one of jets fakes a τ_{had} , the event could end up in the $t_h \tau_{\text{lep}} \tau_{\text{had}}$ regions if the fake
 172 tau has the opposite charge to the lepton or in the $t_l \tau_{\text{had}}$ regions if the fake tau has the same charge as the
 173 lepton.

174 The reducible background except QCD multi-jets fakes is modelled by Monte Carlo but with scale
 175 factors derived from the dedicated $t\bar{t}$ control regions (CRtt) using the SM $t\bar{t}$ decay of dilepton events and
 176 semileptonically double-btagged lepton-jets events listed in Table 4 and explained in Sec. 10.1.

177 The QCD multi-jets also contribute a small fraction of the reducible background by faking both lepton
 178 and taus, especially in the low jet multiplicity region $t_l \tau_{\text{had}} - 1j$. This is modelled by the ABCD method by
 179 cutting on E_T^{miss} and the lepton isolation variable PLIV defined in Sec. 7.6 as explained in Sec. 10.2.

180 5.3 Analysis strategy for in Hadronic channels

181 Similar to the leptonic channels, the $t\bar{t}$ also contributes to the hadronic channels as reducible and irreducible
 182 background. But in the hadronic channels, much larger contribution is observed both from $Z \rightarrow \tau\tau$ plus

Table 4: Overview of the control regions used for fake tau scale factor derivation in leptonic channels compared to signal regions.

Regions		b-jet	light flavor jets	lepton	hadronic taus	charge
CR _{tt}	$t_l t_l 1b\tau_{\text{had}}$	1	any	2	1	$t_l t_l$ OS
	$t_l t_l 2b\tau_{\text{had}}$	2	any	2	1	$t_l t_l$ OS
	$t_l t_h 2b\tau_{\text{had}}\text{-}2j\text{SS}$	2	2	1	1	$t_l \tau_{\text{had}}$ SS
	$t_l t_h 2b\tau_{\text{had}}\text{-}2j\text{OS}$	2	2	1	1	$t_l \tau_{\text{had}}$ OS
	$t_l t_h 2b\tau_{\text{had}}\text{-}3j\text{SS}$	2	≥ 3	1	1	$t_l \tau_{\text{had}}$ SS
	$t_l t_h 2b\tau_{\text{had}}\text{-}3j\text{OS}$	2	≥ 3	1	1	$t_l \tau_{\text{had}}$ OS
SR	$t_l \tau_{\text{had}}\text{-}2j$	1	2	1	1	$t_l \tau_{\text{had}}$ SS
	$t_l \tau_{\text{had}}\text{-}1j$	1	1	1	1	$t_l \tau_{\text{had}}$ SS
	$t_l \tau_{\text{had}}\tau_{\text{had}}$	1	any	1	2	$\tau_{\text{had}}\tau_{\text{had}}$ OS
	$t_h \tau_{\text{lep}}\tau_{\text{had}}\text{-}2j$	1	2	1	1	$\tau_{\text{lep}}\tau_{\text{had}}$ OS
	$t_h \tau_{\text{lep}}\tau_{\text{had}}\text{-}3j$	1	≥ 3	1	1	$\tau_{\text{lep}}\tau_{\text{had}}$ OS

Not reviewed, for internal circulation only

¹⁸³ b -jet and from QCD multi-jets with double fake taus as the excess of data events shown in Figure 3.

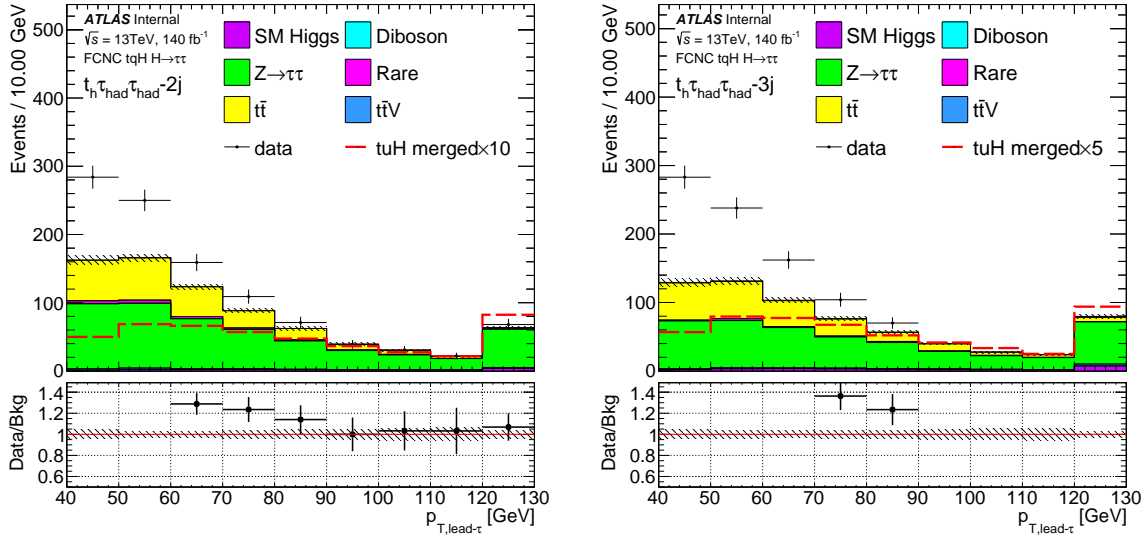


Figure 3: The distributions of leading τ p_T in the $t_h \tau_{\text{had}}\tau_{\text{had}}\text{-}2j$ (a) and $t_h \tau_{\text{had}}\tau_{\text{had}}\text{-}3j$ (b) SR before the fake estimation. Data is more than the MC prediction because the fake tau backgrounds are not yet added due to the fakes from both $t\bar{t}$ and QCD.

¹⁸⁴ The irreducible background is modelled directly by Monte Carlo. The reducible background with sub-
¹⁸⁵ leading tau fake is modelled by Fake Factor (FF) method using the fake-tau enriched control regions. The
¹⁸⁶ FFs are calculated from three different control regions where one of taus failed the medium RNN tau cut,
¹⁸⁷ but passed a minimum RNN cut:

- W+jet control region in the SM $H \rightarrow \tau\tau$ (Calculated by the $H \rightarrow \tau\tau$ group).
- SS control region, the two taus have the same charge and the rest selections are the same as signal region.
- OS control region, the events in the signal region that failing the kinematics cut defined in the Sec. 8.2.

The FF is applied to the fake tau control region where the subleading tau fails the medium requirement, to model the event with sub-leading taus faked in the signal region. The events with leading fake-tau are modelled by Monte Carlo with a conservative uncertainty of 50% according to Sec. 10.1.

5.4 Statistical strategy

After fake estimation, BDT discriminants are trained in order to separate signal and backgrounds in each signal region.

A profile likelihood fit of the BDT discriminant in the SRs with NPs relating to the systematic uncertainties is made in order to set limits on the signal strengths.

5.5 Blinding strategy

In order to keep the analysis unbiased from artificial cut tunings some data histogram bins are blinded. Following the advice in the top group, the blinding threshold is quantified as S/B reaching 0.1 when assuming $B(t \rightarrow Hq)$ is 0.1% which is the limit set by the 36fb^{-1} combined results.

6 Detector, data set and Monte Carlo simulation

6.1 ATLAS detector

The ATLAS detector [22] at the LHC covers nearly the entire solid angle around the collision point. It consists of an inner tracking detector surrounded by a thin superconducting solenoid, electromagnetic and hadronic calorimeters, and a muon spectrometer incorporating three large superconducting toroid magnets.

The inner-detector system (ID) is immersed in a 2 T axial magnetic field and provides charged particle tracking in the range $|\eta| < 2.5$. A high-granularity silicon pixel detector covers the vertex region and

213 typically provides three measurements per track. It is followed by a silicon microstrip tracker, which usually
 214 provides four two-dimensional measurement points per track. These silicon detectors are complemented
 215 by a transition radiation tracker, which enables radially extended track reconstruction up to $|\eta| < 2.0$.
 216 The transition radiation tracker also provides electron identification information based on the fraction of
 217 hits above a higher energy-deposit threshold corresponding to transition radiation. Compared to Run-1,
 218 an Insertable B-Layer [23] (IBL) is inserted as the innermost pixel layer during LS1 for Run-2, which
 219 significantly improves the tracking performance.

220 The calorimeter system covers the pseudorapidity range $|\eta| < 4.9$. Within the region $|\eta| < 3.2$, electromagnetic
 221 calorimetry is provided by barrel and endcap high-granularity liquid-argon (LAr) electromagnetic
 222 calorimeters, with an additional thin LAr presampler covering $|\eta| < 1.8$, to correct for energy loss in
 223 material upstream of the calorimeters. Hadronic calorimetry is provided by a scintillator-tile calorimeter,
 224 segmented into three barrel structures within $|\eta| < 1.7$, and two LAr hadronic endcap calorimeters.

225 A muon spectrometer (MS) comprises separate trigger and high-precision tracking chambers measuring
 226 the deflection of muons in a magnetic field generated by superconducting air-core toroids. The precision
 227 chamber system covers the region $|\eta| < 2.7$ with three layers of monitored drift tubes, complemented by
 228 cathode strip chambers in the forward region, where the background is highest. The muon trigger system
 229 covers the range $|\eta| < 2.4$ with resistive-plate chambers in the barrel, and thin-gap chambers in the endcap
 230 regions.

231 6.2 Data set

232 This analysis is based on the full proton-proton data at a center-of-mass energy $\sqrt{s} = 13$ TeV with a bunch
 233 spacing of 25 ns collected by ATLAS in Run-2. The following good run list (GRL) was used for the 2015
 234 dataset:

```
235           data15_13TeV.periodAllYear_DetStatus-v89-pro21-02
236           _Unknown_PHYS_StandardGRL_All_Good_25ns.xml
```

237 which corresponds to an integrated luminosity of 3.22 fb^{-1} .

238 The GRL used for the 2016 dataset:

```
239           data16_13TeV.periodAllYear_DetStatus-v89-pro21-01
240           _DQDefects-00-02-04_PHYS_StandardGRL_All_Good_25ns.xml
```

241 corresponds to an integrated luminosity of 32.88 fb^{-1} .

242 These GRLs exclude data where the IBL was not fully operational. The uncertainty in the combined
 243 2015+2016 integrated luminosity, 36.1 fb^{-1} , is 2.1%. It is derived, following a methodology similar to

²⁴⁴ that detailed in Ref. [24], from a calibration of the luminosity scale using x-y beam-separation scans
²⁴⁵ performed in August 2015 and May 2016.

²⁴⁶ The GRL used for the 2017 dataset:

```
247           data17_13TeV.periodAllYear_DetStatus-v99-pro22-01
248           _Unknown_PHYS_StandardGRL_All_Good_25ns_Triggerno17e33prim.xml
```

²⁴⁹ corresponds to an integrated luminosity of 44.307 fb^{-1} .

²⁵⁰ The GRL used for the 2018 dataset:

```
251           data18_13TeV.periodAllYear_DetStatus-v102-pro22-04
252           _Unknown_PHYS_StandardGRL_All_Good_25ns_Triggerno17e33prim.xml
```

²⁵³ corresponds to an integrated luminosity of 59.937 fb^{-1} . The final luminosity used for the analysis is
²⁵⁴ 140.45 fb^{-1} .

²⁵⁵ 6.3 Signal and background simulation

²⁵⁶ The overview of the major samples generated is summarized in Table 5.

²⁵⁷ The TopFCNC UFO model [25, 26] with 5-flavour scheme is used for signal simulation.

²⁵⁸ The targeted signal in this analysis is $t\bar{t}(qH)/tH$ with $H \rightarrow \tau\tau$ (samples 411170-411177 and 412098-
²⁵⁹ 412105) in App. A).

²⁶⁰ The FCNC ST signal is simulated using MadGraph5_aMC@NLO v2.6.2 [27] interfaced with Pythia 8
²⁶¹ [28] with the A14 tune [29] for the generation of parton showers, hadronisation and multiple interactions
²⁶² and the NNPDF30NLO [30] parton distribution functions (PDF) is used to generate qg events at next-to-
²⁶³ leading order (NLO) in QCD. Depending on either up quark or charm quark involved in the FCNC decay
²⁶⁴ and either the W bosons decaying hadronically or leptonically, 4 samples are generated for each term of
²⁶⁵ effective Lagrangian, so eight samples in total.

²⁶⁶ The FCNC TT signal is simulated using Powheg-Box [31] V2 interfaced with Pythia8 [28] with the
²⁶⁷ A14 tune [29] for the generation of parton showers, hadronisation and multiple interactions and the
²⁶⁸ NNPDF30NLO [30] parton distribution functions (PDF) is used to generate $t\bar{t}$ events at next-to-leading
²⁶⁹ order (NLO) in QCD. Depending on either the top or the anti-top quark decaying to bW , either up quark or
²⁷⁰ charm quark involved in the FCNC decay and either the W bosons decaying hadronically or leptonically,
²⁷¹ eight samples are produced with the Higgs decaying into a τ -lepton pair.

²⁷² Considering the other decays of the Higgs can be part of the signal, these samples are also included:

- ²⁷³ • 411420-411427: production mode with $H \rightarrow ZZ$ and $H \rightarrow WW$.

- 274 • xxxxxx-xxxxxx: inclusive W and Higgs decays are also included. These sample have a one-lepton
 275 (electron or muon) filter at truth level (either coming from W or Higgs decays).

276 The events in xxxxxx-xxxxxx with $H \rightarrow \tau\tau$ decay are removed based on truth information.

277 It is checked that after the final selection, there are 110 overlapped signal events caused by different overlap
 278 removal and object definition in xTauFramework and ttHMultiAna (27140 in total for hadhad channel and
 279 95253 in total for lepton channels) but there is no overlap in the signal enriched region ($BDT > 0.5$).

280 The total FCNC signal with fake taus in this analysis is not used in the MVA training, but is regarded as
 281 part of the total signal in the fit. The normalization factor of the other components is common with the
 282 signal, so that their yields are fully correlated in the fit.

283 The dominant background is the $t\bar{t}$ production. The $t\bar{t}$ process and the single top process are generated
 284 with Powheg-Box [31] V2, and Pythia8 is used for the parton shower. NNPDF30NLO [30] and A14
 285 tune [29] are used for $t\bar{t}$ (single top). The $t\bar{t}$ sample is also generated with different generators and parton
 286 showers models, as well as different amount of radiations, for systematics as detailed in Sec. 12.

287 The $t\bar{t}X$, where $X=W, ee, \mu\mu, \tau\tau$ or $Z(qq, vv)$ are generated with MadGraph5_aMC@NLO and interfaced
 288 with Pythia8 for the parton shower. The NNPDF30NLO [30] is used for the matrix element PDF. The $t\bar{t}$,
 289 single top and $t\bar{t}X$ are combined into a single process named top background in the analysis.

290 The W +jets, Z +jets and diboson backgrounds are simulated using Sherpa 2.2.1 [32] with NNPDF30NNLO
 291 PDF [30].

292 The τ decay in the single top samples is handled by Tauola [33]. All samples showered by Pythia8
 293 (Sherpa) have the τ decays also handled by Pythia8 (Sherpa). All the decay modes of the τ lepton are
 294 allowed in the event generators (but may be subject to generator filters). The summary of used generators
 295 for matrix element and parton shower is given in Table 5.

296 The SM higgs background includes ggH , VH , VBF and $t\bar{t}H$, generated from Powheg-Box [31] V2
 297 interfaced with Pythia8. The overall contribution is pretty small. Various PDF and tune options are use
 298 for those samples depending on the decay modes.

299 The tH associated production is negligible but we still considered it. The sample is generated using
 300 MadGraph5 and interfaced with pythia8 for parton shower. CT10 PDF and A14 tune are used. It is treated
 301 as part of SM higgs background explained in above.

302 Except the major background V +jets, $t\bar{t}$, SM higgs, Diboson, the other minor background are categorised
 303 into "Rare" processes in this analysis, which doesn't necessarily mean it's rare in the pp collision.

304 All Monte-Carlo (MC) samples were passed through the full GEANT4 [34] simulation of the ATLAS
 305 detector, except for two extra $t\bar{t}$ samples with Pythia8 and Herwig7 [35] parton showering which are

Table 5: Overview of the MC generators used for the main signal and background samples

Process	Generator		PDF set		Tune	Order
	ME	PS	ME	PS		
<i>T</i> T Signal	Powheg	Pythia8	NNPDF30NLO	NNPDF23LO	A14	NLO
<i>S</i> T Signal	MadGraph5_aMC@NLO	Pythia8	NNPDF30NLO	NNPDF23LO	A14	NLO
<i>W/Z+jets</i>	Sherpa 2.2.1		NNPDF30NNLO		Sherpa	NLO/LO
<i>t</i> <i>t̄</i>	Powheg	Pythia8	NNPDF30NLO	NNPDF23LO	A14	NLO
Single top	Powheg	Pythia6	CT10(NLO)	CTEQ6L1[44]	Perugia2012	NLO
<i>t</i> <i>t̄X</i>	MadGraph5_aMC@NLO	Pythia8	NNPDF30NLO	NNPDF23LO	A14	NLO
Diboson	Sherpa 2.2.1		NNPDF30NNLO		Sherpa	NLO/LO

306 simulated with ATLFAST-II [36] for systematics (Sec. 12). In the analysis, the simulated events were
 307 reweighted based on their pile-up to match the pile-up profile observed in data.

308 The full list of MC samples are given in App. A. The single boson and diboson cross sections are
 309 calculated to NNLO [37]. The *t**t̄* cross section is calculated at NNLO in QCD including resummation
 310 of NNLL soft gluon terms for a top-quark mass of 172.5 GeV [38]. The *t**tH* and *t**tV* are normalized to
 311 NLO cross sections according to [39] and [40]. The *t*-channel and *s*-channel single top cross sections are
 312 calculated at NLO with Hathor v2.1 [41, 42], while the *Wt* channel is calculated at NLO+NNLL [43].

313 7 Object reconstruction

314 In this section, various objects used in this analysis are defined, namely jets, electrons, muons, hadronically
 315 decaying taus and missing transverse energy.

316 7.1 Jets

317 Jets are reconstructed using the anti- k_t algorithm [45] with a distance parameter $R = 0.4$ applied to the
 318 particle flow candidates. Only jets with $p_T > 25$ GeV and $|\eta| < 4.5$ are considered by the E_T^{miss} calculation
 319 and overlap removal procedure. To suppress jets produced in additional pile-up interactions, jets with
 320 $p_T < 60$ GeV and $|\eta| < 2.4$ are required to have a Jet Vertex Tagger (JVT [46]) parameter larger than
 321 0.2 (Medium working point). The JVT is the output of the jet vertex tagger algorithm used to identify
 322 and select jets originating from the hard-scatter interaction through the use of tracking and vertexing
 323 information. About 10% of selected jets in the signal are in the forward detector region. After the above
 324 selection and overlap removal, a “jet cleaning” cut performed by JetCleaningTool with LooseBad working
 325 point is applied on all the jets, and the events with jets not passing this cut are discarded. Only the central
 326 jets with $|\eta| < 2.4$ are considered in the analysis to reject pile-up contamination.

327 7.2 b-tagging

328 The DL1r [47] algorithm is used to identify the jets initiated by b -quarks. A working point corresponding
 329 to an average efficiency of 70% for jets containing b -quarks is chosen.

330 7.3 Light leptons

331 Electron candidates are identified by tracks reconstructed in the inner detector and the matched cluster of
 332 energy deposited in the electromagnetic calorimeter. Electrons candidates are required to have $E_T > 15$
 333 GeV and $|\eta| < 2.47$. The transition region, $1.37 < |\eta| < 1.52$, between the barrel and end-cap calorimeters
 334 is excluded. They are further required to pass a loose + b-layer likelihood-based identification point
 335 [48] and a FCLoose isolation working point [49]. The electrons are further removed if its cluster is
 336 affected by the presence of a dead frontend board in the first or second sampling or by the presence of a
 337 dead high voltage region affecting the three samplings or by the presence of a masked cell in the core. The
 338 electron is required to be consistent with the primary vertex by imposing on the trasverse impact parameter
 339 significance ($|d_0|/\sigma_{d0} < 5$) and the longituinal impact parameter ($|\Delta z_0 \sin\theta_l| < 0.5$ mm) cuts.

340 Muon reconstruction begins with tracks reconstructed in the MS and is matched to tracks reconstructed
 341 in the inner detector. Muon candidates are required to have $p_T > 10$ GeV and $|\eta| < 2.5$. A Loose
 342 identification selection [50] based on the requirements on the number of hits in the ID and the MS
 343 is satisfied. A FCLoose isolation [49] criterion is also required. The transverse impact parameter
 344 requirement for muon is slightly tighter than for electron ($|d_0|/\sigma_{d0} < 3$), while the longitudinal impact
 345 parameter selection is the same.

346 Tight isolation working points are also applied in some channels to reduce fake and non-prompt lepton
 347 contributions based a trained isolation boosted decision tree `PromptLeptonVeto` (PLIV), as described in
 348 Sec. 7.6.

349 7.4 Hadronic tau decays

350 The hadronic tau candidates [51] are seeded by jets reconstructed by the anti- k_t algorithm [45], which
 351 is applied on calibrated topo clusters [52] with a distance parameter of R=0.4. They are required to
 352 have $p_T > 20$ GeV and $|\eta| < 2.5$. The transition region between the barrel and end-cap calorimeters
 353 ($1.37 < |\eta| < 1.52$) is excluded.

354 In the hadronic channels, these tau candidates are considered in the overlap removal procedure and
 355 missing transverse energy calculation, following the Htautau group [53]. In the analysis event selection,
 356 the hadronic tau candidates are required to have one or three charged tracks and an absolute charge of one.

357 An identification algorithm based on Recursive Neural Network (RNN) [54] is applied to discriminate the
 358 visible decay products of hadronically decaying tau lepton τ_{had} from jets initiated by quarks or gluons.
 359 Different RNN working points are used at different levels depending on the analysis channel. Only events
 360 with RNN Medium taus are considered to be signal in the hadronic channels while taus not passing the
 361 RNN Medium are only used in the control regions for fake tau estimation.

362 In the leptonic channels, the taus passing the RNN Loose working point are considered in the overlap
 363 removal procedure and missing transverse energy calculation, following the ttW multi-lepton group [55],
 364 which is more focused on leptons.

365 The OLR and MET calculation procedures in hadronic channels are more forgiving in terms of taus since
 366 there are constantly two hadronic taus, and in the fake estimation, the taus not passing the RNN Medium
 367 are also used. This way we can benefit from better statistics and also be consistent with the W+jet regions
 368 used in the SM $H \rightarrow \tau\tau$ group where the Fake Factors are derived.

369 For the Medium ID, the tau efficiency is about 75% (60%) for 1-prong (3-prong) candidates. The ID
 370 efficiencies are optimized to be flat versus the tau p_T and pileup.

371 The tau candidates are required to not overlap with a very loose electron candidate, and a dedicated BDT
 372 variable is also used to veto the taus which are actually electrons.

373 Efficiency scale factors for tau reconstruction, ID and electron BDT rejection [56] are applied on tau
 374 candidates in MC.

375 7.5 Missing transverse energy

376 The missing transverse energy E_T^{miss} is computed using the fully calibrated and reconstructed physics
 377 objects as described above. The TrackSoftTerm (TST) algorithm is used to compute the SoftTerm of the
 378 E_T^{miss} [57].

379 7.6 Tight lepton isolation: PromptLeptonImprovedVeto(PLIV)

380 A dedicated isolation boosted decision tree has been trained to better reject non-prompt leptons and
 381 fakes produced in hadron decays [58]. The main idea is to identify non-prompt light leptons using
 382 lifetime information associated with a track jet that matches the selected light lepton. These additional
 383 reconstructed charged particle tracks inside the jet can be used to increase the precision of identifying the
 384 displaced decay vertex of heavy flavor (b, c) hadrons that produced a non-prompt leptons.

385 The PLIV is trained on leptons selected from the Powheg+Pythia8 non-allhad $t\bar{t}$ sample using eight input
 386 variables:

- Three of them are used to identify b-tagged jets by ATLAS flavor tagging algorithms;
- Two of them are the ratio of the track lepton p_T with respect to the track jet p_T and ΔR between the lepton and the track jet axis;
- Three of them are the number of tracks collected by the track jet and the lepton track and calorimeter isolation variables.

The PLIV shows a significant improvement for non-prompt-lepton rejection compared to the cut-based isolation variables.

The tight working points are: $PLIV < -0.6734$ for high p_T muonss and $PLIV < -0.704$ for hight p_T barrel electrons. The scale factors for the efficiencies of the tight PLIV working points are measured using the tag and probe method with $Z \rightarrow l^+l^-$ events.

7.7 Overlap removal

For the objects passing the selection above, a geometric overlap removal is applied to eliminate the ambiguity in the object identification. When two objects are close geometrically with ΔR less than a certain threshold, or satisfy some certain requirements, one of them will be removed.

In the hadronic channels, the overlap removal is done by the official overlap removal tool provided by ASG group. The "Standard" working point is used. The rules are discribed as follows in sequence:

- If two electrons have overlapped second-layer cluser, or shared tracks, the electron with lower p_T is removed.
- τ_{had} within a $\Delta R = 0.2$ cone of an electron or muon are removed.
- If a muon sharing an ID track with an electron and the muon is calo-tagged, the muon is removed. Otherwise the electron is removed.
- Jets within a $\Delta R = 0.2$ cone of an electron are removed.
- Electrons within a $\Delta R = 0.4$ cone of a jet are removed.
- When a muon ID track is ghost associated to a jet or within a $\Delta R = 0.2$ cone of a jet, the jet is removed if it has less than 3 tracks with $p_T > 500$ MeV or has a relative small p_T ($p_T^\mu > 0.5 p_T^{\text{jet}}$ and $p_T^\mu > 0.7$ [the scalar sum of the p_T 's of the jet tracks with $p_T > 500$ MeV]).
- Muons within a $\Delta R = 0.4$ cone of a jet are removed.

- Jets within a $\Delta R = 0.2$ cone of the leading τ_{had} ($\tau_{\text{lep}} \tau_{\text{had}}$), or with the two leading τ_{had} 's ($\tau_{\text{had}} \tau_{\text{had}}$), are excluded. The overlap also works for the reverted tau ID regions used in the analysis, since the tau ID information is not used.

- If a tau candidate is tagged as b-jet with 70% working point, the tau is removed.

In the leptonic channels, the overlap removal is done using the heavy flavor overlap removal working point, which gives precedence to the b-tagged jet as follows:

- If two electrons have overlapped second-layer cluster, or shared tracks, the electron with lower p_T is removed.
- τ_{had} within a $\Delta R = 0.2$ cone of an electron or muon are removed.
- If a muon sharing an ID track with an electron and the muon is calo-tagged, the muon is removed. Otherwise the electron is removed.
- Jet is not tagged as b-jet and within a $\Delta R = 0.2$ cone of an electron is removed.
- When a muon ID track is ghost associated to a jet or within a $\Delta R = 0.2$ cone of a jet, the jet is removed if it is not tagged as b-jet and has either less than 3 tracks with $p_T > 500$ MeV or has a relative small p_T ($p_T^\mu > 0.5 p_T^{\text{jet}}$ and $p_T^\mu > 0.7$ [the scalar sum of the p_T 's of the jet tracks with $p_T > 500$ MeV]).
- Muons within a $\Delta R = 0.4$ cone of a jet are removed.
- Jet is not tagged as b-jet and within a $\Delta R = 0.2$ cone of the τ_{had} is removed. The overlap also works for the reverted tau ID regions used in the analysis.
- The event is removed if a tau candidate is tagged as b-jet with 70% working point.

Note that the E_T^{miss} calculation package has its own overlap removal procedure. Only two leading taus are considered in the calculation.

435 8 Signal regions

436 In the leptonic channels, the p_T of the lepton is required to be 1 GeV above the trigger threshold. The
 437 leptons are required to have **Tight ID** as defined in Sec. 7. The trigger matching between the offline and
 438 trigger level lepton objects is also required for the corresponding leptons selected for the analysis.

439 In the hadronic channels, the two tau candidates with the highest p_T are chosen. They should also pass
 440 the **Medium tau ID** and overlap removal. To account for the trigger thresholds, the two hadronic taus are
 441 required to pass the $p_T > 40$ GeV and $p_T > 30$ GeV cuts.

442 The details of implementation of the event selection before the n-tuples and n-tuple level object quality
 443 cuts are listed in App. B.

444 8.1 Trigger

445 In the leptonic channels, the single-lepton triggers are required to select the candidate events. In general,
 446 the lowest unprescaled triggers are used in every data-taking periods:

447 Single electron:

- 448 • 2015: HLT_e24_lhmedium_L1EM20VH,
 449 HLT_e60_lhmedium, HLT_e120_lhloose
- 450 • 2016, 2017, 2018: HLT_e26_lhtight_nod0_ivarloose,
 451 HLT_e60_lhmedium_nod0, HLT_e140_lhloose_nod0

452 Single muon:

- 453 • 2015: HLT_mu20_iloose_L1MU15, HLT_mu50
- 454 • 2016, 2017, 2018: HLT_mu26_ivarmedium, HLT_mu50

455 The di-lepton control regions to estimate fake taus are required to pass di-lepton triggers:

456 Di-electron:

- 457 • 2015: HLT_2e12_lhloose_L12EM10VH
- 458 • 2016: HLT_2e17_lhvloose_nod0
- 459 • 2017, 2018: HLT_2e24_lhvloose_nod0

460 Di-muon:

Not reviewed, for internal circulation only

- 461 • 2015: HLT_mu18_mu8noL1
 462 • 2016, 2017, 2018: HLT_mu22_mu8noL1

463 Electron+Muon:

- 464 • 2015: HLT_e17_lhloose_mu14
 465 • 2016, 2017, 2018: HLT_e17_lhloose_nod0_mu14

466 The trigger used for hadronic channels in each year are listed as follow:

- 467 • 2015: HLT_tau35_medium1_tracktwo_tau25_medium1_tracktwo_L1TAU20IM_2TAU12IM
 468 • 2016: HLT_tau35_medium1_tracktwo_tau25_medium1_tracktwo
 469 • 2017: HLT_tau35_medium1_tracktwo_tau25_medium1_tracktwo_03dR30_L1DR_TAU20ITAU12I_J25
 470 • 2018: HLT_tau35_medium1_tracktwoEF_tau25_medium1_tracktwoEF_03dR30_L1DR_TAU20ITAU12I_J25

471 The two τ_{had} candidates are matched to the respective legs of the di-tau trigger using the individual single
 472 tau trigger objects. The p_T thresholds are chosen such that the selected τ_{had} candidate p_T already lies
 473 in the plateau of the respective trigger efficiency curve. Due to the rising instantaneous luminosity, the
 474 trigger used in the 2016-2018 data taking includes a requirement for an additional level-1 calorimeter
 475 trigger jet . The leading jet in those events is required to be matched within $\Delta R < 0.4$ with the jet ROI
 476 that fulfilled the jet part of the trigger criteria (trigger jet). The $p_T > 60 \text{ GeV}$ cut is applied to make sure
 477 that the jet is in the trigger p_T plateau.

478 8.2 Cuts

479 Kinematics cuts are carefully selected to reduce background and provide control region for fake tau
 480 estimation in the hadronic channels:

- 481 • $m_{\tau\tau,\text{vis}} > 60$
 482 • $m_{\tau\tau,\text{vis}} < 120$
 483 • $\Delta R(\tau, \tau) < 3.4$
 484 • $100 \text{ GeV} < m_{\tau\tau} < 150 \text{ GeV}$
 485 • $m_{t,\text{FCNC}} > 140 \text{ GeV}$

486 The S/B is significantly improved after applying these cuts as shown in Table 31 and 32. The yield of the
487 CR generated are shown in Table 16 indicated by “OS CR”.

488 In the leptonic channels, except $t_l\tau_{\text{had}}\tau_{\text{had}}$, a $E_T^{\text{miss}} > 20\text{GeV}$ cut and PLIV tight is used to reduce QCD
489 background and also provide QCD enriched control regions. The yield are shown in Table 10 - 11.

490 The yields of signal regions for both hadronic and leptonic channels are shown in Table 3. For the $tt(cH)$
491 channel tcH coupling search, the FCNC jet is from a c-quark. Regarding the similarity between the b-jet
492 and c-jet, the very loose b-tagging is attempted on the FCNC jet in order to further select the $t \rightarrow cH$
493 signal. However, the dominating background is $t\bar{t}$ where there are 2 b-jets. This resort does not help with
494 the significance.

495 9 Reconstruction of event topology

496 To comply with the signal topology, in each channel, exactly one jet should be tagged as a b -jet.

497 In $t_h t(qH)$ events, the jet from $t \rightarrow qH$, denoted as the FCNC jet, should be a hard narrow jet considering
 498 it's from the decay chain $t \rightarrow qH \rightarrow q\tau\tau$, with taus reconstructed as leptons or τ_{had} . So all jets from the
 499 top hadronic decay and the FCNC jet should pass the jet selection mentioned in the Sec 7. There should
 500 be at least four jets among which the one with smallest $\Delta R(p_{\text{jet}}^{\mu}, p_{\tau_1}^{\mu} + p_{\tau_2}^{\mu})$ is considered as FCNC jet
 501 since the top decay products are likely boosted close together than other jets, as shown in Figure 4. If
 502 there are more than 2 jets beside FCNC jet and b -jet, the jets from W boson decay are chosen from the
 503 combination which have the invariant mass closest to W resonance. There is the chance that one of the
 504 jets fails the p_T requirement and not reconstructed. This kind of events will fall into $t_h H$ channel. The
 505 FCNC top resonance is still reconstructable given the big chance that the jet which is missing is from W
 506 decay.

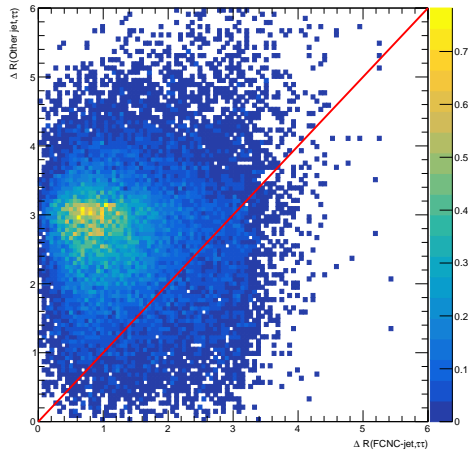


Figure 4: The ΔR between FCNC jet and di-tau candidates (visible) versus ΔR between other jet and di-tau candidates.

507 In $t_h H$ events, there are 3 jets coming from top hadronic decay including the b -jet. So a Higgs resonance
 508 formed by the taus and a top resonance formed by the jets are expected.

509 In $t_h H$ and $t_h t(qH)$ channels, the χ^2 fit is used to reconstruct the ditau mass and momentum by taking the
 510 τ decay kinematics into account. To determine the 4-momenta of the invisible decay products of the tau
 511 decays, the following χ^2 in Eq. 3, based on the collinear approximation is used.

$$\chi^2 = \left(\frac{m_H^{\text{fit}} - 125}{\sigma_{\text{Higgs}}} \right)^2 + \left(\frac{E_{x,\text{miss}}^{\text{fit}} - E_{x,\text{miss}}}{\sigma_{\text{miss}}} \right)^2 + \left(\frac{E_{y,\text{miss}}^{\text{fit}} - E_{y,\text{miss}}}{\sigma_{\text{miss}}} \right)^2, \quad (3)$$

512 In Eq. 3, the free parameters are the energy ratio of invisible decay products for each tau decay. The
 513 Higgs mass resolution is set to 20 GeV according to the [59]. The E_T^{miss} resolution is parametrized as

$$\sigma_{\text{miss}} = 13.1 + 0.50\sqrt{\Sigma E_T}, \quad (4)$$

514 where ΣE_T (in GeV) is the scalar sum of transverse energy depositions of all objects and clusters. The
 515 invisible 4-momenta are obtained by minimizing the combined χ^2 for each event. By adding the Higgs
 516 mass constraint term in the kinematic fit, not only is the Higgs mass resolution improved, but also the
 517 resolutions of the Higgs boson's four-momentum, and the mass of the top from which the Higgs comes.
 518 Figure 5 shows the distributions of χ^2 in different regions. Good agreement between data and background
 519 predictions are achieved.

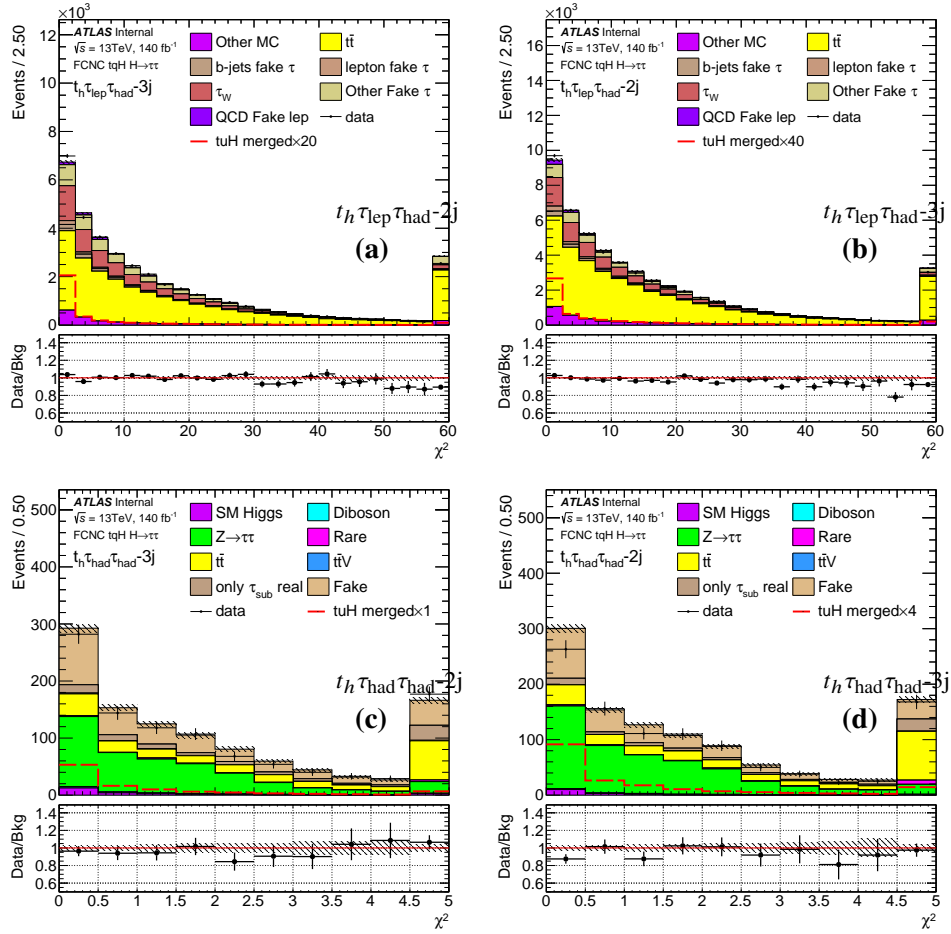


Figure 5: The distributions of χ^2 in Eq. 3 in the hadronic channels.

21st April 2021 – 22:47

25

Not reviewed, for internal circulation only

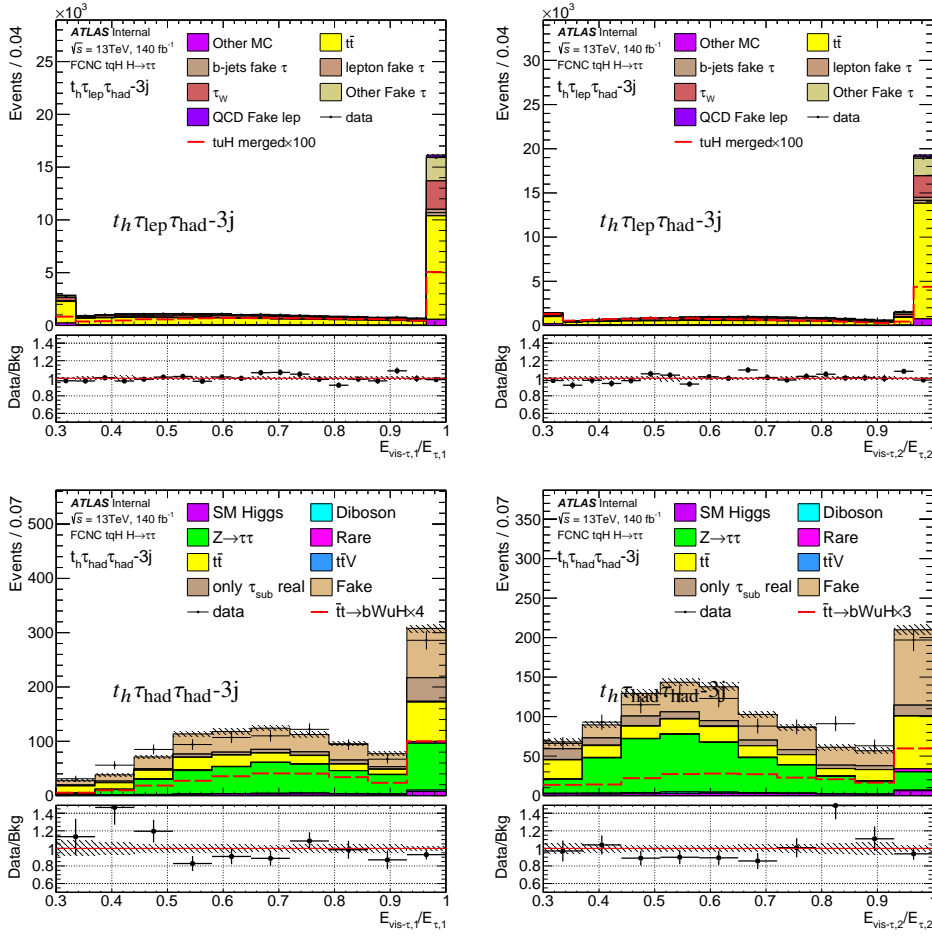


Figure 6: The distributions of $E_{\nu,i}/E_{\tau,i}$, $i = 1, 2$ in the $t_h \tau_{lep} \tau_{had}-3j$ (top) and $\tau_{had} \tau_{had}$ (bottom) channels.

520 In $t_l \tau_{had} \tau_{had}$ channels, a Higgs resonance formed by the taus is expected. Additionally for $t_l t(qH)$ with
521 $H \rightarrow \tau_{had} \tau_{had}$ events, a top resonance formed by the c/u jet and Higgs is expected.

522 Due to the large amount of neutrinos produced in leptonic channels with a huge degree of freedom. The
523 kinematic fit to reconstruct the neutrinos is given up in $t_l \tau_{had} \tau_{had}$ and $t_l \tau_{had}$ channels. The kinematics
524 calculated directly from visible particles and E_T^{miss} are used as BDT input.

525 With the event topology reconstructed, a number of variables are defined for signal and background
526 separation. Their distributions can be found later in this section, and some of their explanations are as
527 follows. In the following explanations, di-tau point to the visible decay product of both τ_{had} and τ_{lep} .

- 528 1. E_{miss}^T is the missing transverse momentum.
529 2. $p_{T,\tau}$ is the transverse momentum of the leading tau candidate.
530 3. $p_{T,\text{sub-}\tau}$ is the transverse momentum of the sub-leading tau candidate.

Not reviewed, for internal circulation only

- 531 4. $p_{T,l}$ is the transverse momentum of the leading lepton.
 532 5. χ^2 is derived from kinematic fitting for the neutrinos.
 533 6. $m_{t,SM}$ is the invariant mass of the b -jet and the two jets from the W decay, and reflects the top mass
 534 in the decay $t \rightarrow Wb \rightarrow j_1 j_2 b$. This variable is only defined for the 4-jet $t_h H$ and $t_h t(qH)$ events.
 535 7. m_W^T is the transverse mass calculated from the lepton and E_T^{miss} in the leptonic channels, defined as

$$m_W^T = \sqrt{2p_{T,\text{lep}}E_T^{\text{miss}}(1 - \cos\Delta\phi_{\text{lep,miss}})}. \quad (5)$$

- 536 8. $m_{\tau,\tau}$ is the invariant mass of the tau candidates and reconstructed neutrinos in $t_h H$ and $t_h t(qH)$
 537 channels.
 538 9. m_W is the reconstructed invariant mass of the hadronic W boson from SM top quark.
 539 10. $m_{t,FCNC}$ is the visible invariant mass of the FCNC-decaying top quark reconstructed from di-tau
 540 candidates, FCNC-jet and reconstructed neutrinos.
 541 11. $m_{\tau\tau,vis}$ is the visible invariant mass of the di-tau candidates
 542 12. $p_{T,\tau\tau,vis}$ is the p_T of the di-tau candidates.
 543 13. $m_{t,FCNC,vis}$ is the reconstructed visible mass of the FCNC-decaying top quark.
 544 14. $m_{t,SM,vis}$ is the invariant mass of the lepton and the b -jet, which reflects the visible SM top mass.
 545 15. $M(\tau q jet, min)$ is the visible mass of the di-tau candidates (include leptonic tau) and the light-
 546 flavor jet, minimized by choosing different jet, reflects the invariant masss of the visible FCNC top
 547 decaying product, an alternative of variable $m_{t,FCNC,vis}$.
 548 16. $M(w jet1, w jet2, min)$ is the invariant mass of two light-flavor jet, minimized by choosing different
 549 jets, reflects the invariant mass of the W candidate, an alternative of m_W .
 550 17. E_{miss}^T centrality is a measure of how central the E_T^{miss} lies between the two tau candidates in the
 551 transverse plane, and is defined as

$$\begin{aligned} E_T^{\text{miss}} \text{ centrality} &= (x + y)/\sqrt{x^2 + y^2}, \\ \text{with } x &= \frac{\sin(\phi_{\text{miss}} - \phi_{\tau_1})}{\sin(\phi_{\tau_2} - \phi_{\tau_1})}, y = \frac{\sin(\phi_{\tau_2} - \phi_{\text{miss}})}{\sin(\phi_{\tau_2} - \phi_{\tau_1})}, \end{aligned} \quad (6)$$

- 552 18. $E_{\nu,i}/E_{\tau,i}, i = 1, 2$ is the momentum fraction carried by the visible decay products from the tau
 553 mother. It is based on the best-fit 4-momentum of the neutrino(s) according to the event reconstruc-
 554 tion algorithm in this section. For the τ_{had} decay mode, the visible decay products carry most of
 555 the tau energy since there is only a single neutrino in the final state, which is evident in the excess
 556 around 1 in Figure 6.

Not reviewed, for internal circulation only

- 557 19. $\Delta R(l + b\text{jet}, \tau\tau)$ is the angular distance between the lepton+b-jet and di-tau candidates.
- 558 20. $\Delta R(l, b\text{jet})$ is the angular distance between the lepton and b-jet.
- 559 21. $\Delta R(\tau, b\text{jet})$ is the angular distance between the tau and b-jet. If there are two taus in the event, the
560 leading one is selected for the calculation.
- 561 22. $\eta_{\tau,\max}$ is the maximum η value among the tau candidates.
- 562 23. $\Delta R(l, \tau)$ is the angular distance between the lepton and the closest tau candidate in the leptonic
563 channels.
- 564 24. $\Delta R(\tau, q\text{jet})$ is the angular distance between the tau and the reconstructed fcnc jet.
- 565 25. $\Delta R(\tau, \tau)$ is the angular distance between two tau candidates, in case of $t_h\tau_{\text{lep}}\tau_{\text{had}}$ channels, the
566 definition is the same as $\Delta R(l, \tau)$.
- 567 26. $\Delta\phi(\tau\tau, P_{\text{miss}}^T)$ is the azimuthal angle between the $E_{\text{T}}^{\text{miss}}$ and di-tau p_{T} .

568 The distributions of those variables in the signal regions (SRs) are shown in:

- 569 • $t_l\tau_{\text{had}}\text{-1j}$: Figure 7 - 8
- 570 • $t_l\tau_{\text{had}}\text{-2j}$: Figure 9 - 10
- 571 • $t_h\tau_{\text{lep}}\tau_{\text{had}}\text{-2j}$: Figure 11 - 13
- 572 • $t_h\tau_{\text{lep}}\tau_{\text{had}}\text{-3j}$: Figure 14 - 16
- 573 • $t_l\tau_{\text{had}}\tau_{\text{had}}$: Figure 17 - 18
- 574 • $t_h\tau_{\text{had}}\tau_{\text{had}}\text{-2j}$: Figure 19 - 20
- 575 • $t_h\tau_{\text{had}}\tau_{\text{had}}\text{-3j}$: Figure 21 - 22

576 The data are in good agreement with the background prediction of the standard model.

Not reviewed, for internal circulation only

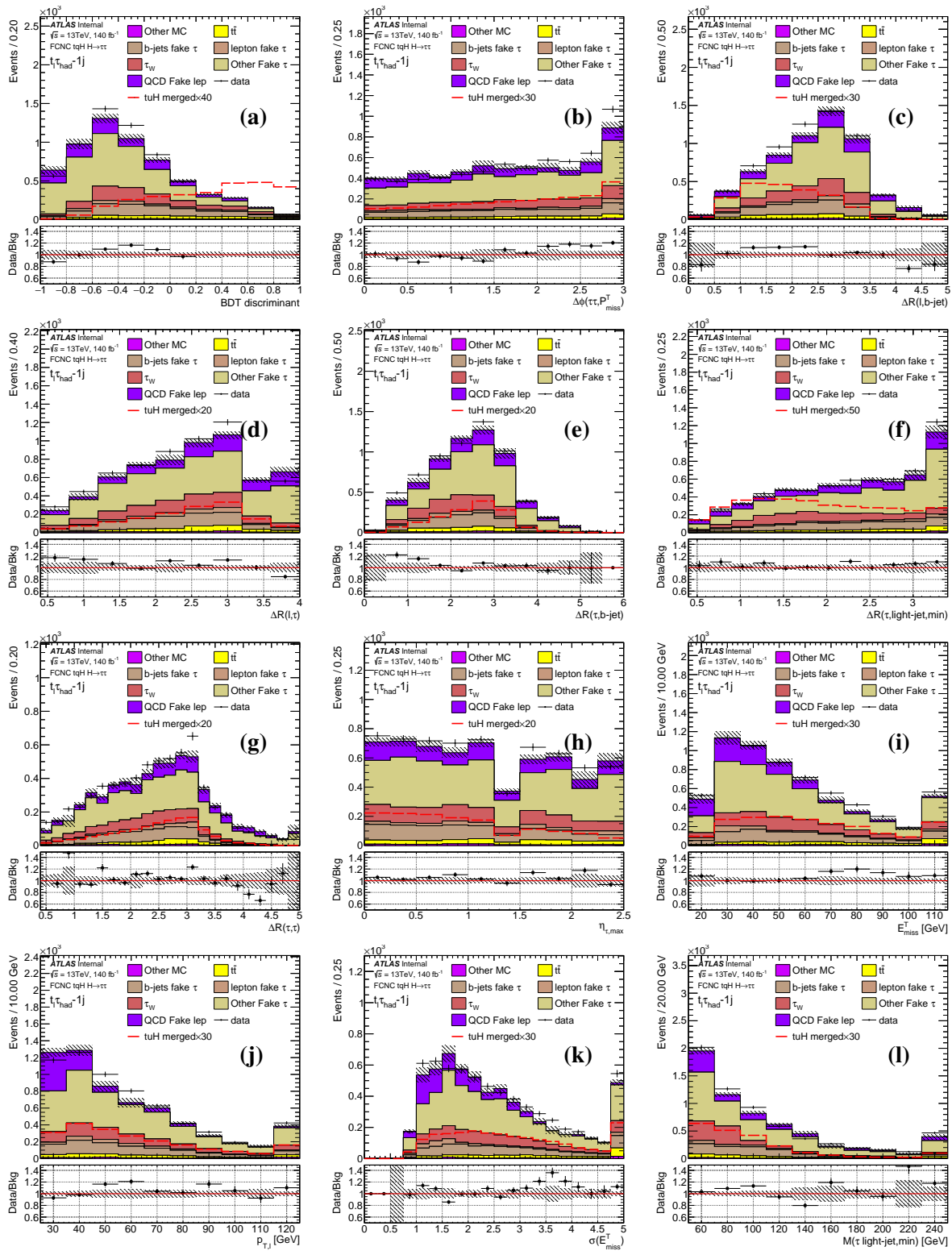


Figure 7: The variables distributions for the background and merged tuH signal in the $t_l \tau_{had-1j}$

Not reviewed, for internal circulation only

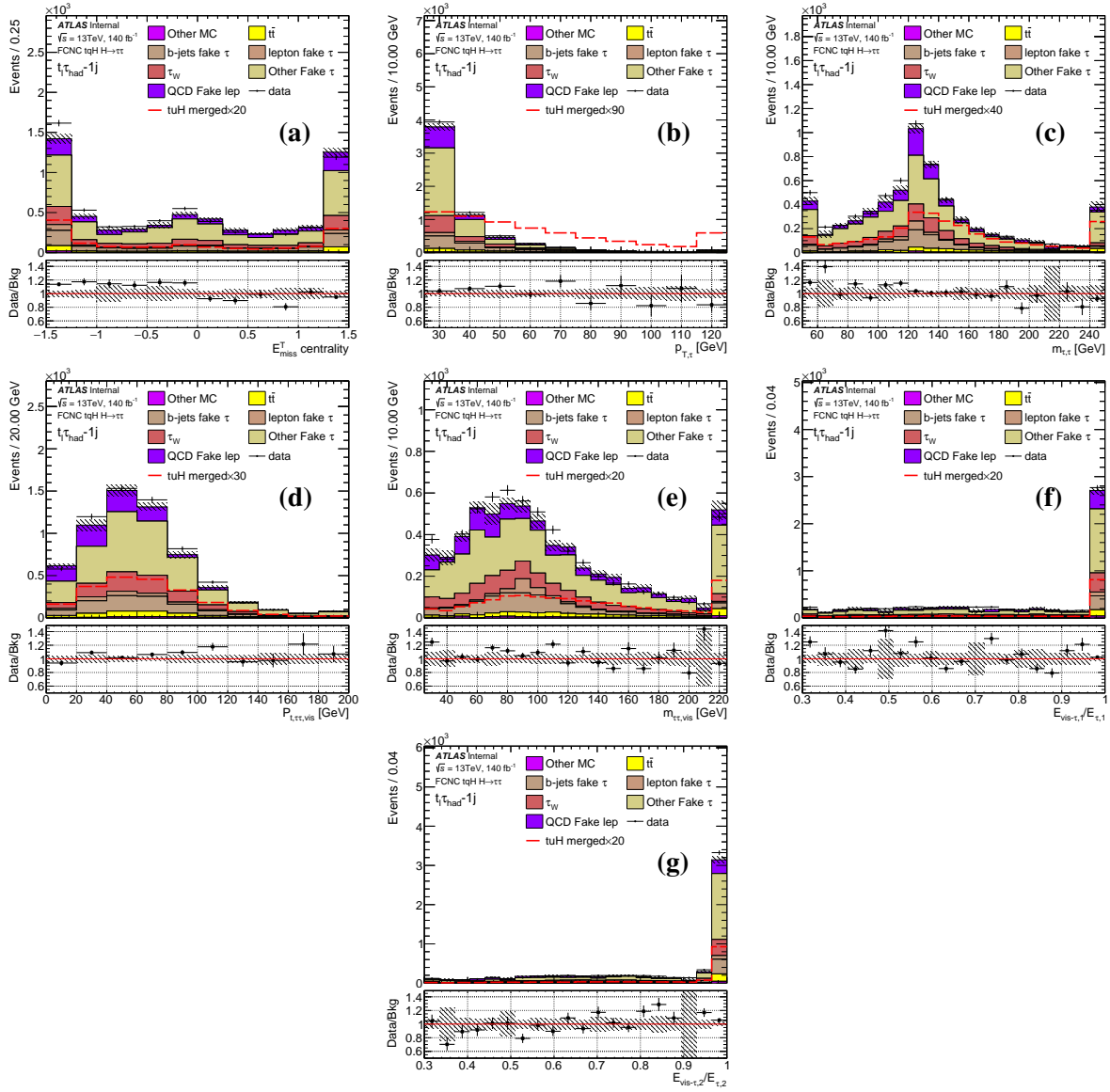


Figure 8: The variables distributions for the background and merged tuH signal in the $t_l \tau_{\text{had}}-1j$

Not reviewed, for internal circulation only

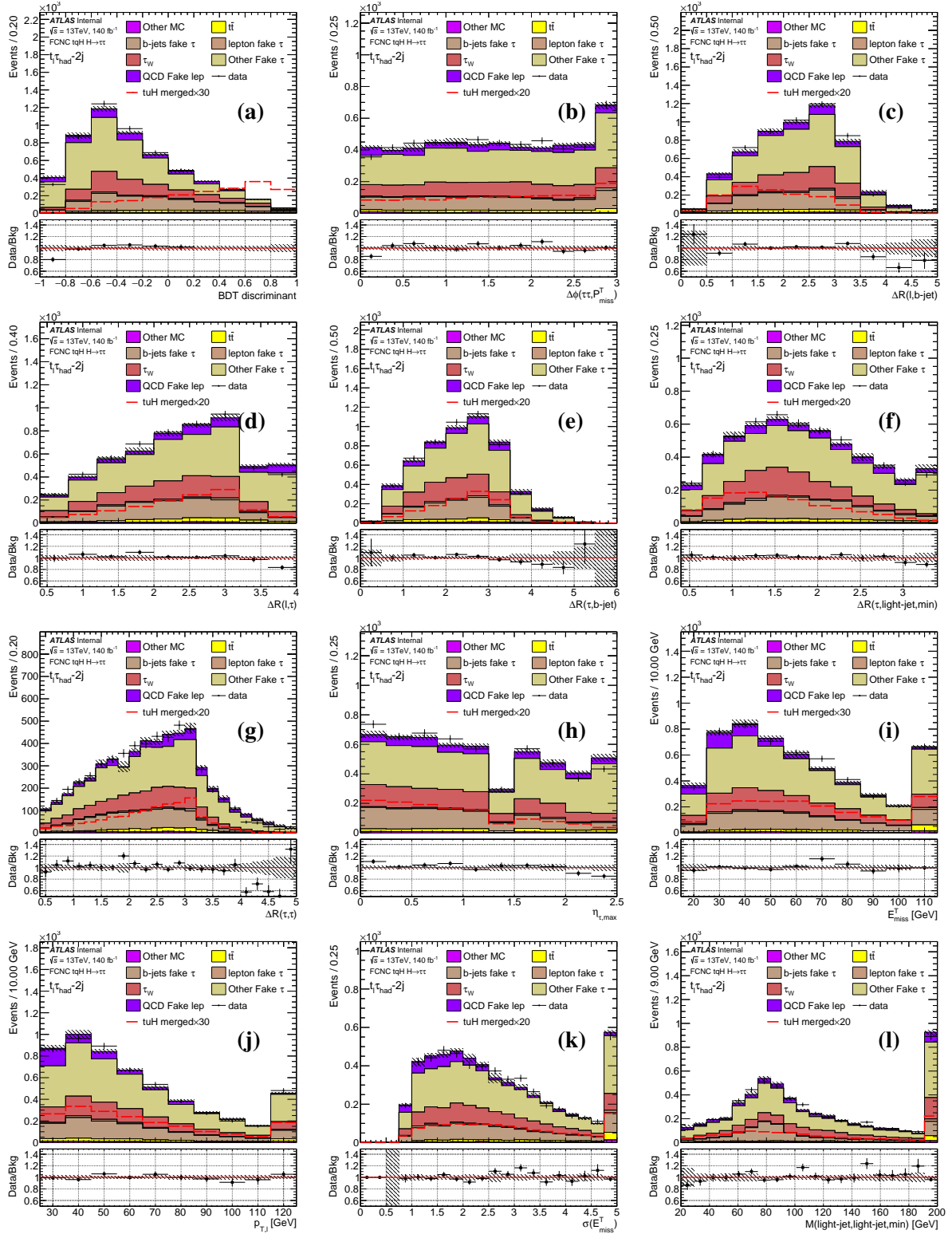


Figure 9: The variables distributions for the background and merged tuH signal in the $t_l \tau_{had-2j}$

Not reviewed, for internal circulation only

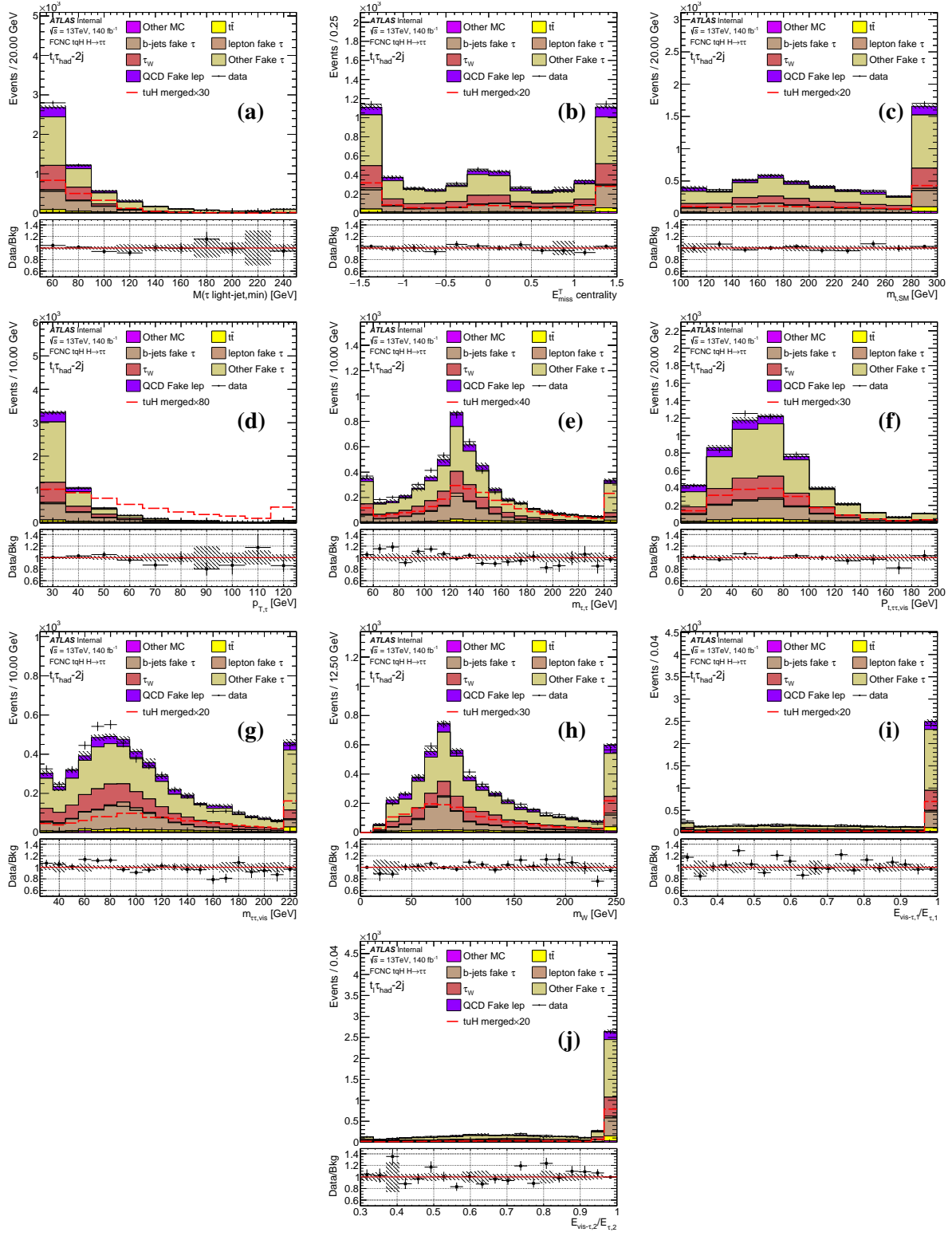


Figure 10: The variables distributions for the background and merged tuH signal in the $t_l \tau_{\text{had}}-2j$

Not reviewed, for internal circulation only

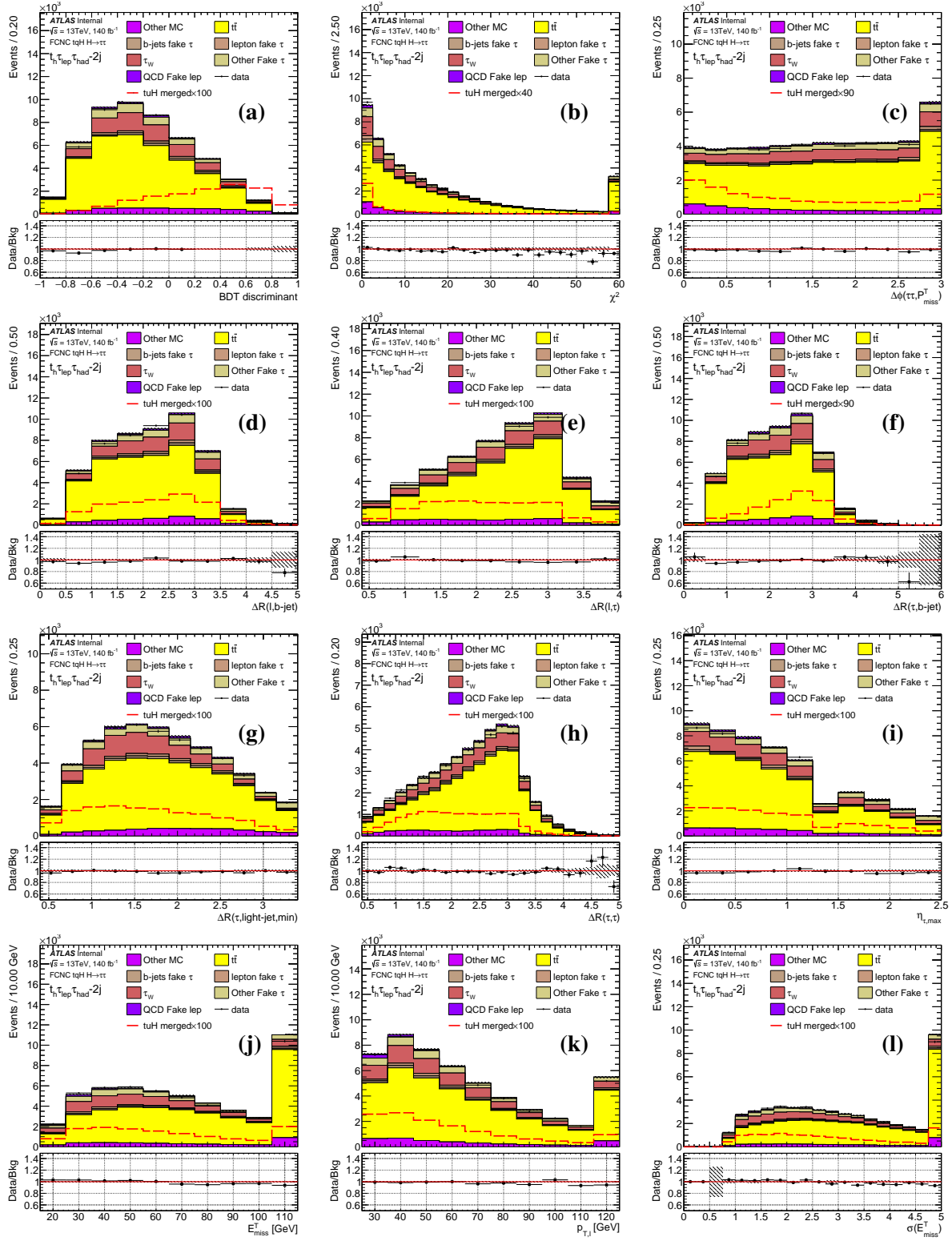


Figure 11: The variables distributions for the background and merged tuH signal in the $t_h \tau_{\text{lep}} \tau_{\text{had-2j}}$

Not reviewed, for internal circulation only

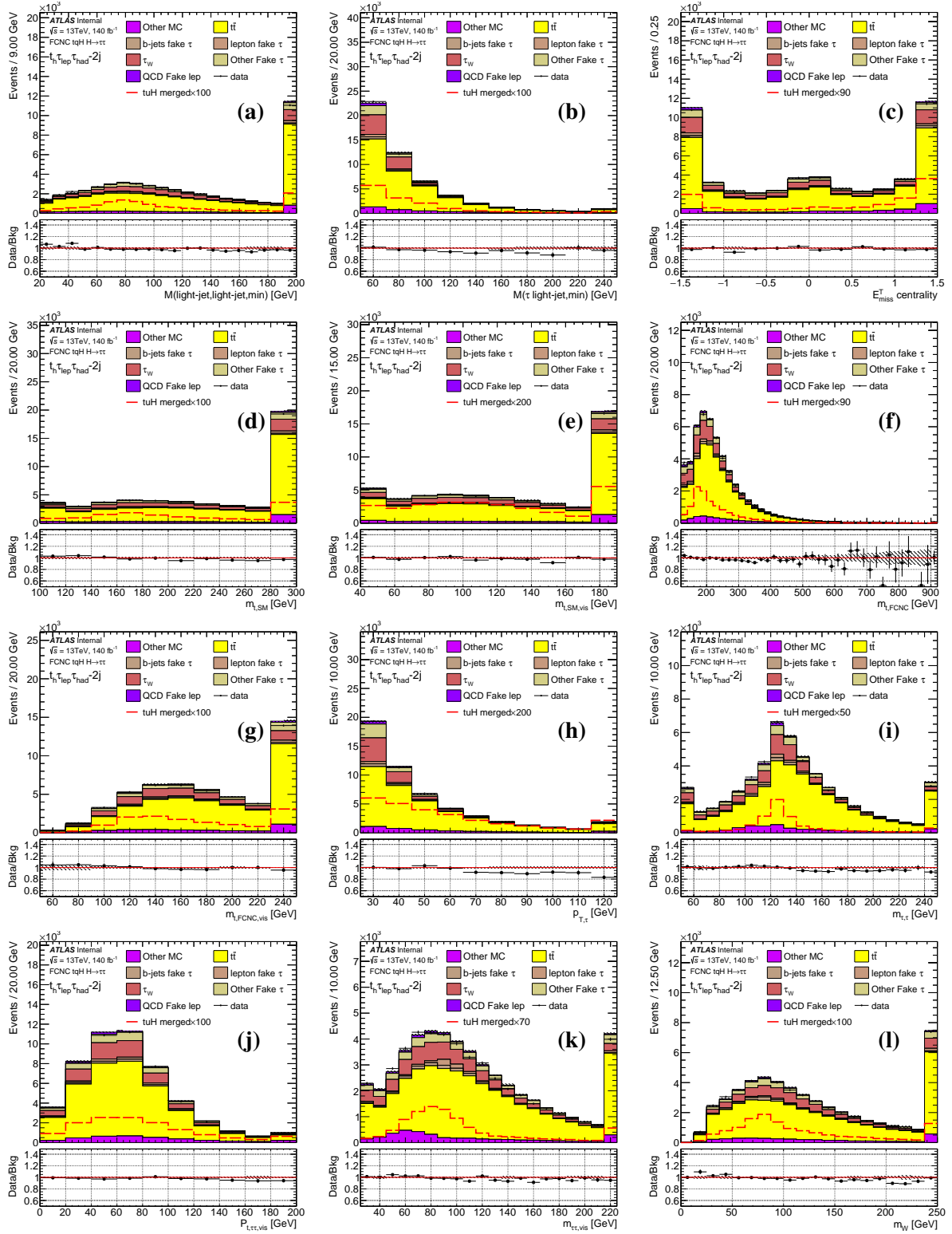


Figure 12: The variables distributions for the background and merged tuH signal in the $t_h \tau_{\text{lep}} \tau_{\text{had}}-2j$

Not reviewed, for internal circulation only

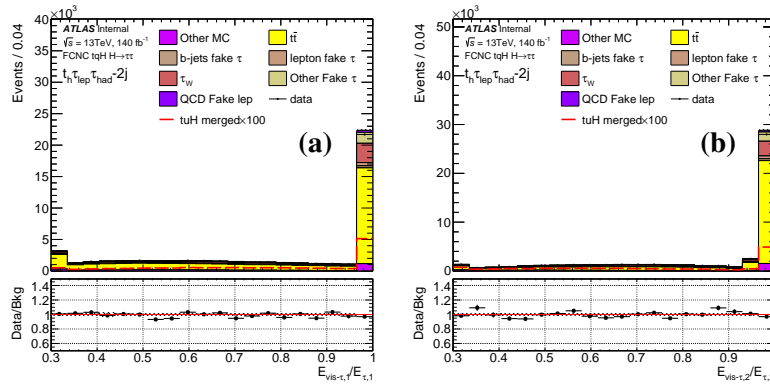


Figure 13: The variables distributions for the background and merged $t\bar{H}$ signal in the $t_h \tau_{\text{lep}} \tau_{\text{had}} - 2j$

Not reviewed, for internal circulation only

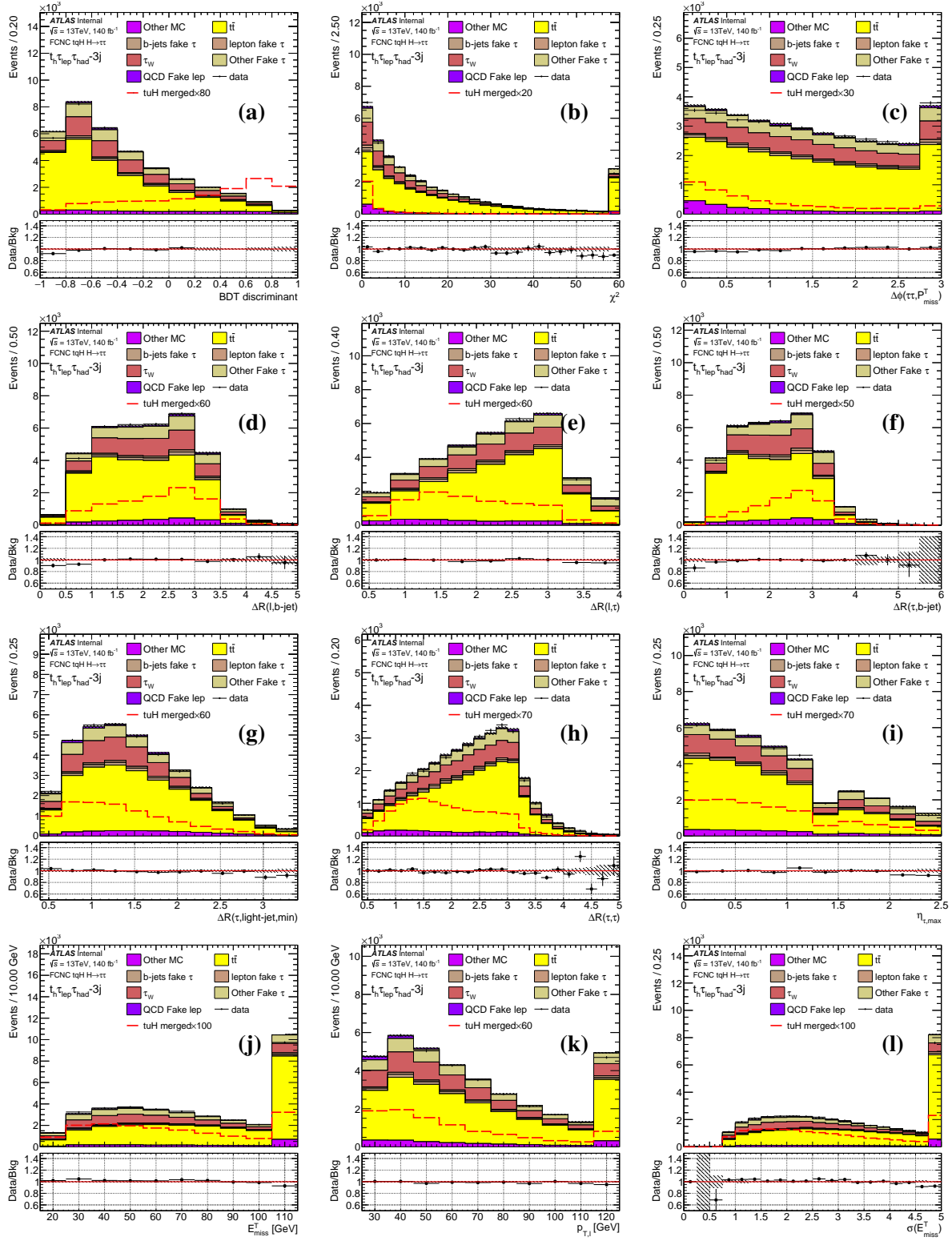


Figure 14: The variables distributions for the background and merged tuH signal in the $t_h \tau_{\text{lep}} \tau_{\text{had}} - 3j$

Not reviewed, for internal circulation only

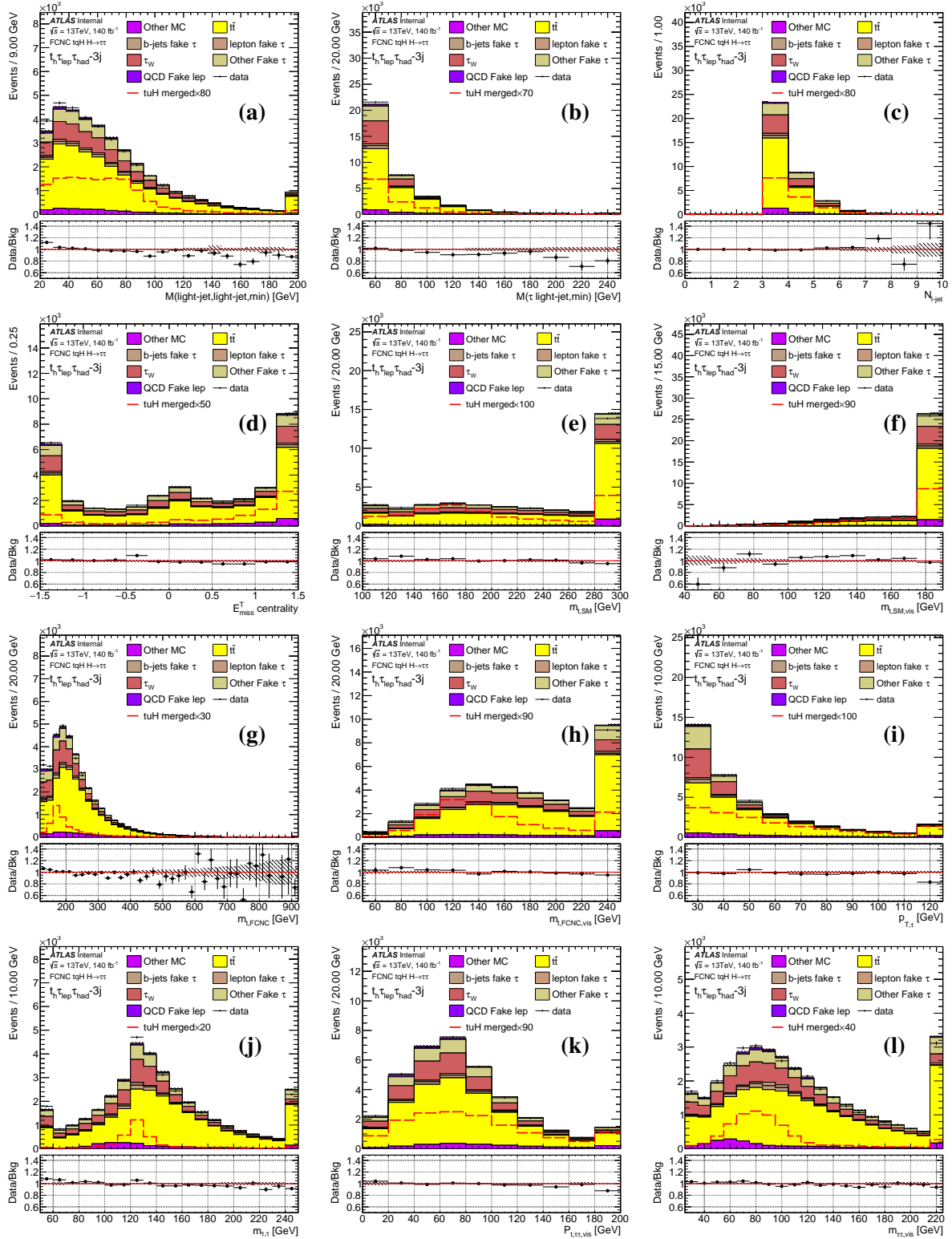


Figure 15: The variables distributions for the background and merged tuH signal in the $t_h \tau_{\text{lep}} \tau_{\text{had}}\text{-}3j$

Not reviewed, for internal circulation only

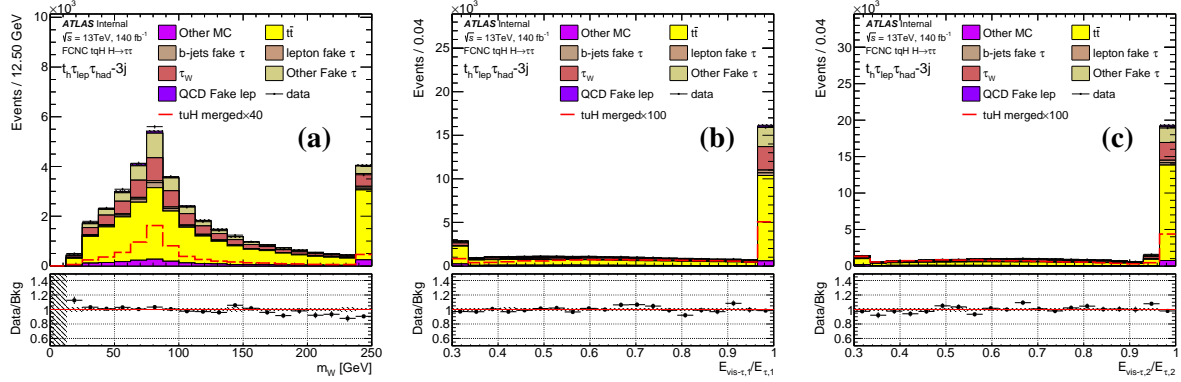


Figure 16: The variables distributions for the background and merged tuH signal in the $t_h \tau_{\text{lep}} \tau_{\text{had}}\text{-}3j$

Not reviewed, for internal circulation only

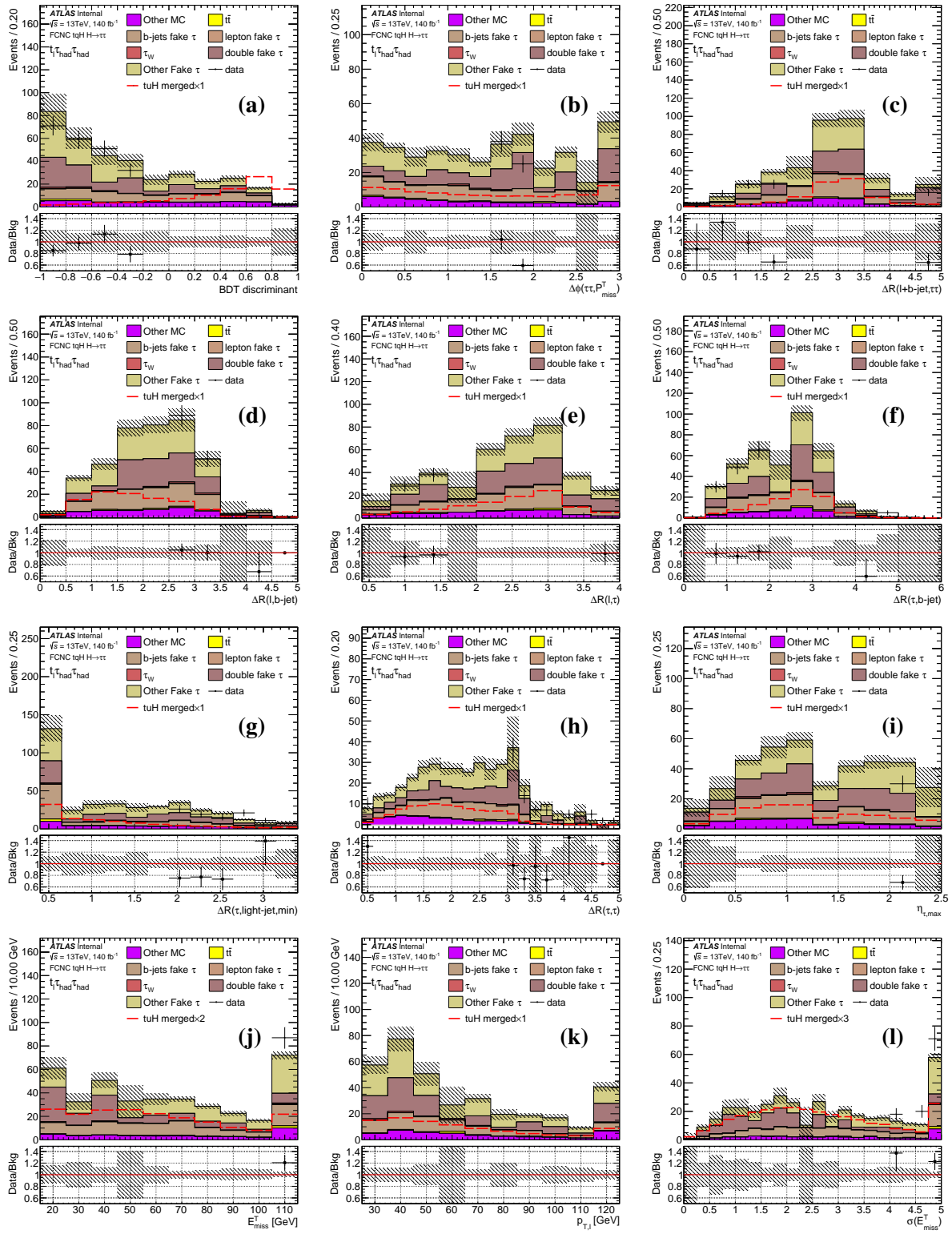


Figure 17: The variables distributions for the background and merged tuH signal in the $t_1 \tau_{\text{had}} \tau_{\text{had}}$

Not reviewed, for internal circulation only

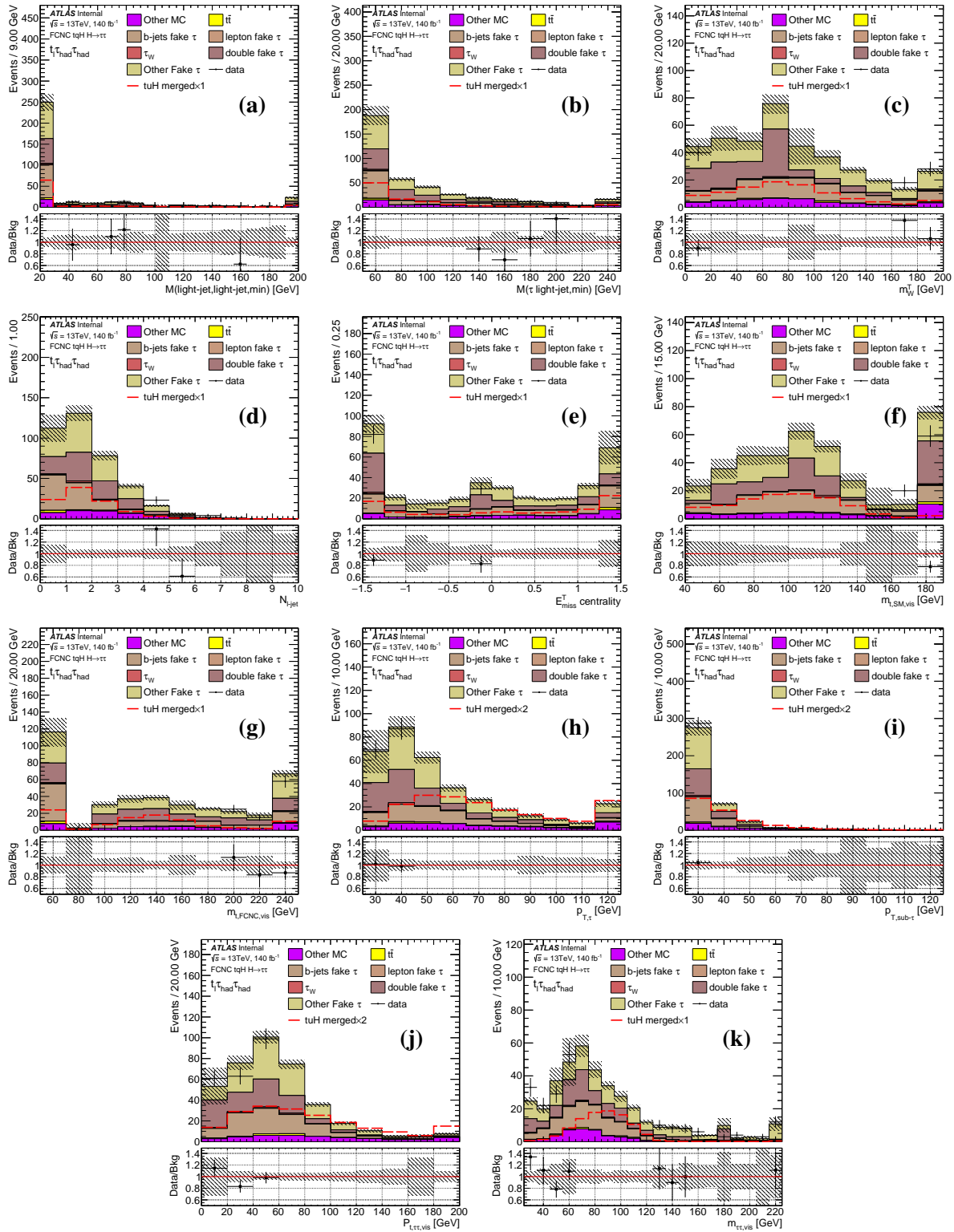


Figure 18: The variables distributions for the background and merged tuH signal in the $t_1 t_2 \text{had} \tau_1 \tau_2 \text{had}$

Not reviewed, for internal circulation only

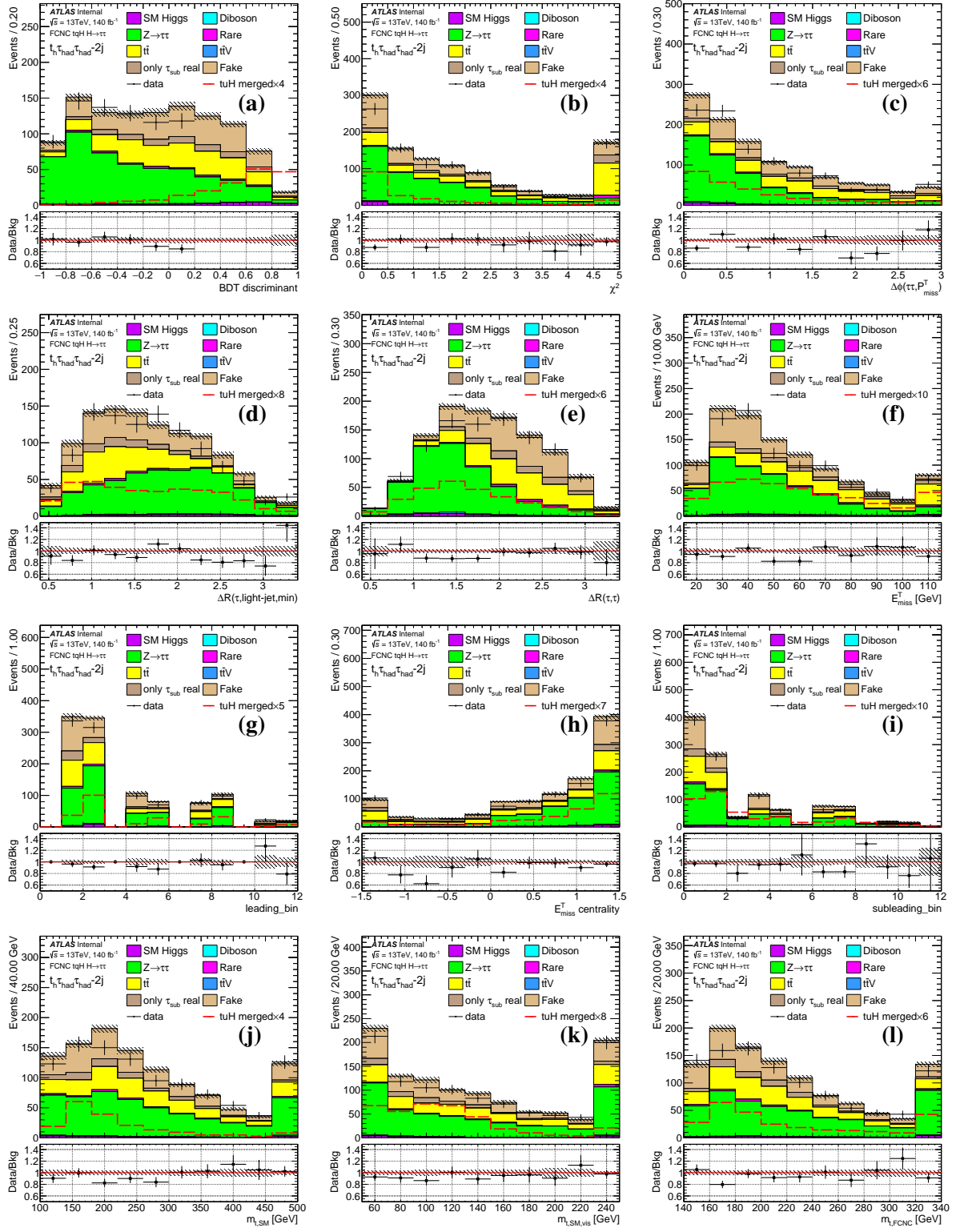


Figure 19: The variables distributions for the background and merged tuH signal in the $t_h \tau_{had} \tau_{had-2j}$

Not reviewed, for internal circulation only

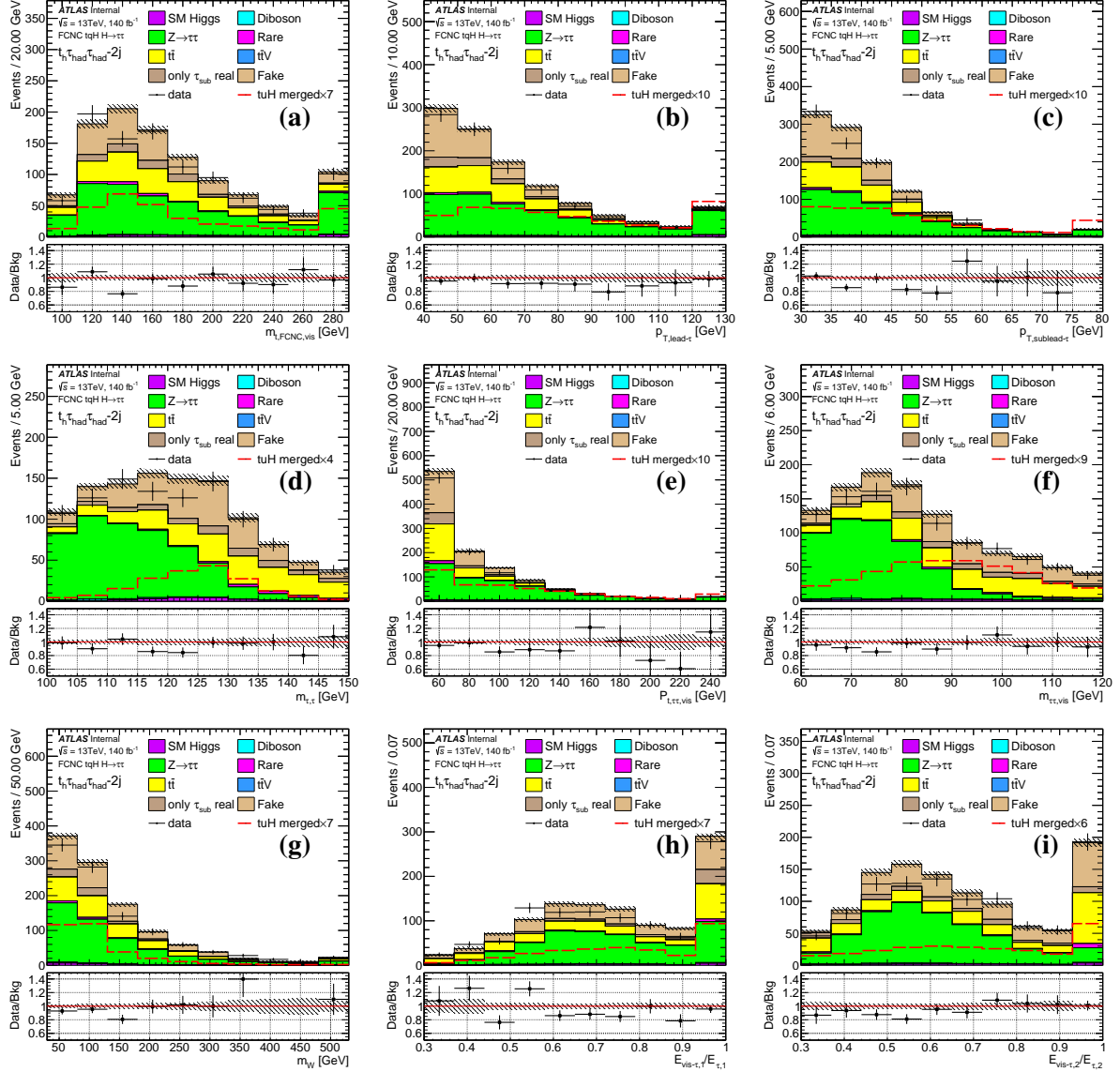


Figure 20: The variables distributions for the background and merged tuH signal in the $t_h \tau_{had} \tau_{had-2j}$

Not reviewed, for internal circulation only

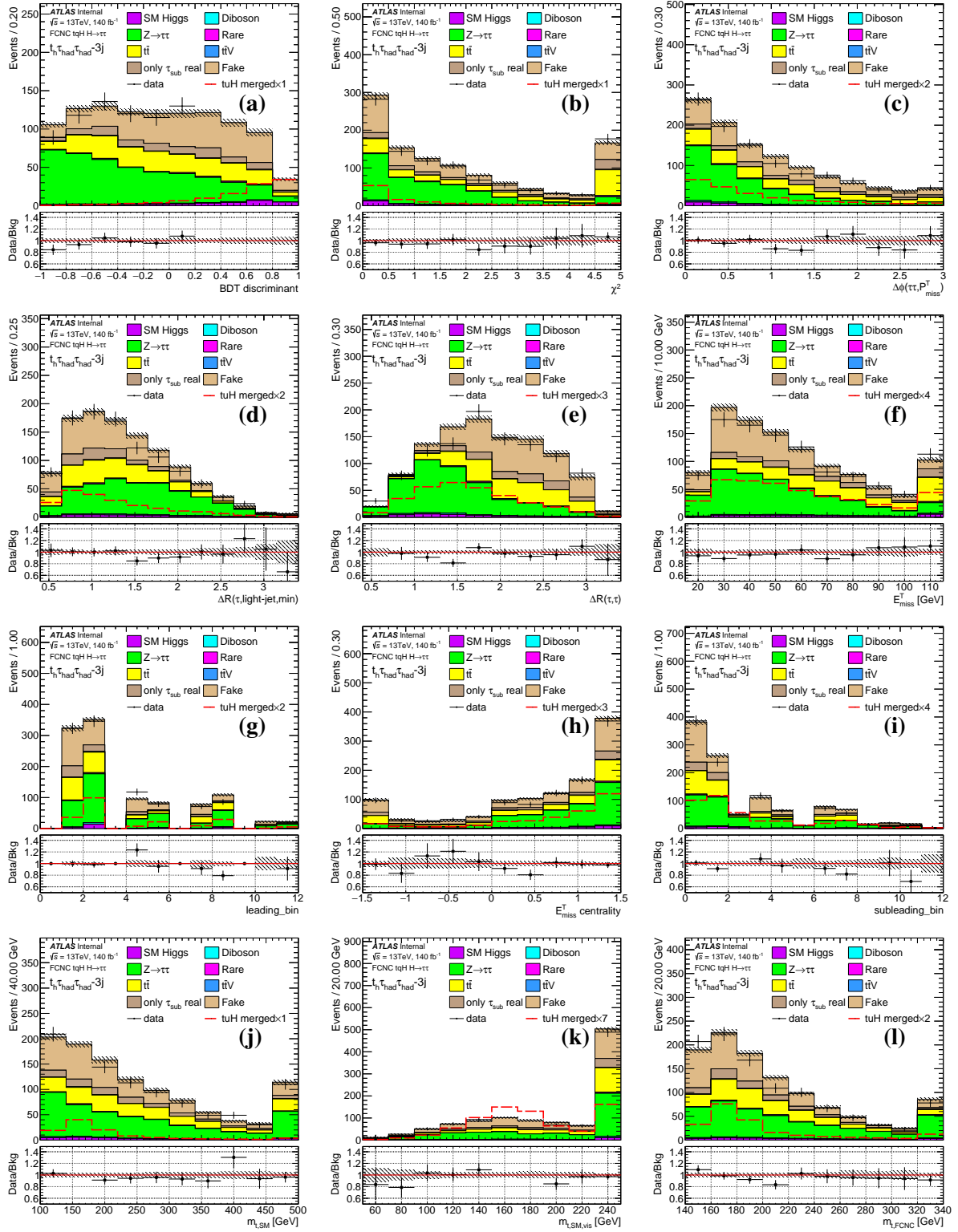


Figure 21: The variables distributions for the background and merged tuH signal in the $t_h \tau_{had} \tau_{had-3j}$

Not reviewed, for internal circulation only

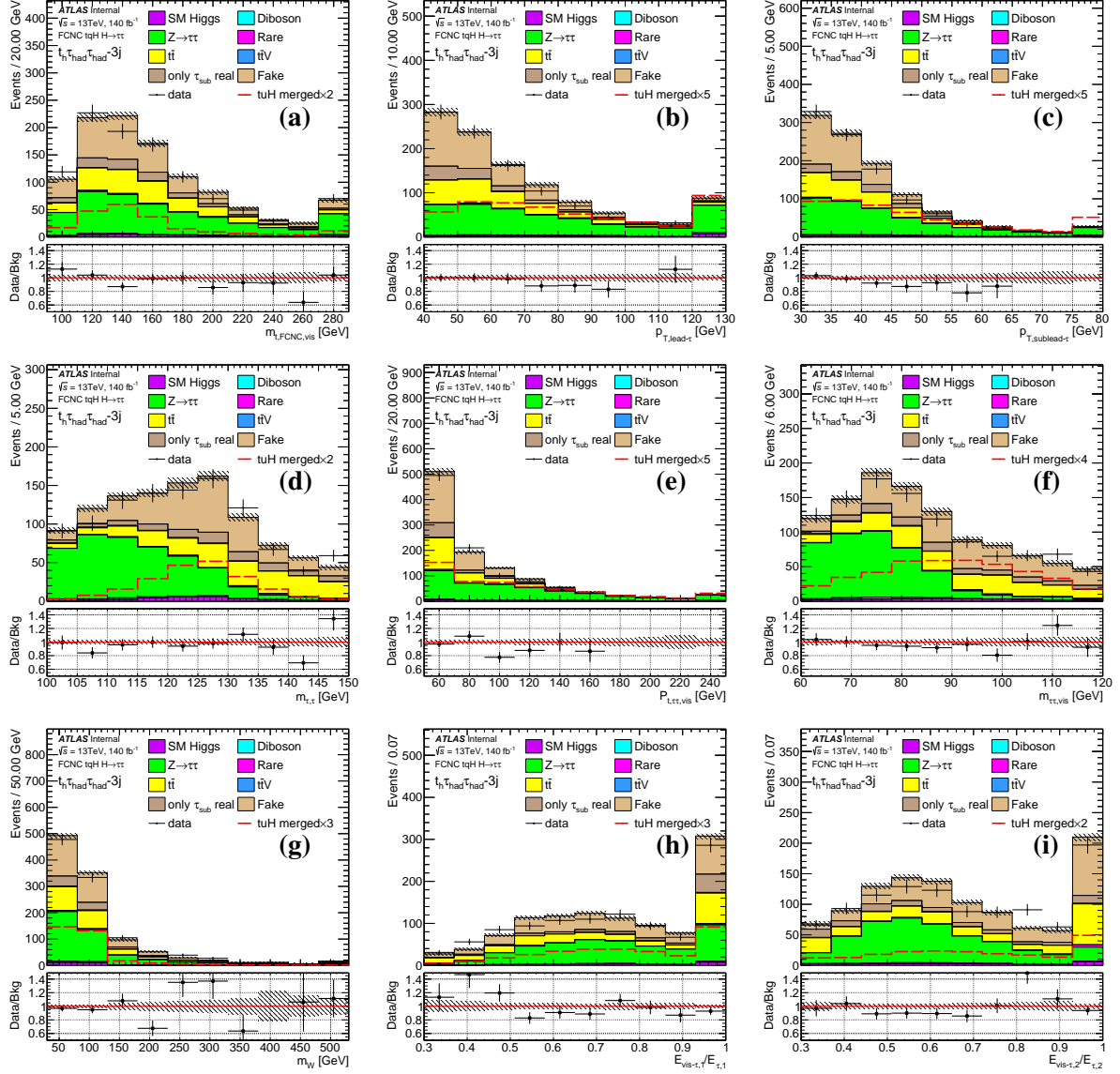


Figure 22: The variables distributions for the background and merged tuH signal in the $t_h \tau_{had} \tau_{had-3j}$

577 10 Background estimation

- 578 The background events with real tau leptons are represented by Monte Carlo (MC) samples. These include
579 $t\bar{t}$, $t\bar{t} + H/V$ and single top events with real taus, and $Z \rightarrow \tau\tau + \text{jets}$.
- 580 The $Z \rightarrow ee, \mu\mu$ processes are included for lepton faking tau background. The lepton faking taus are
581 dominated by electrons which is studied by the tau working group. The e-veto BDT cut is used to reduce
582 this kind of background as mentioned in the Section 7.4. The corresponding scale factors are applied
583 separately to true electrons and true taus with dedicated uncertainties [56].
- 584 The fake background with one or more taus faked by jets consists of the top fake (with at least one fake
585 tau from jets in the top events), QCD multijet, $W + \text{jets}$ and diboson events.
- 586 In the hadronic channels, the real tau background is mostly from $Z \rightarrow \tau\tau + \text{jets}$ and $t\bar{t}$ as shown in Figure 23
587 where the MC only includes real taus while the excess of data events consists of fakes from both QCD
588 multijet and $t\bar{t}$.
- 589 However, the $t\bar{t}$ is dominant in the leptonic channels as shown in Figure 24 where the MC contains both
590 fake tau and real tau contributions.

Not reviewed, for internal circulation only

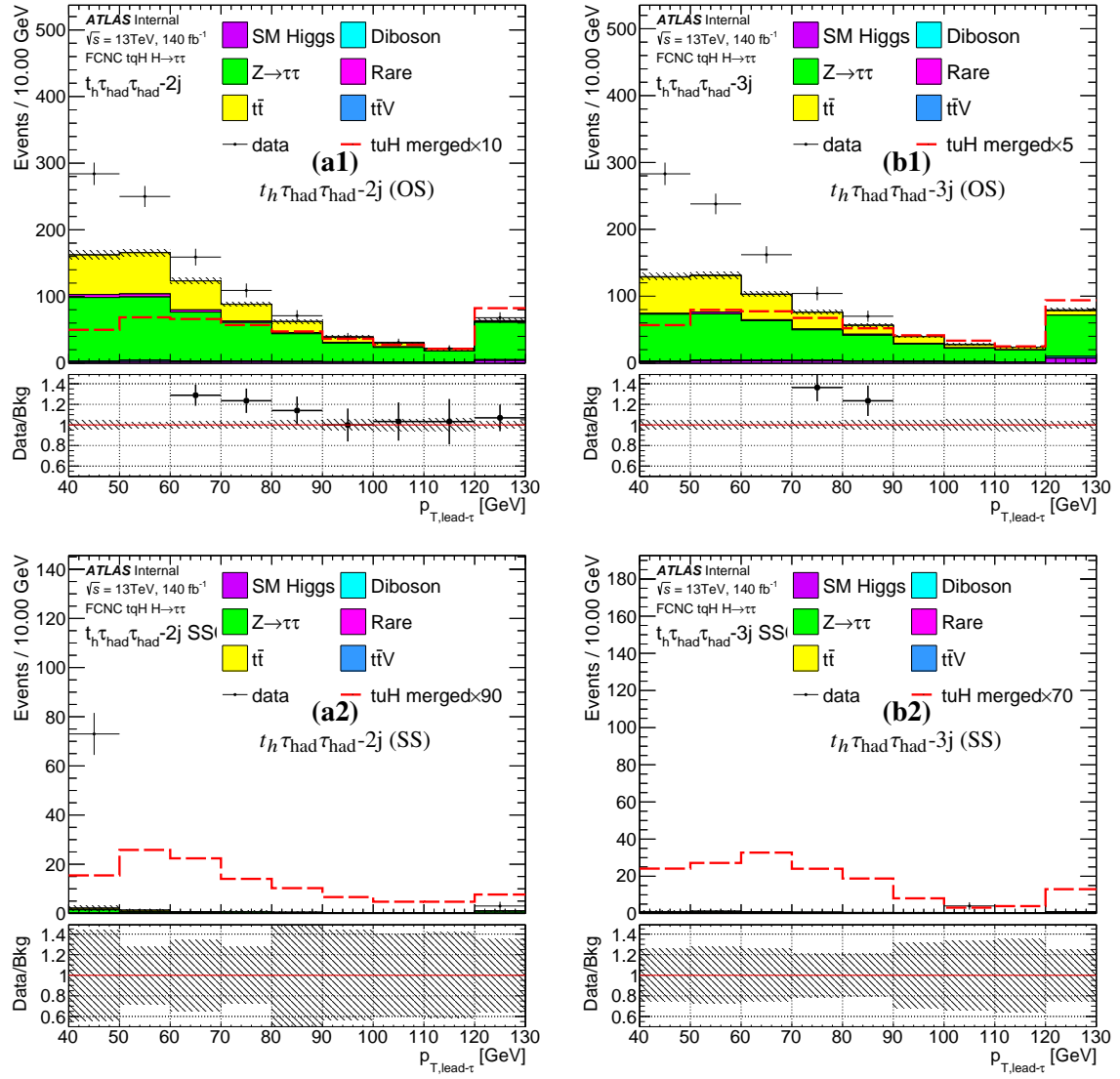


Figure 23: The distributions of leading τ p_T in the $t_h \tau_{had} \tau_{had}-2j$ (a), and $t_h \tau_{had} \tau_{had}-3j$ (b) SR (1) and SS CR (2) before the fake estimation. Data is more than the MC prediction because the fake tau backgrounds are not yet added.

Not reviewed, for internal circulation only

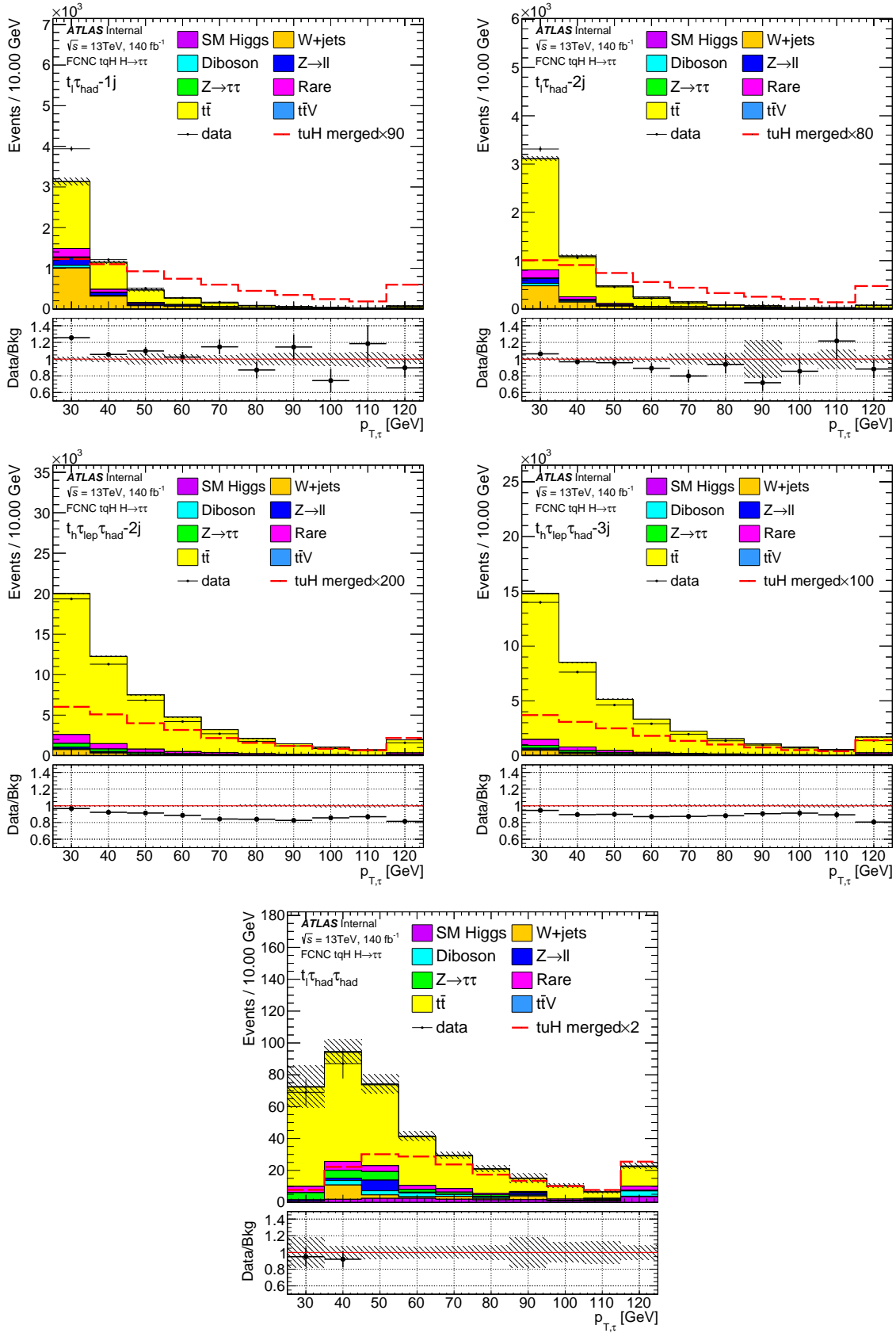


Figure 24: The distributions of τp_T in the signal regions.

591 10.1 Fake tau estimation in leptonic channels

592 Due to the large yield in the leptonic channels, tighter tau selection is applied to reduce disk space
 593 usage, which limits the use of control regions with loosened tau identifications. Instead, the fake taus
 594 background are modelled by the MC events calibrated with Data-Driven (DD) Scale Factors (SF) derived
 595 from dedicated $t\bar{t}$ control regions by comparing MC to data using dilepton and double b-tagged lepton
 596 jets events.

597 The QCD multi-jet background is dominated by the fake taus as well as the fake lepton. These events will
 598 be modelled by ABCD method in the next section.

599 The fake tau from the $t\bar{t}$ events is the largest background in the total fake in the leptonic channels as
 600 shown in Figure 24, which contributes around 70% to 99% in different regions. They in turn can be
 601 used to derive the fake tau SFs from $t\bar{t}$ control regions (CR $t\bar{t}$) using the SM $t\bar{t}$ decay of dilepton events
 602 and semileptonically double-btagged lepton-jets events listed in Table 4, aimed at fake taus from different
 603 origins. Within the top fake events, fake taus can come from different origins, i.e., from jets (heavy/light
 604 flavor quark or gluon initiated) or leptons (electron or muon). The tau fake origins are checked with the
 605 top MC. Dedicated top pair production control regions are defined in the following:

- 606 • W-jet faking tau from the double b-tagged $t\bar{t}$ semileptonically decay: exactly 1 lepton, exactly 1
 607 tau candidate, at least 4 jets with exactly 2 b-tagged. Tau candidate and lepton have the same-sign
 608 (SS) or opposite-sign (OS) charge, separated into $t_l t_h 2b\tau_{had-2jSS}$, $t_l t_h 2b\tau_{had-3jSS}$, $t_l t_h 2b\tau_{had-2jOS}$,
 609 $t_l t_h 2b\tau_{had-3jOS}$.
- 610 • B-jet faking tau from the single b-tagged $t\bar{t}$ dilepton events: 2 leptons with different flavors or same
 611 flavors away from Z pole ($M_{ll} > 100\text{GeV}$ or $M_{ll} < 80\text{GeV}$), exactly 1 tau candidate, exactly 1
 612 b-tagged jet, referred as $t_l t_l 1b\tau_{had}$.
- 613 • Other jets faking tau from the double b-tagged $t\bar{t}$ dilepton events: 2 leptons with different flavors
 614 or same flavors away from Z pole, exactly 1 tau candidate, at least two jets with exactly 2 b-tagged
 615 jets, referred as $t_l t_l 2b\tau_{had}$.

Not reviewed, for internal circulation only

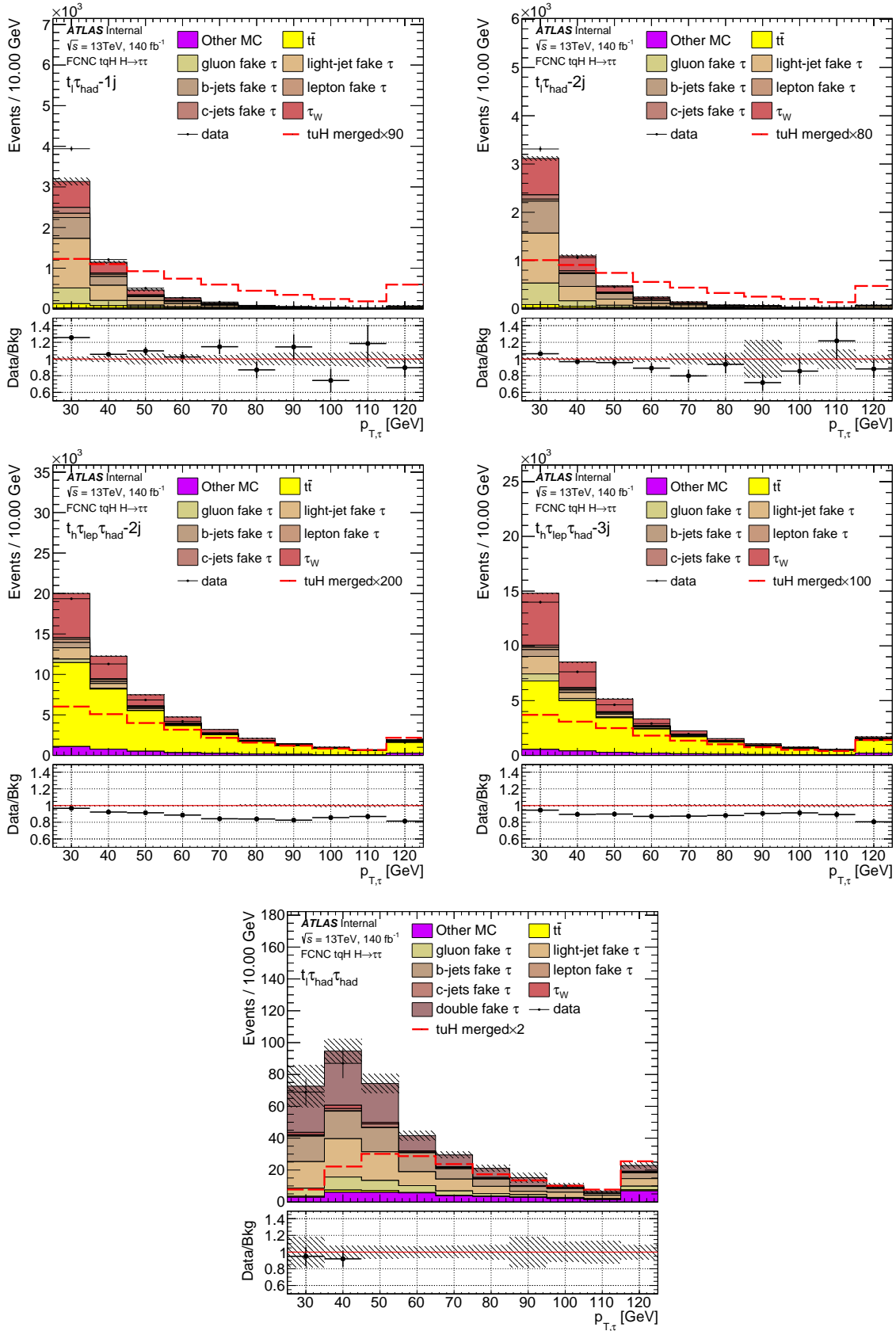


Figure 25: The distributions of τp_T in the signal regions with fake tau origin shown.

As shown in the Figure 25, most of the fake taus come from quark initiated jets, but the flavor distributions in OS are similar to those in SS. The data is generally over-estimated in the OS regions while it is opposite in the SS region. If the fake taus are corrected by the same scale factors, this mismodelling will never get solved. This asymmetry of the SS and OS fake taus can be interpreted by the mis-modelling of the fake tau charges. Since the fake taus mainly come from light-flavored jets as shown in Figure 25, the mis-modelling is related to the charge carried by the original jet that is faking a tau. So the parent of the jet is believed to be charge correlated with the lepton. Considering the main background is $t\bar{t}$ process. The only suspect is the hadronic W boson. In order to find the contribution of w -jet faking taus (τ_W), the truth information is used to match between the w -jet and the fake tau with $\Delta R < 0.4$. As shown in the Figure 25, there is a considerable amount of τ_W 's in both SS and OS regions. There are four kinds of fake taus that need to be calibrated: Type1) τ_W 's with the opposite charge to the lepton; Type2) τ_W 's with the same charge as the lepton; Type 3) the fake taus from b-jets; Type4) the fake taus from other origins (mainly radiations). The following $t\bar{t}$ control regions are used to calibrate these four fake tau types.

These control regions are similar to the signal regions but with an additional b-jet or lepton as defined below. In the control regions with single lepton, $E_T^{\text{miss}} > 20\text{GeV}$ and at least 2 light jets and 2 b-tagged jets are required to ensure that QCD contribution is negligible. The yield of the control regions are listed in Table 6 and 7.

- $t_l t_l 1b \tau_{\text{had}}$: 2 leptons with different flavors or away from Z pole, exactly 1 tau candidate, exactly 1 b-tagged jets.
- $t_l t_l 2b \tau_{\text{had}}$: 2 leptons with different flavors or away from Z pole, exactly 1 tau candidate, exactly 2 b-tagged jets.
- $t_l t_h 2b \tau_{\text{had}}\text{-}2j\text{SS}$: Exactly 1 lepton, exactly 1 tau candidate, exactly 4 jets with exactly 2 b-tagged. Tau candidate and lepton have the same charge.
- $t_l t_h 2b \tau_{\text{had}}\text{-}2j\text{OS}$: Exactly 1 lepton, exactly 1 tau candidate, exactly 4 jets with exactly 2 b-tagged. Tau candidate and lepton have the opposite charge.
- $t_l t_h 2b \tau_{\text{had}}\text{-}3j\text{SS}$: Exactly 1 lepton, exactly 1 tau candidate, at least 5 jets with exactly 2 b-tagged. Tau candidate and lepton have the same charge.
- $t_l t_h 2b \tau_{\text{had}}\text{-}3j\text{OS}$: Exactly 1 lepton, exactly 1 tau candidate, at least 5 jets with exactly 2 b-tagged. Tau candidate and lepton have the opposite charge.

Where di-lepton regions ($t_l t_l 1b \tau_{\text{had}}$ and $t_l t_l 2b \tau_{\text{had}}$) are used to calibrate the Type3 and Type4 fake taus. These regions are dominated by the bjet and the radiation jet faking taus. The regions of $t_l t_h 2b \tau_{\text{had}}\text{-}2j\text{OS}$ and $t_l t_h 2b \tau_{\text{had}}\text{-}3j\text{OS}$ are used to calibrate Type1 fake taus. Compared to the signal region, this region has an additional b-jet. So the $t\bar{t}$ background is enhanced in this region and signal is depleted. Similarly for the Type2, the regions of $t_l t_h 2b \tau_{\text{had}}\text{-}2j\text{SS}$ and $t_l t_h 2b \tau_{\text{had}}\text{-}3j\text{SS}$ are chosen. The components of these

Table 6: The yield in the control regions used to derive fake tau SFs.

	$t_l t_h 2b\tau_{had}-2jOS$	$t_l t_h 2b\tau_{had}-2jSS$	$t_l t_h 2b\tau_{had}-3jOS$
Other MC	644.38 ± 8.42	41.49 ± 0.76	402.12 ± 5.53
$t\bar{t}$	13973.95 ± 43.13	87.85 ± 3.41	7633.30 ± 31.79
<i>gluon fake τ</i>	342.15 ± 7.06	313.82 ± 6.46	406.41 ± 7.36
<i>light – jet fake τ</i>	988.09 ± 11.89	794.60 ± 10.51	986.09 ± 11.57
<i>b – jets fake τ</i>	71.09 ± 3.10	67.54 ± 3.02	61.82 ± 2.87
<i>lepton fake τ</i>	320.87 ± 7.12	23.80 ± 1.79	168.43 ± 4.80
<i>c – jets fake τ</i>	180.21 ± 4.96	66.52 ± 2.95	135.56 ± 4.28
τ_W	5794.20 ± 27.73	675.30 ± 9.46	3700.89 ± 22.00
background	22314.94 ± 54.55	2070.92 ± 16.58	13494.62 ± 41.98
data	20217.00 ± 142.19	1967.00 ± 44.35	12246.00 ± 110.66
$\bar{t}t \rightarrow bWcH$	11.90 ± 0.36	4.84 ± 0.18	11.61 ± 0.36
$cg \rightarrow tH$	0.31 ± 0.02	0.06 ± 0.01	0.19 ± 0.02
tcH merged	12.21 ± 0.36	4.90 ± 0.18	11.81 ± 0.36
$\bar{t}t \rightarrow bWuH$	5.65 ± 0.23	2.27 ± 0.12	6.43 ± 0.26
$ug \rightarrow tH$	1.42 ± 0.09	0.30 ± 0.03	1.00 ± 0.09
tuH merged	7.07 ± 0.25	2.57 ± 0.13	7.43 ± 0.27
	$t_l t_h 2b\tau_{had}-3jSS$	$t_l t_l 1b\tau_{had}$	$t_l t_l 2b\tau_{had}$
Other MC	56.61 ± 0.79	72.48 ± 1.08	36.69 ± 0.40
$t\bar{t}$	57.14 ± 2.75	23.45 ± 1.77	4.57 ± 0.77
<i>gluon fake τ</i>	385.18 ± 7.19	382.80 ± 9.85	214.14 ± 5.76
<i>light – jet fake τ</i>	830.37 ± 10.52	1054.64 ± 26.16	521.64 ± 8.62
<i>b – jets fake τ</i>	61.92 ± 2.89	878.41 ± 11.33	24.39 ± 1.81
<i>lepton fake τ</i>	12.94 ± 1.29	2.42 ± 0.29	0.73 ± 0.17
<i>c – jets fake τ</i>	65.49 ± 2.87	77.78 ± 9.27	28.89 ± 2.00
τ_W	439.33 ± 7.54	40.96 ± 2.24	20.25 ± 1.54
background	1908.99 ± 15.67	2532.95 ± 31.70	851.31 ± 10.86
data	1884.00 ± 43.41	2505.00 ± 50.05	903.00 ± 30.05
$\bar{t}t \rightarrow bWcH$	3.69 ± 0.15	28.39 ± 0.43	2.43 ± 0.12
$cg \rightarrow tH$	0.04 ± 0.01	2.16 ± 0.04	0.07 ± 0.01
tcH merged	3.73 ± 0.15	30.55 ± 0.43	2.50 ± 0.13
$\bar{t}t \rightarrow bWuH$	1.97 ± 0.11	29.56 ± 0.44	0.63 ± 0.07
$ug \rightarrow tH$	0.19 ± 0.03	10.26 ± 0.20	0.17 ± 0.03
tuH merged	2.16 ± 0.12	39.81 ± 0.49	0.80 ± 0.07

Table 7: The yield in the control regions used to derive fake tau SFs.

	$t_l t_h 2b\tau_{had}$ -3jSS	$t_l t_l 1b\tau_{had}$	$t_l t_l 2b\tau_{had}$
SM Higgs	21.58 ± 0.18	23.11 ± 0.63	16.04 ± 0.12
Diboson	1.27 ± 0.08	16.00 ± 0.50	0.92 ± 0.06
$Z \rightarrow \tau\tau$	0.98 ± 0.25	0.32 ± 0.31	0.02 ± 0.02
Rare	8.86 ± 0.57	9.93 ± 0.54	3.52 ± 0.25
$t\bar{t}$	57.14 ± 2.75	23.45 ± 1.77	4.57 ± 0.77
$t\bar{t}V$	23.93 ± 0.44	23.12 ± 0.36	16.20 ± 0.29
<i>gluon fake τ</i>	385.18 ± 7.19	382.80 ± 9.85	214.14 ± 5.76
<i>light-jet fake τ</i>	830.37 ± 10.52	1054.64 ± 26.16	521.64 ± 8.62
<i>b-jets fake τ</i>	61.92 ± 2.89	878.41 ± 11.33	24.39 ± 1.81
<i>lepton fake τ</i>	12.94 ± 1.29	2.42 ± 0.29	0.73 ± 0.17
<i>c-jets fake τ</i>	65.49 ± 2.87	77.78 ± 9.27	28.89 ± 2.00
τ_W	439.33 ± 7.54	40.96 ± 2.24	20.25 ± 1.54
background	1908.99 ± 15.67	2532.95 ± 31.70	851.31 ± 10.86
data	1884.00 ± 43.41	2505.00 ± 50.05	903.00 ± 30.05
$\bar{t}t \rightarrow bWcH$	3.69 ± 0.15	28.39 ± 0.43	2.43 ± 0.12
$cg \rightarrow tH$	0.04 ± 0.01	2.16 ± 0.04	0.07 ± 0.01
tcH merged	3.73 ± 0.15	30.55 ± 0.43	2.50 ± 0.13
$\bar{t}t \rightarrow bWuH$	1.97 ± 0.11	29.56 ± 0.44	0.63 ± 0.07
$ug \rightarrow tH$	0.19 ± 0.03	10.26 ± 0.20	0.17 ± 0.03
tuH merged	2.16 ± 0.12	39.81 ± 0.49	0.80 ± 0.07

regions are shown in Figure 26. A simultaneous fit to data is made to derive the scale factors for the fake taus. There are four parameters needed to be decided (the scale factors for the 4 types). But considering the p_T and number of tracks dependence of the tau reconstruction, the scale factors are derived in 3 p_T slices (25-35, 35-45, 45-)GeV for 1 and 3 prong taus separately. So there are total 24 parameters to be determined. The results are shown in Table 8 and 9. Where the errors are statistical only. The post-fit plots are shown in Figure 27. Then the scale factors are applied to the corresponding signal regions with single b-tagged jet. In $t_l \tau_{had}$ channel, both taus can be fake, so the calibration is applied to each tau separately, following the same procedure as $\tau_{lep} \tau_{had}$ channels using the lepton and fake tau charges, then the scale factors are multiplied together. The nominal value of the scale factors will vary along with other uncertainties from combined preformance (CP) recommendations and theory uncertainties in the final fit.

Not reviewed, for internal circulation only

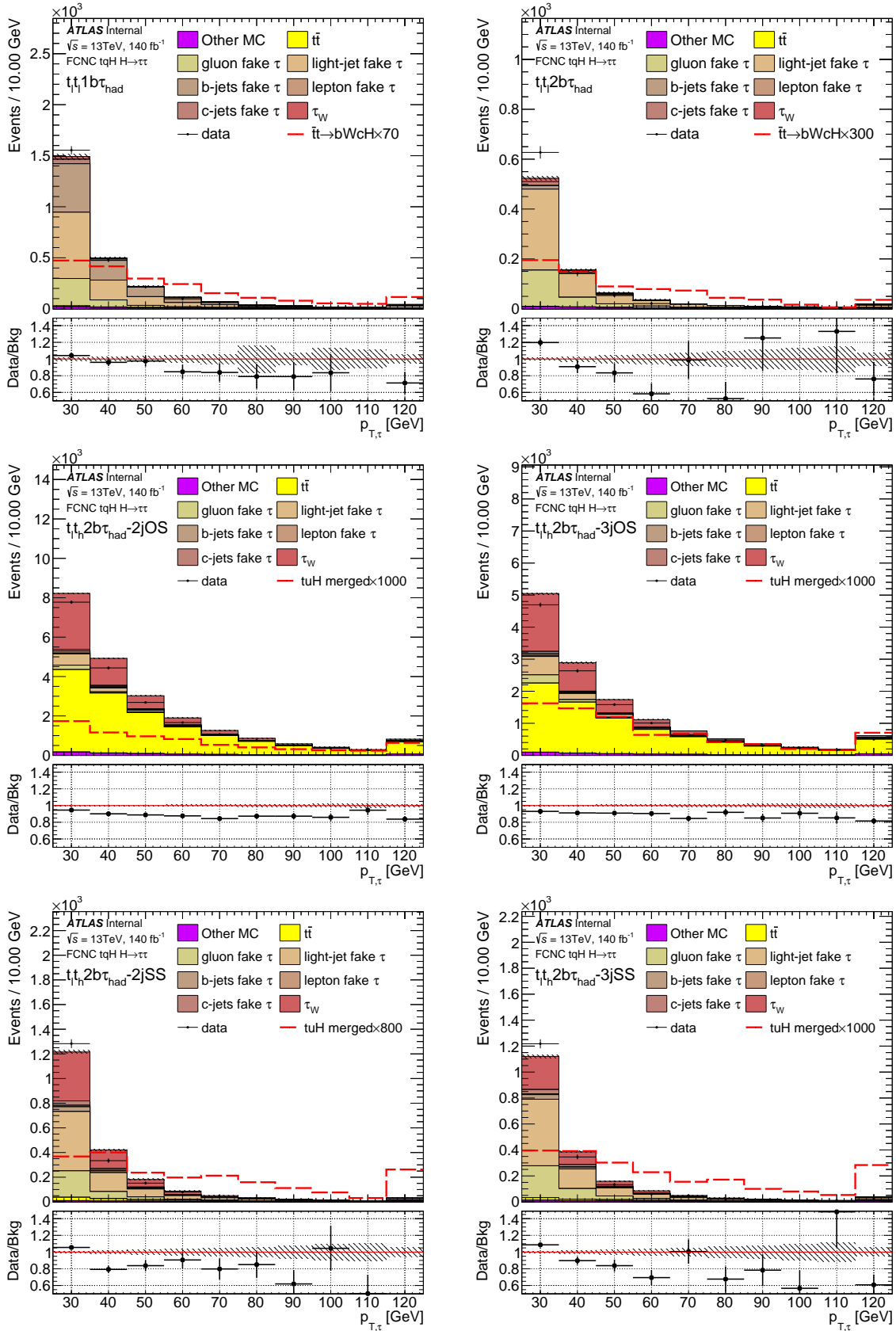


Figure 26: The distributions of τ p_T in the control regions used to calibrate the fake taus.

Not reviewed, for internal circulation only

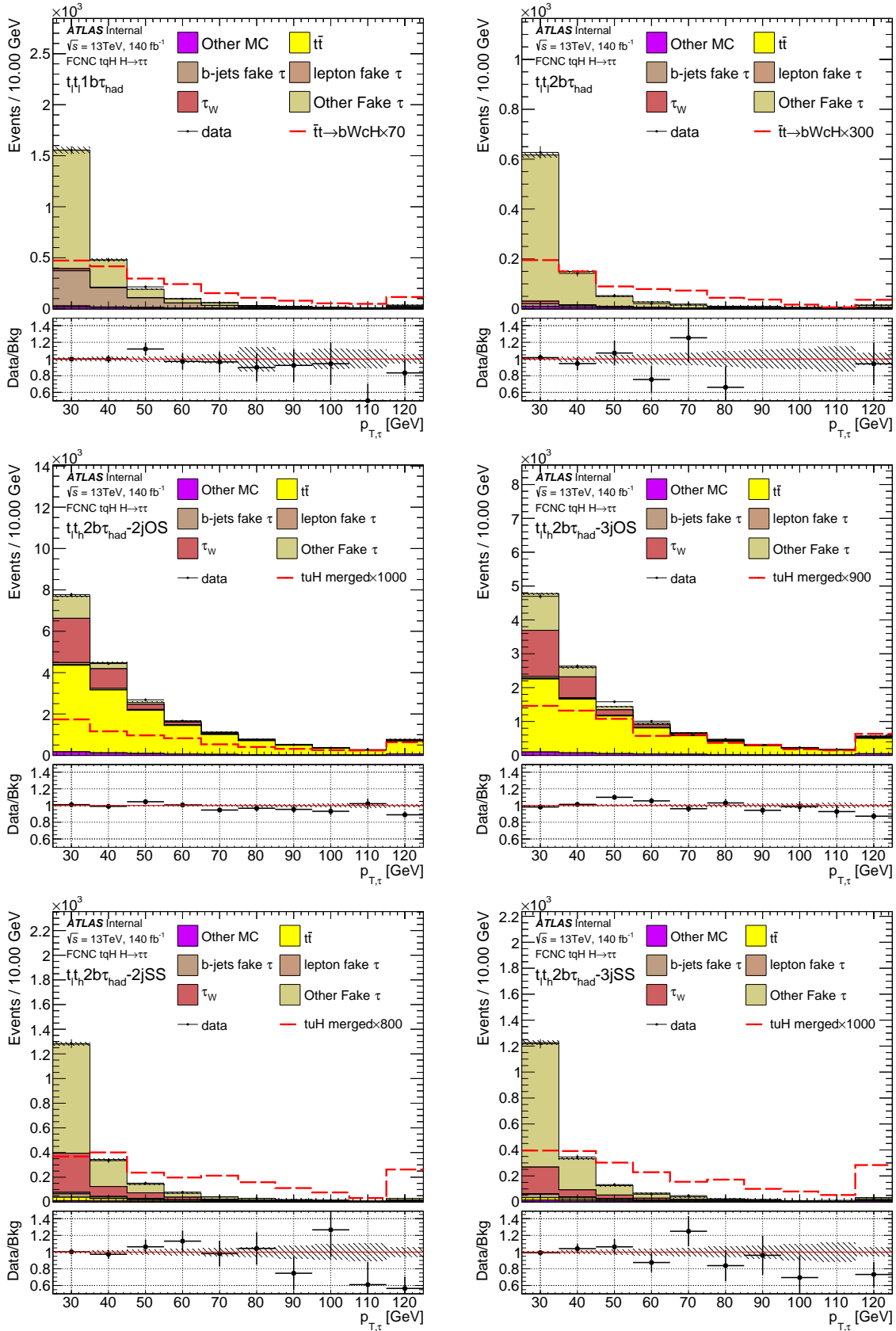


Figure 27: The post-fit distributions of τp_T in the control regions after the fake tau correction.

Table 8: The scale factors for 1 prong fake taus in different p_T bins derived from the fit.

	25 – 35 GeV	35 – 45 GeV	45GeV–
$\tau_{b\ fake}$	0.62 ± 0.10	0.83 ± 0.09	0.94 ± 0.07
τ_{other}	1.20 ± 0.02	1.01 ± 0.04	0.76 ± 0.03
τ_W os	0.71 ± 0.01	0.61 ± 0.02	0.38 ± 0.02
τ_W ss	0.76 ± 0.06	0.37 ± 0.08	0.74 ± 0.08

Table 9: The scale factors for 3 prong fake taus in different p_T bins derived from the fit.

	25 – 35 GeV	35 – 45 GeV	45GeV–
$\tau_{b\ fake}$	1.07 ± 0.13	1.39 ± 0.12	1.25 ± 0.10
τ_{other}	1.28 ± 0.07	0.66 ± 0.08	0.71 ± 0.07
τ_W os	1.01 ± 0.03	1.09 ± 0.04	0.30 ± 0.05
τ_W ss	0.93 ± 0.10	1.05 ± 0.09	0.79 ± 0.09

660 10.2 QCD fake background in $t_h\tau_{lep}\tau_{had}$ and $t_l\tau_{had}$ regions

661 After the fake tau calibration, the fake contribution from QCD with both lepton and tau fakes is estimated
 662 using ABCD method. For each $t_h\tau_{lep}\tau_{had}$ and $t_l\tau_{had}$ signal regions, 3 control regions (ABC) are defined
 663 as follows compared to signal region (D):

- 664 • A: $E_T^{miss} < 20\text{GeV}$, PLIV not tight
- 665 • B: $E_T^{miss} < 20\text{GeV}$, PLIV tight
- 666 • C: $E_T^{miss} > 20\text{GeV}$, PLIV not tight
- 667 • D: $E_T^{miss} > 20\text{GeV}$, PLIV tight (SR)

668 The yields in each A, B, C, D regions are shown in Table 10 - 11.

669 In each signal region, a transfer factor is measured as $r = \frac{N_B}{N_A}$. Where N_A and N_B are the yields calculated
 670 by data-MC where MC includes real lepton background with real taus or calibrated fake taus. The results
 671 are shown in Table 12. The uncertainties in the table for each region contain statistical uncertainties and
 672 the potential signal contamination ($BR = 0.2\%$). In principle for the QCD estimation, the transfer factor
 673 should not depend on the number of jets and charge. So all the measurements in four signal regions are
 674 taken into consideration to derive a universal transfer factor. The central value and statistical uncertainty of
 675 the transfer factor are derived using likelihood method separately for electron and muons. The systematics
 676 variation is taken by calculating the second moment of the four measurements (The power is $1/\sigma^2$). The
 677 combined result is shown as the last line in the table with both statistics and systematics considered, where
 678 the statistical uncertainty for electron and muon are 0.13 and 0.07 respectively, which indicates that the

Table 10: The yields in each A, B, C, D regions.

	$t_l \tau_{\text{had}-1j} \text{ C}$	$t_l \tau_{\text{had}-1j} \text{ A}$	$t_l \tau_{\text{had}-1j} \text{ D}$	$t_l \tau_{\text{had}-1j} \text{ B}$
Other MC	8.71 ± 1.73	2.50 ± 1.45	84.62 ± 6.19	10.57 ± 3.32
$t\bar{t}$	22.35 ± 1.75	1.28 ± 0.41	280.14 ± 6.27	20.26 ± 1.69
$b - \text{jets fake } \tau$	71.10 ± 3.25	6.14 ± 1.20	811.72 ± 10.82	93.22 ± 4.60
$\text{lepton fake } \tau$	6.88 ± 8.37	-1.51 ± 5.38	221.68 ± 16.47	55.99 ± 13.93
τ_W	79.57 ± 2.96	8.40 ± 0.94	839.60 ± 10.20	104.06 ± 3.39
<i>Other Fake τ</i>	419.34 ± 59.88	35.62 ± 11.01	2918.71 ± 106.64	525.13 ± 44.70
QCD Fake lep	/	/	916.84 ± 53.16	/
background	607.95 ± 60.67	52.43 ± 12.44	6073.31 ± 121.52	809.23 ± 47.31
data	1948.00 ± 44.14	721.00 ± 26.85	6353.00 ± 79.71	1221.00 ± 34.94
$\bar{t}t \rightarrow bWcH$	5.28 ± 0.18	0.58 ± 0.06	57.59 ± 0.61	5.54 ± 0.19
$cg \rightarrow tH$	0.19 ± 0.01	0.01 ± 0.00	2.23 ± 0.04	0.21 ± 0.01
tcH merged	5.47 ± 0.18	0.59 ± 0.06	59.82 ± 0.61	5.75 ± 0.19
$\bar{t}t \rightarrow bWuH$	4.72 ± 0.18	0.40 ± 0.05	59.72 ± 0.62	5.17 ± 0.18
$ug \rightarrow tH$	1.03 ± 0.06	0.08 ± 0.02	11.36 ± 0.21	0.95 ± 0.06
tuH merged	5.75 ± 0.19	0.48 ± 0.06	71.08 ± 0.66	6.12 ± 0.19
	$t_h \tau_{\text{lep}} \tau_{\text{had}-2j} \text{ C}$	$t_h \tau_{\text{lep}} \tau_{\text{had}-2j} \text{ A}$	$t_h \tau_{\text{lep}} \tau_{\text{had}-2j} \text{ D}$	$t_h \tau_{\text{lep}} \tau_{\text{had}-2j} \text{ B}$
Other MC	427.27 ± 13.25	60.87 ± 5.60	3616.76 ± 36.46	383.91 ± 16.39
$t\bar{t}$	2753.18 ± 19.34	149.04 ± 4.50	33758.95 ± 68.11	2038.00 ± 16.73
$b - \text{jets fake } \tau$	81.67 ± 3.21	7.55 ± 0.96	1007.05 ± 11.53	113.52 ± 4.10
$\text{lepton fake } \tau$	94.41 ± 7.96	24.42 ± 7.64	1120.54 ± 30.89	229.60 ± 16.12
τ_W	632.71 ± 8.06	56.64 ± 2.60	7256.82 ± 26.72	830.41 ± 9.13
<i>Other Fake τ</i>	342.27 ± 33.23	40.05 ± 9.43	3829.90 ± 80.98	435.80 ± 38.91
QCD Fake lep	/	/	821.77 ± 58.67	/
background	4331.53 ± 42.34	338.56 ± 14.37	51411.79 ± 133.30	4031.24 ± 49.22
data	5542.00 ± 74.44	645.00 ± 25.40	50412.00 ± 224.53	4400.00 ± 66.33
$\bar{t}t \rightarrow bWcH$	13.42 ± 0.37	1.62 ± 0.13	102.58 ± 0.97	12.56 ± 0.36
$cg \rightarrow tH$	0.73 ± 0.03	0.09 ± 0.01	5.66 ± 0.08	0.68 ± 0.03
tcH merged	14.16 ± 0.37	1.71 ± 0.13	108.24 ± 0.98	13.24 ± 0.36
$\bar{t}t \rightarrow bWuH$	13.69 ± 0.36	1.74 ± 0.14	105.62 ± 0.96	12.98 ± 0.35
$ug \rightarrow tH$	5.28 ± 0.17	0.57 ± 0.05	28.60 ± 0.40	3.07 ± 0.13
tuH merged	18.97 ± 0.40	2.31 ± 0.15	134.22 ± 1.04	16.06 ± 0.38

Table 11: The yields in each A, B, C, D regions.

	$t_l \tau_{\text{had}-2j}$ C	$t_l \tau_{\text{had}-2j}$ A	$t_l \tau_{\text{had}-2j}$ D	$t_l \tau_{\text{had}-2j}$ B
Other MC	8.03 ± 0.67	0.34 ± 0.07	83.30 ± 2.55	8.29 ± 1.95
$t\bar{t}$	18.39 ± 1.61	1.51 ± 0.46	178.80 ± 4.97	10.51 ± 1.19
$b - \text{jets fake } \tau$	81.99 ± 3.25	7.55 ± 0.97	1015.84 ± 11.49	111.78 ± 3.82
$\text{lepton fake } \tau$	9.04 ± 1.98	2.84 ± 1.32	87.81 ± 5.45	19.03 ± 3.34
τ_W	85.69 ± 3.20	8.32 ± 0.93	963.47 ± 10.41	109.50 ± 3.41
<i>Other Fake</i> τ	294.73 ± 22.40	42.55 ± 8.72	2625.87 ± 49.02	334.01 ± 20.86
QCD Fake lep	/	/	434.65 ± 27.74	/
background	497.87 ± 23.01	63.11 ± 8.93	5389.74 ± 58.93	593.11 ± 21.86
data	1135.00 ± 33.69	243.00 ± 15.59	5410.00 ± 73.55	740.00 ± 27.20
$\bar{t}t \rightarrow bWcH$	4.61 ± 0.17	0.38 ± 0.05	52.80 ± 0.58	4.90 ± 0.18
$cg \rightarrow tH$	0.12 ± 0.01	0.02 ± 0.00	1.38 ± 0.03	0.11 ± 0.01
tcH merged	4.73 ± 0.17	0.40 ± 0.05	54.19 ± 0.58	5.01 ± 0.18
$\bar{t}t \rightarrow bWuH$	4.84 ± 0.18	0.37 ± 0.05	55.47 ± 0.60	4.98 ± 0.18
$ug \rightarrow tH$	0.63 ± 0.05	0.05 ± 0.01	7.51 ± 0.17	0.63 ± 0.05
tuH merged	5.47 ± 0.18	0.42 ± 0.05	62.98 ± 0.62	5.61 ± 0.19
	$t_h \tau_{\text{lep}} \tau_{\text{had}-3j}$ C	$t_h \tau_{\text{lep}} \tau_{\text{had}-3j}$ A	$t_h \tau_{\text{lep}} \tau_{\text{had}-3j}$ D	$t_h \tau_{\text{lep}} \tau_{\text{had}-3j}$ B
Other MC	266.81 ± 7.02	26.16 ± 2.56	2054.94 ± 17.48	152.66 ± 6.44
$t\bar{t}$	1858.94 ± 15.86	84.80 ± 3.40	21766.04 ± 54.57	1029.13 ± 11.83
$b - \text{jets fake } \tau$	85.05 ± 3.27	6.03 ± 0.86	924.32 ± 10.69	89.95 ± 3.41
$\text{lepton fake } \tau$	61.60 ± 3.18	8.38 ± 1.15	650.24 ± 11.32	84.10 ± 4.49
τ_W	552.26 ± 7.18	45.29 ± 2.02	6236.96 ± 24.82	629.30 ± 7.79
<i>Other Fake</i> τ	490.62 ± 41.82	33.20 ± 2.98	4372.94 ± 32.42	433.96 ± 11.50
QCD Fake lep	/	/	484.10 ± 53.60	/
background	3315.28 ± 46.06	203.87 ± 5.75	36489.54 ± 89.81	2419.10 ± 20.15
data	4025.00 ± 63.44	374.00 ± 19.34	35942.00 ± 189.58	2540.00 ± 50.40
$\bar{t}t \rightarrow bWcH$	20.32 ± 0.48	2.28 ± 0.17	133.14 ± 1.19	15.05 ± 0.41
$cg \rightarrow tH$	0.63 ± 0.03	0.06 ± 0.01	4.47 ± 0.08	0.39 ± 0.02
tcH merged	20.95 ± 0.48	2.35 ± 0.17	137.61 ± 1.19	15.44 ± 0.41
$\bar{t}t \rightarrow bWuH$	21.86 ± 0.48	2.78 ± 0.18	139.67 ± 1.18	16.68 ± 0.42
$ug \rightarrow tH$	4.61 ± 0.17	0.35 ± 0.05	24.78 ± 0.40	1.83 ± 0.10
tuH merged	26.46 ± 0.51	3.13 ± 0.18	164.45 ± 1.25	18.51 ± 0.44

Table 12: The QCD transfer factor derived from different low E_T^{miss} control regions

	Electron	Muon
$t_l \tau_{had-1j}$	0.68 ± 0.17	0.59 ± 0.11
$t_h \tau_{lep} \tau_{had-2j}$	1.57 ± 0.69	1.07 ± 0.32
$t_l \tau_{had-2j}$	1.07 ± 0.52	0.75 ± 0.23
$t_h \tau_{lep} \tau_{had-3j}$	1.15 ± 0.85	0.60 ± 0.37
Combined	0.77 ± 0.27	0.66 ± 0.16

679 systematic uncertainties are comparable with the statistical uncertainties, meaning that there is no big
 680 deviation among the four measurements.

681 Finally the QCD contribution in D is then estimated as rC . The data and background comparison after the
 682 fake tau and fake lepton estimation is shown in Figure 29.

683 A closure test is made for the background estimations in the low BDT region (BDT score < -0.6). The
 684 transfer factor derived in the low BDT region is shown in the Table 14. The leading lepton p_T distribution
 685 in the low BDT is shown in Figure 28. The yields are shown in Table 13. The data are in good agreement
 686 with the background prediction in the $t_l \tau_{had}$ channels where the QCD fake lepton is more important, while
 687 the QCD fake lepton is negligible in the $t_h \tau_{lep} \tau_{had}$ channels. No additional uncertainty is needed for the
 688 QCD fake lepton estimation.

Not reviewed, for internal circulation only

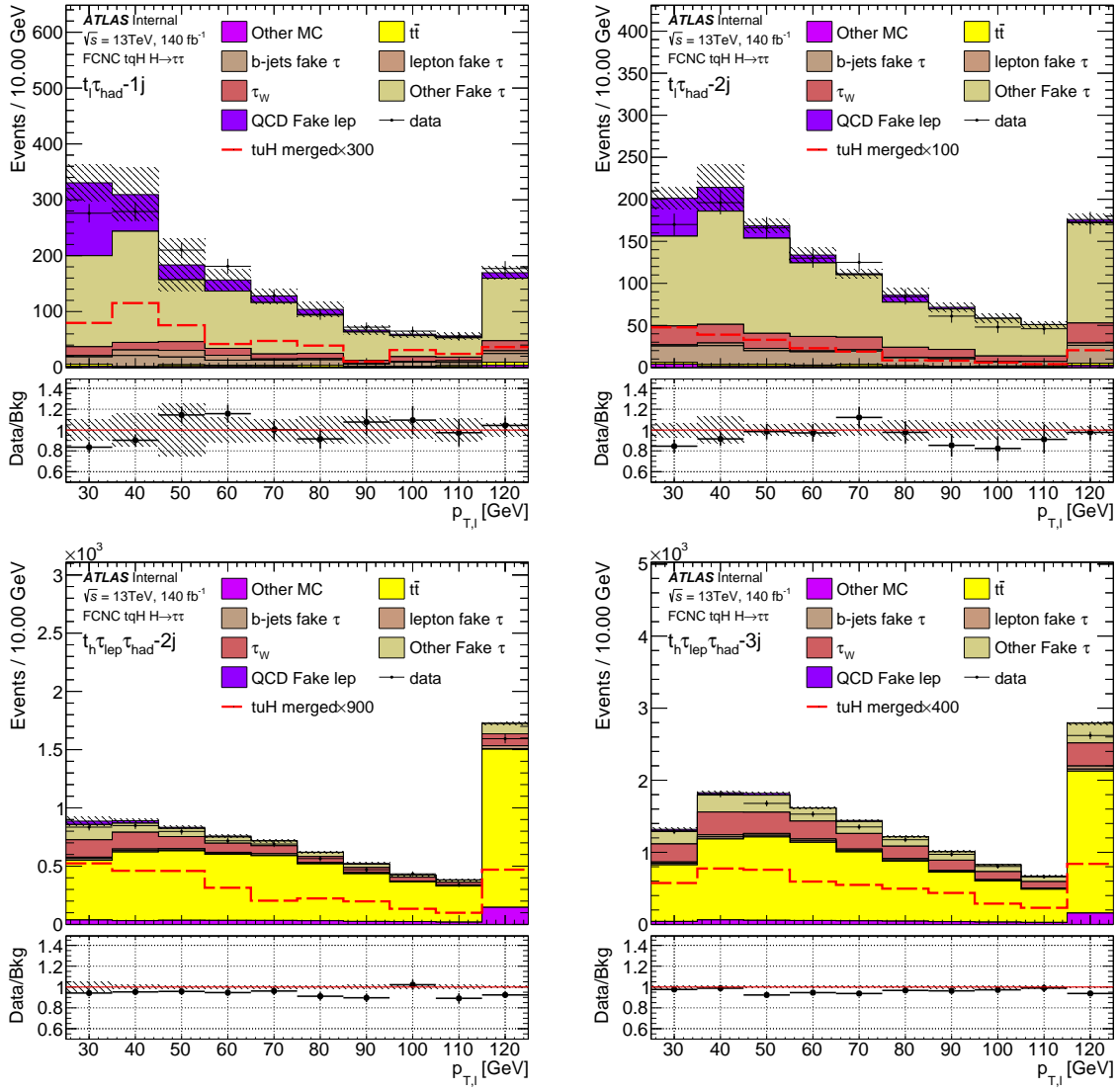


Figure 28: The data-MC comparison of lepton p_T in the low BDT score regions after the fake tau correction and QCD estimation.

Not reviewed, for internal circulation only

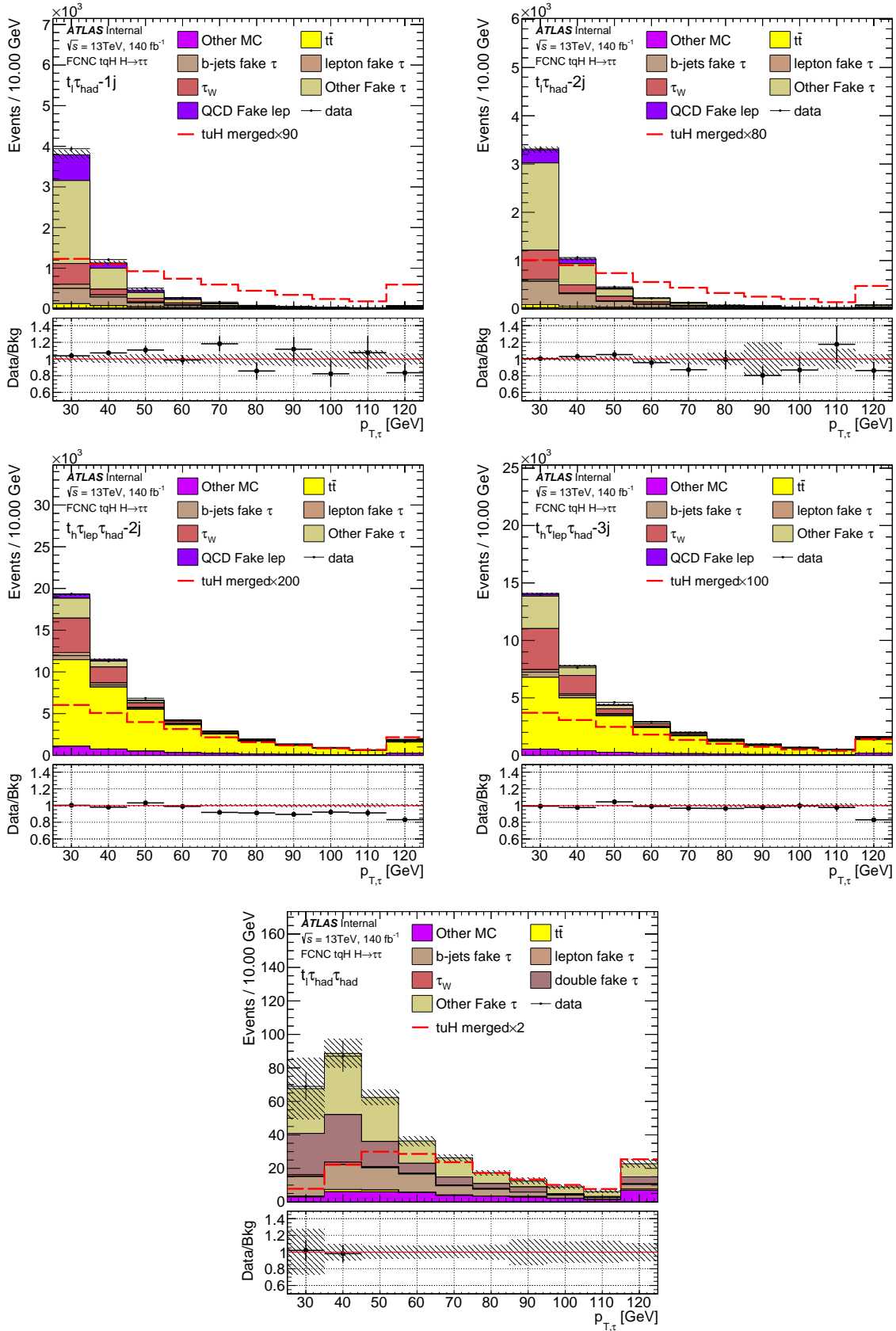


Figure 29: The data-MC comparison of τp_T in the signal regions after the fake tau correction and QCD estimation.

Table 13: The yield in the low BDT region where the QCD faking estimation in the leptonic channels are tested.

	$t_l \tau_{\text{had}-1j}$	$t_h \tau_{\text{lep}} \tau_{\text{had}-2j}$	$t_l \tau_{\text{had}-2j}$	$t_h \tau_{\text{lep}} \tau_{\text{had}-3j}$
Other MC	8.16 ± 5.09	418.47 ± 7.51	12.00 ± 1.93	560.17 ± 7.71
$t\bar{t}$	30.78 ± 2.07	5725.79 ± 28.16	18.13 ± 1.58	9622.23 ± 36.37
$b - \text{jets fake } \tau$	107.77 ± 3.94	53.65 ± 2.54	140.19 ± 4.04	187.88 ± 4.76
$\text{lepton fake } \tau$	47.42 ± 10.39	120.94 ± 4.82	15.76 ± 3.08	212.53 ± 5.53
τ_W	114.84 ± 4.31	796.01 ± 9.05	152.83 ± 4.52	2159.41 ± 14.85
<i>Other Fake</i> τ	970.64 ± 77.05	564.72 ± 42.07	820.95 ± 32.84	1682.29 ± 18.98
QCD Fake lep	283.65 ± 19.42	79.42 ± 17.10	111.21 ± 11.66	109.88 ± 23.17
background	1563.26 ± 80.53	7759.02 ± 54.99	1271.07 ± 35.60	14534.39 ± 50.53
data	1538.00 ± 39.22	7291.00 ± 85.39	1198.00 ± 34.61	13888.00 ± 117.85
$\bar{t}t \rightarrow bWcH$	1.79 ± 0.11	3.14 ± 0.15	1.58 ± 0.11	13.06 ± 0.30
$cg \rightarrow tH$	0.08 ± 0.01	0.09 ± 0.01	0.06 ± 0.01	0.21 ± 0.01
tcH merged	1.87 ± 0.11	3.22 ± 0.15	1.64 ± 0.11	13.27 ± 0.30
$\bar{t}t \rightarrow bWuH$	1.33 ± 0.09	2.84 ± 0.14	1.76 ± 0.11	12.27 ± 0.29
$ug \rightarrow tH$	0.34 ± 0.04	0.59 ± 0.05	0.32 ± 0.03	1.58 ± 0.08
tuH merged	1.67 ± 0.10	3.43 ± 0.15	2.08 ± 0.12	13.85 ± 0.30

Table 14: The QCD transfer factor derived from low BDT regions as closure test.

	Electron	Muon
lowBDT $t_l \tau_{\text{had}-1j}$	0.63 ± 0.20	0.51 ± 0.19
lowBDT $t_h \tau_{\text{lep}} \tau_{\text{had}-2j}$	2.77 ± 1.60	2.08 ± 2.24
lowBDT $t_l \tau_{\text{had}-2j}$	0.87 ± 0.91	0.69 ± 0.47
lowBDT $t_h \tau_{\text{lep}} \tau_{\text{had}-3j}$	3.05 ± 2.06	0.50 ± 0.77
Combined	0.69 ± 0.39	0.54 ± 0.22

689 10.3 Fake tau estimate in hadronic channels

690 In the hadronic channels, the QCD also contributes to the fake tau background which we don't have MC
 691 samples. The τ_{had} p_T spectra in the $\tau_{\text{had}}\tau_{\text{had}}$ SS and OS are shown in Figure 23, where the data have an
 692 excess above the background prediction, which only contains real tau background. A Fake Factor Method
 693 developed by $H \rightarrow \tau\tau$ group [53] is adopted and customized for this analysis. The QCD and part of MC
 694 fake background are estimated together using anti-tau ID control regions defined below. The yield in the
 695 Fake-CR is shown in the Table 15.

- 696 • Fake-CR: 2 opposite charged τ_{had} with leading one passing RNN medium, subleading one failing
 697 RNN medium, other requirements are the same as SR (one for each $t_h \tau_{\text{had}}\tau_{\text{had}-2j}$ and $t_h \tau_{\text{had}}\tau_{\text{had}-3j}$)

Table 15: The yield in the not-medium region.

	$t_h \tau_{\text{had}} \tau_{\text{had-2j}}$	$t_h \tau_{\text{had}} \tau_{\text{had-3j}}$
SM Higgs	3.75 ± 0.20	6.46 ± 0.21
Diboson	1.47 ± 0.26	3.35 ± 0.47
$Z \rightarrow \tau\tau$	121.29 ± 4.03	107.10 ± 3.31
Rare	5.07 ± 0.85	2.24 ± 0.55
$t\bar{t}$	60.32 ± 3.18	59.17 ± 3.12
$t\bar{t}V$	0.19 ± 0.04	1.40 ± 0.13
<i>only $\tau_{\text{sub real}}$</i>	14.77 ± 1.57	23.05 ± 1.99
data	1504.00 ± 38.78	1790.00 ± 42.31
$\bar{t}t \rightarrow bWcH$	7.77 ± 0.32	21.30 ± 0.54
$cg \rightarrow tH$	0.71 ± 0.03	0.94 ± 0.04
tcH merged	8.48 ± 0.32	22.23 ± 0.54
$\bar{t}t \rightarrow bWuH$	6.70 ± 0.30	22.26 ± 0.56
$ug \rightarrow tH$	3.53 ± 0.16	4.89 ± 0.19
tuH merged	10.23 ± 0.34	27.15 ± 0.60

698 SR).

699 Since the sub-leading tau ID is reversed, the Fake-CR contains most of events with fake sub-leading
700 tau. However there are also events with two medium taus in the SR that the leading tau is fake and the
701 sub-leading tau is real. These events can not be modelled by the events in Fake-CR. Fortunately the
702 contribution of these events is minor compared to the other fake background as shown in the Table 3 and
703 Figure 31 defined as “Only $\tau_{\text{sub real}}$ ”. So they can be modelled by MC with the fake tau SFs measured
704 from the CRtt in the leptonic channels.

705 Then the events with fake sub-leading tau can be calculated by rescaling the templates of fake taus in
706 the Fake-CR with proper fake factors. The templates are acquired by subtracting all MC background
707 contributions with real sub-leading taus from data.

708 The Fake-factors (FF) were computed in the W+jets control region (1 lepton + 1 tau, no b-jet) by the
709 $H \rightarrow \tau\tau$ group [53] as listed in Table 18. They are computed in two regions with different tau ID
710 requirement. The FFs are the ratio of the Data–MC_{real tau} yields passing the medium tau ID to which
711 failing the medium tau ID. The FFs are calculated in 12 bins ($2\eta \times 3p_T \times 2N_{\text{track}}$).

712 The uncertainties of this method consists of three parts:

- 713 1. The statistical uncertainties during the FF derivation, one for each bin, 12 in total.
714 2. The FF is rederived in the SS CR (2 taus with the same-sign charge, at least 3 jets with exactly
715 1 b-tagged) to account for any possible difference in the parameterized fake-factors as shown in

716 Figure 30. The fake factors are also presented in Table 19. The difference between the FF derived
717 in the SS CR and W+jet control region is treated as one of the systematics.

718 3. The FF is rederived in the OS CR (2 taus with the opposite-sign charge, at least 3 jets with exactly
719 1 b-tagged) with the events failing the signal cuts defined in Table 31 and 32 to account for the
720 different contribution from each origin of the fake taus as shown in Figure 30. The fake factors are
721 summarized in Table 20. The difference between the FF derived in the OS CR and W+jet control
722 region is treated as another systematics.

723 The yields in SS CR and OS CR regions for passing and failing the medium tau selection are shown
724 in Table 16 and 17.

Table 16: The yield in SS CR and OS CR.

	$t_h \tau_{\text{had}} \tau_{\text{had}}\text{-}2j$ SSCR	$t_h \tau_{\text{had}} \tau_{\text{had}}\text{-}3j$ SSCR
SM Higgs	0.26 ± 0.04	0.80 ± 0.05
Diboson	0.31 ± 0.07	0.38 ± 0.07
$Z \rightarrow \tau\tau$	4.02 ± 1.01	3.29 ± 0.41
Rare	0.15 ± 0.15	0.12 ± 0.12
$t\bar{t}$	1.60 ± 0.49	0.82 ± 0.42
$t\bar{t}V$	0.23 ± 0.04	0.88 ± 0.09
<i>only $\tau_{\text{sub real}}$</i>	11.84 ± 1.51	17.79 ± 1.82
data	182.00 ± 13.49	222.00 ± 14.90
$\bar{t}t \rightarrow bWcH$	1.08 ± 0.10	1.80 ± 0.13
$cg \rightarrow tH$	0.05 ± 0.01	0.05 ± 0.01
tcH merged	1.14 ± 0.10	1.85 ± 0.13
$\bar{t}t \rightarrow bWuH$	0.95 ± 0.09	1.89 ± 0.14
$ug \rightarrow tH$	0.29 ± 0.04	0.32 ± 0.04
tuH merged	1.24 ± 0.10	2.21 ± 0.15
	$t_h \tau_{\text{had}} \tau_{\text{had}}\text{-}2j$	$t_h \tau_{\text{had}} \tau_{\text{had}}\text{-}3j$
SM Higgs	3.04 ± 0.17	7.31 ± 0.19
Diboson	11.59 ± 0.74	16.94 ± 0.80
$Z \rightarrow \tau\tau$	528.42 ± 6.51	515.44 ± 5.89
Rare	34.90 ± 2.27	31.19 ± 2.10
$t\bar{t}$	357.25 ± 7.79	405.41 ± 8.26
$t\bar{t}V$	1.65 ± 0.12	13.07 ± 0.38
<i>only $\tau_{\text{sub real}}$</i>	71.54 ± 3.75	110.02 ± 4.21
data	1304.00 ± 36.11	1454.00 ± 38.13
$\bar{t}t \rightarrow bWcH$	5.51 ± 0.24	14.76 ± 0.42
$cg \rightarrow tH$	0.60 ± 0.03	0.81 ± 0.03
tcH merged	6.11 ± 0.24	15.57 ± 0.42
$\bar{t}t \rightarrow bWuH$	6.11 ± 0.26	14.59 ± 0.42
$ug \rightarrow tH$	3.87 ± 0.15	4.98 ± 0.19
tuH merged	9.97 ± 0.30	19.57 ± 0.46

Table 17: The yield in the not-medium SS CR and OS CR.

	$t_h \tau_{\text{had}} \tau_{\text{had}-2j}$ SSCR	$t_h \tau_{\text{had}} \tau_{\text{had}-3j}$ SSCR
SM Higgs	0.13 ± 0.03	0.29 ± 0.04
Diboson	0.04 ± 0.05	0.10 ± 0.02
$Z \rightarrow \tau\tau$	1.40 ± 0.34	2.19 ± 0.34
$t\bar{t}$	0.63 ± 0.32	0.94 ± 0.43
$t\bar{t}V$	0.02 ± 0.02	0.29 ± 0.05
<i>only $\tau_{\text{sub real}}$</i>	2.52 ± 0.66	4.86 ± 0.88
Rare	/	0.00 ± 0.00
data	943.00 ± 30.71	1126.00 ± 33.56
$\bar{t}t \rightarrow bWcH$	0.21 ± 0.04	0.66 ± 0.08
$cg \rightarrow tH$	0.02 ± 0.01	0.02 ± 0.00
tcH merged	0.23 ± 0.04	0.68 ± 0.08
$\bar{t}t \rightarrow bWuH$	0.40 ± 0.06	0.69 ± 0.09
$ug \rightarrow tH$	0.18 ± 0.03	0.18 ± 0.03
tuH merged	0.58 ± 0.07	0.87 ± 0.09
	$t_h \tau_{\text{had}} \tau_{\text{had}-2j}$ OSCR	$t_h \tau_{\text{had}} \tau_{\text{had}-3j}$ OSCR
SM Higgs	0.51 ± 0.06	1.72 ± 0.09
Diboson	1.96 ± 0.29	3.23 ± 0.36
$Z \rightarrow \tau\tau$	104.35 ± 2.85	110.88 ± 2.69
Rare	11.23 ± 1.27	7.61 ± 1.03
$t\bar{t}$	90.67 ± 3.93	119.44 ± 4.51
$t\bar{t}V$	0.45 ± 0.06	3.10 ± 0.18
<i>only $\tau_{\text{sub real}}$</i>	18.77 ± 1.74	33.39 ± 2.35
data	2231.00 ± 47.23	2480.00 ± 49.80
$\bar{t}t \rightarrow bWcH$	1.45 ± 0.12	3.28 ± 0.20
$cg \rightarrow tH$	0.11 ± 0.01	0.18 ± 0.02
tcH merged	1.56 ± 0.12	3.46 ± 0.20
$\bar{t}t \rightarrow bWuH$	1.40 ± 0.12	3.62 ± 0.21
$ug \rightarrow tH$	0.73 ± 0.06	1.02 ± 0.08
tuH merged	2.13 ± 0.14	4.63 ± 0.23

Not reviewed, for internal circulation only

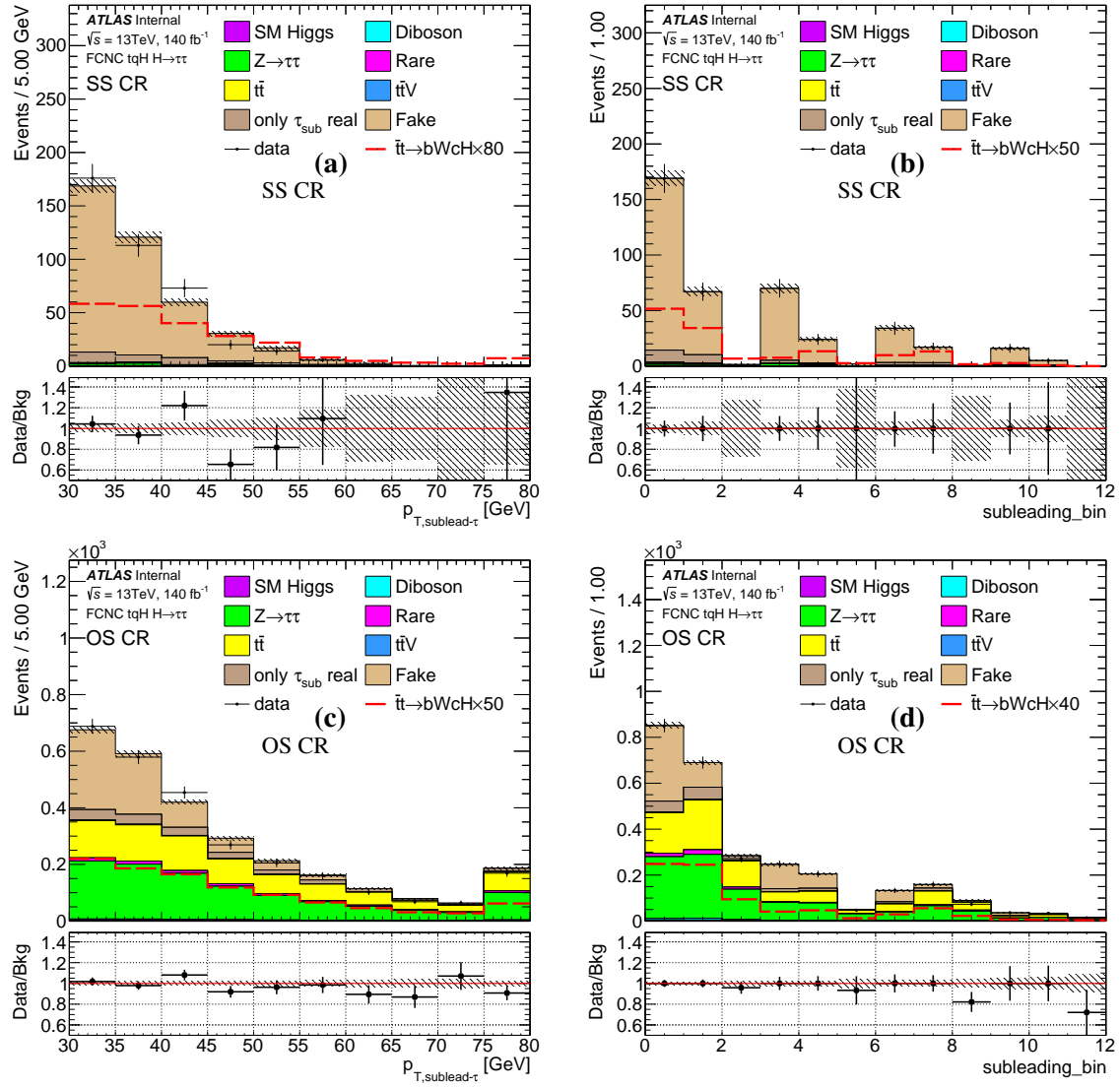


Figure 30: The distributions of sub-leading τ p_T and sub-leading tau index (bin 1-6 are for 1 prong, 7-12 are for 3 prong; bin 1-3, 7-9 are for $|\eta| < 1.37$ with 3 p_T slices and the rest are for $|\eta| > 1.52$) in the SS CR and OS CR. The fake estimation of the index is perfect by definition but in some high p_T bins MC is higher than data where the estimation is treated as 0.

725 Due to the low statistics in the high p_T region, some fake factors are negative in SS CR or OS CR. Those
 726 FFs are reset to zero.

727 The tau p_T distributions after fake estimation are shown in Figure 31 using three FFs derived for nominal
 728 and two systematics samples (SS CR and OS CR). The small difference indicates that the three sets of FFs
 729 are consistent with each other.

Not reviewed, for internal circulation only

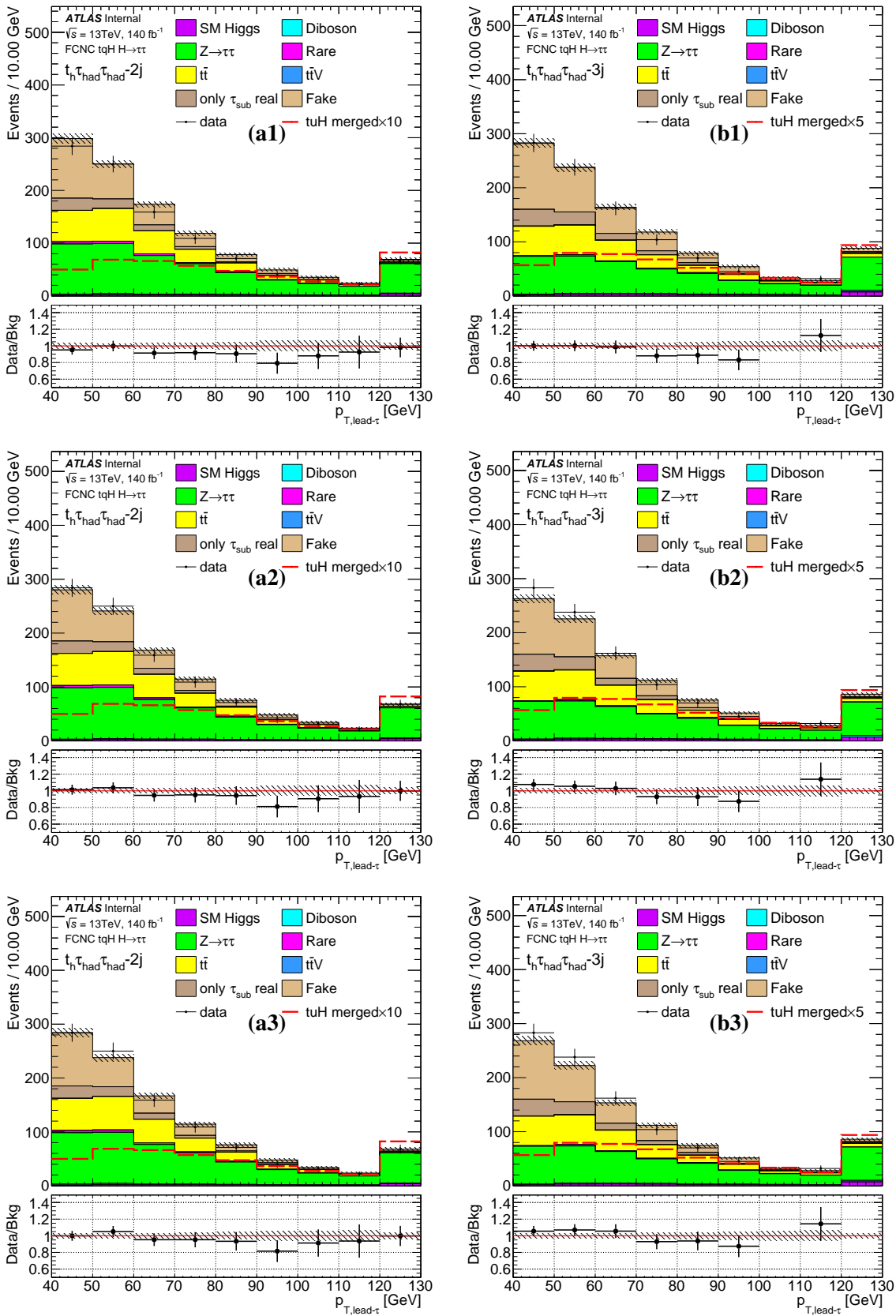


Figure 31: The distributions of τ p_T in the $t_h \tau_{\text{had}} \tau_{\text{had}}-2j$ (SS)(a1-3), $t_h \tau_{\text{had}} \tau_{\text{had}}-3j$ (OS) (b1-3), using the nominal (1), SS CR derived (2), OS CR derived FFs.

Not reviewed, for internal circulation only

Table 18: FF derived by the $H \rightarrow \tau\tau$ group. The errors in the tables are treated as systematics.

		30 – 40 GeV	40 – 60 GeV	60 GeV-
1p	$ \eta \leq 1.37$	0.297 ± 0.020	0.258 ± 0.021	0.192 ± 0.027
	$ \eta \geq 1.52$	0.242 ± 0.021	0.166 ± 0.023	0.131 ± 0.030
3p	$ \eta \leq 1.37$	0.131 ± 0.018	0.104 ± 0.017	0.158 ± 0.032
	$ \eta \geq 1.52$	0.074 ± 0.023	0.086 ± 0.020	0.057 ± 0.030

Table 19: FF derived in SS CR. The difference between median value and those in 18 is treated as one of the systematics.

		30 – 40 GeV	40 – 60 GeV	60 GeV-
1p	$ \eta \leq 1.37$	0.24 ± 0.02	0.24 ± 0.04	-0.10 ± 0.04
	$ \eta \geq 1.52$	0.19 ± 0.03	0.14 ± 0.04	0.30 ± 0.28
3p	$ \eta \leq 1.37$	0.11 ± 0.02	0.10 ± 0.03	-0.07 ± 0.04
	$ \eta \geq 1.52$	0.10 ± 0.03	0.05 ± 0.03	-0.01 ± 0.01

Table 20: FF derived in OS CR. The difference between median value and those in 18 is treated as one of the systematics.

		30 – 40 GeV	40 – 60 GeV	60 GeV-
1p	$ \eta \leq 1.37$	0.30 ± 0.03	0.16 ± 0.04	-0.09 ± 0.14
	$ \eta \geq 1.52$	0.19 ± 0.03	0.17 ± 0.04	-0.05 ± 0.12
3p	$ \eta \leq 1.37$	0.11 ± 0.03	0.04 ± 0.03	-0.20 ± 0.12
	$ \eta \geq 1.52$	0.05 ± 0.03	0.02 ± 0.03	-0.19 ± 0.16

730 11 MVA analysis

731 In this section, we investigate the sensitivity of probing signal using one of the Multi-Variate Analysis
 732 (MVA) methods, the Gradient Boosted Decision Trees (BDT) method [60, 61], with the TMVA software
 733 package. The BDT output score is in the range between -1 and 1. The most signal-like events have scores
 734 near 1 while the most background-like events have scores near -1.

735 The signal topology and kinematics are different across all the channels. To maximize the overall
 736 sensitivity, separated BDTG trainings are applied to each signal region. A number of variables as the
 737 BDT inputs are used to train and test events in each signal region for maximal signal acceptance and
 738 background rejection. They are listed in Table 21 and Table 22.

739 The signal and background samples are randomly divided into two equal parts (denoted as even and odd
 740 parity events). The BDT is trained with one part, and tested on the other part. It is always ensured that
 741 the BDT derived from the training events is not applied to the same events, but only to the independent
 742 test ones. The sum of MC all background processes, corrected normalized, are used in the training and
 743 testing. With the `IgnoreNegWeightsInTraining` option, only MC events with positive MC weights are
 744 used in the training. In The hadronic channels, due to the fake is modelled by the not-medium tau control
 745 region, the data events in the not-medium tau control region is also used in the training with a weight of
 746 0.3 to take the FFs into account. The comparison of BDT performances in test-odd and test-even samples
 747 is given in Figure 35-37.

748 The BDT parameters `NTrees` and `nCuts` are tuned based on the integration of the ROC's. The best choice
 749 for each channel depends on the number of variables used and the statistics. The optimisation factor is
 750 defined as $L = S_{\text{avg}} - xS_{\text{diff}}$, where S_{avg} is the average integration value of the two folds, indicating the
 751 separation power of the model, meaning the larger it is, the better. S_{diff} is the difference between the
 752 integration values of the two folds, indicating the instability of the models, meaning the smaller it is, the
 753 better. The factor x is chosen depending on how important the stability is regarded over the separation
 754 power, where there is no common standard. In this analysis $x = 1$ is chosen.

755 The optimisation process uses a gradient method with a step of 5 for `nCuts` and 10 for `NTrees`. The
 756 optimisation stops when the maximum value of the optimisation factor L is found. The steps taken is
 757 listed in the App. C. The final result is shown in Table 23.

Table 21: The importance (in %) of each variables used in the BDTG training for leptonic channels, the two numbers in the each block are from the two training folds.

	$t_l \tau_{\text{had}-1j}$	$t_h \tau_{\text{lep}} \tau_{\text{had}-2j}$	$t_l \tau_{\text{had}-2j}$	$t_h \tau_{\text{lep}} \tau_{\text{had}-3j}$	$t_l \tau_{\text{had}} \tau_{\text{had}}$
$p_{T,\tau}$	20.96 / 19.55	6.51 / 6.35	6.93 / 7.00	5.09 / 5.32	6.33 / 7.21
E_{miss}^T	9.82 / 9.95	9.22 / 8.50	7.03 / 7.42	9.64 / 9.08	6.86 / 5.54
$m_{\tau\tau,vis}$	7.17 / 6.31	8.55 / 8.67	4.70 / 5.65	8.84 / 8.63	13.21 / 13.13
$\Delta R(\tau, \text{light jet}, \text{min})$	13.64 / 14.27	6.52 / 5.83	6.48 / 6.10	4.51 / 4.38	7.22 / 8.84
$\Delta R(l, b \text{ jet})$	18.28 / 17.76	5.82 / 4.19	8.14 / 6.32	2.94 / 2.94	6.52 / 6.51
$\Delta R(l, \tau)$	10.69 / 11.76	8.09 / 9.29	6.78 / 6.97	7.90 / 7.58	4.17 / 4.21
$\Delta R(\tau, b \text{ jet})$	10.88 / 11.27	5.90 / 5.18	6.59 / 6.34	3.40 / 3.38	4.70 / 3.04
$p_{T,l}$	8.55 / 9.12	1.96 / 1.86	4.33 / 3.94	3.75 / 3.60	1.75 / 1.26
$\Delta\phi(\tau\tau, P_{miss}^T)$	/	4.55 / 5.88	8.26 / 8.09	5.56 / 5.95	/
$E_{miss}^T \text{ centrality}$	/	5.88 / 5.70	4.84 / 5.48	4.59 / 4.77	/
$m_{\tau,\tau}$	/	11.23 / 11.63	10.31 / 9.17	5.87 / 6.22	/
$E_{vis\ \tau,1}/E_{\tau,1}$	/	9.20 / 10.05	9.12 / 9.78	7.76 / 7.69	/
$E_{vis\ \tau,2}/E_{\tau,2}$	/	8.06 / 8.49	6.85 / 8.28	7.29 / 6.78	/
$m_{t,SM}$	/	4.93 / 5.33	4.62 / 4.28	4.60 / 4.45	/
$M(\text{light jet}, \text{light jet}, \text{min})$	/	3.58 / 3.04	5.02 / 5.20	3.07 / 3.90	/
m_W	/	/	/	3.08 / 3.26	/
χ^2	/	/	/	12.12 / 12.09	/
$\Delta R(\tau, \tau)$	/	/	/	/	8.43 / 8.52
$m_{t,SM,vis}$	/	/	/	/	8.81 / 7.64
$M(\tau \text{ light jet}, \text{min})$	/	/	/	/	2.99 / 3.02
$\eta_{\tau,max}$	/	/	/	/	6.93 / 6.37
m_W^T	/	/	/	/	3.45 / 7.20
$\Delta R(l + b \text{ jet}, \tau\tau)$	/	/	/	/	5.75 / 7.79
$P_{t,\tau\tau,vis}$	/	/	/	/	6.12 / 4.47
$m_{t,FCNC,vis}$	/	/	/	/	6.74 / 5.27

Table 22: The importance (in %) of each variables used in the BDTG training for hadronic channels, the two numbers in the each block are from the two training folds.

Not reviewed, for internal circulation only

	$t_h \tau_{had} \tau_{had-2j}$	$t_h \tau_{had} \tau_{had-3j}$
$p_{T,\tau}$	6.69 / 6.31	4.49 / 5.29
E_{miss}^T	8.69 / 8.13	7.02 / 6.72
$m_{\tau\tau,vis}$	12.43 / 11.58	8.29 / 7.84
$\Delta R(\tau, light\ jet, min)$	8.59 / 7.34	7.42 / 8.02
$\Delta R(\tau, \tau)$	10.45 / 9.89	8.81 / 9.24
$m_{t,FCNC}$	7.45 / 7.06	8.12 / 7.48
E_{miss}^T centrality	7.22 / 9.56	7.60 / 6.93
$m_{\tau,\tau}$	13.22 / 12.41	11.53 / 11.82
$E_{\nu,2}/E_{\tau,2}$	7.47 / 6.86	6.47 / 6.66
$m_{t,SM}$	10.54 / 11.20	8.56 / 9.14
m_W	7.25 / 9.66	7.52 / 8.23
$\Delta\phi(\tau\tau, P_{miss}^T)$	/	7.47 / 6.67
$E_{\nu,1}/E_{\tau,1}$	/	6.70 / 5.97

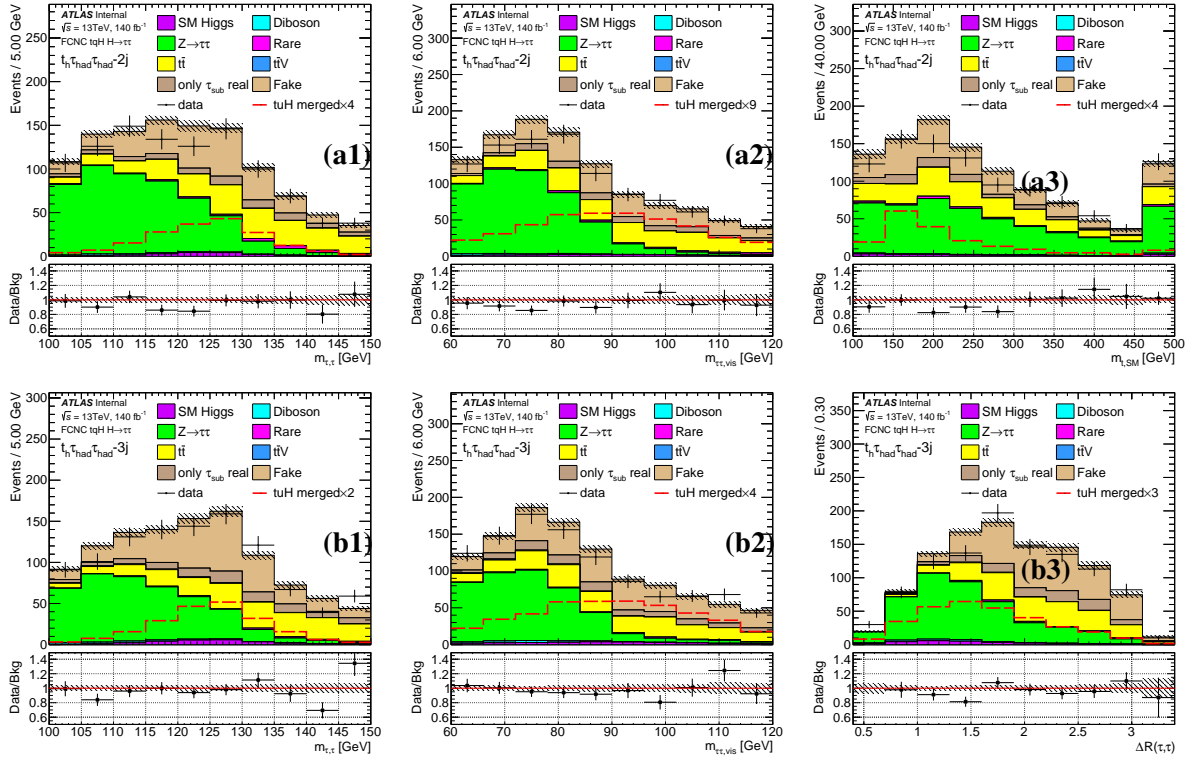


Figure 32: The BDT input distributions for the background and merged signal in the $t_h \tau_{had} \tau_{had-2j}$ (a1-3), $t_h \tau_{had} \tau_{had-3j}$ (b1-3)

Not reviewed, for internal circulation only

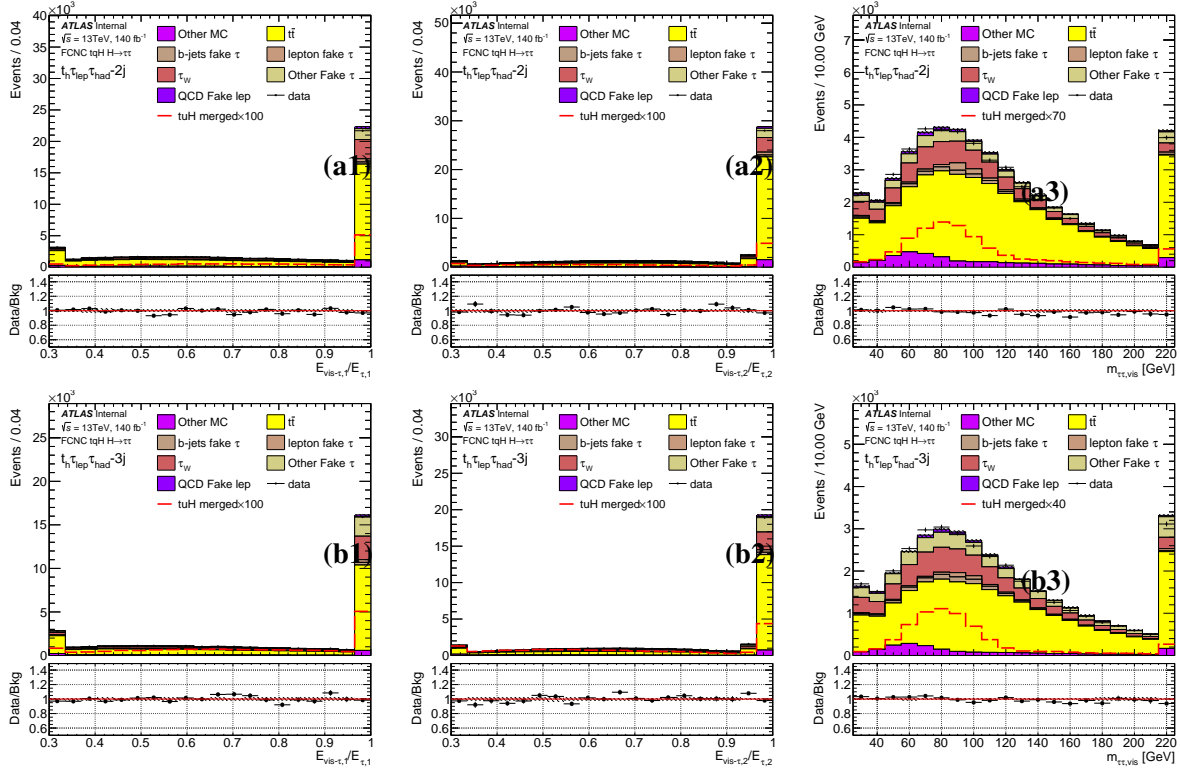


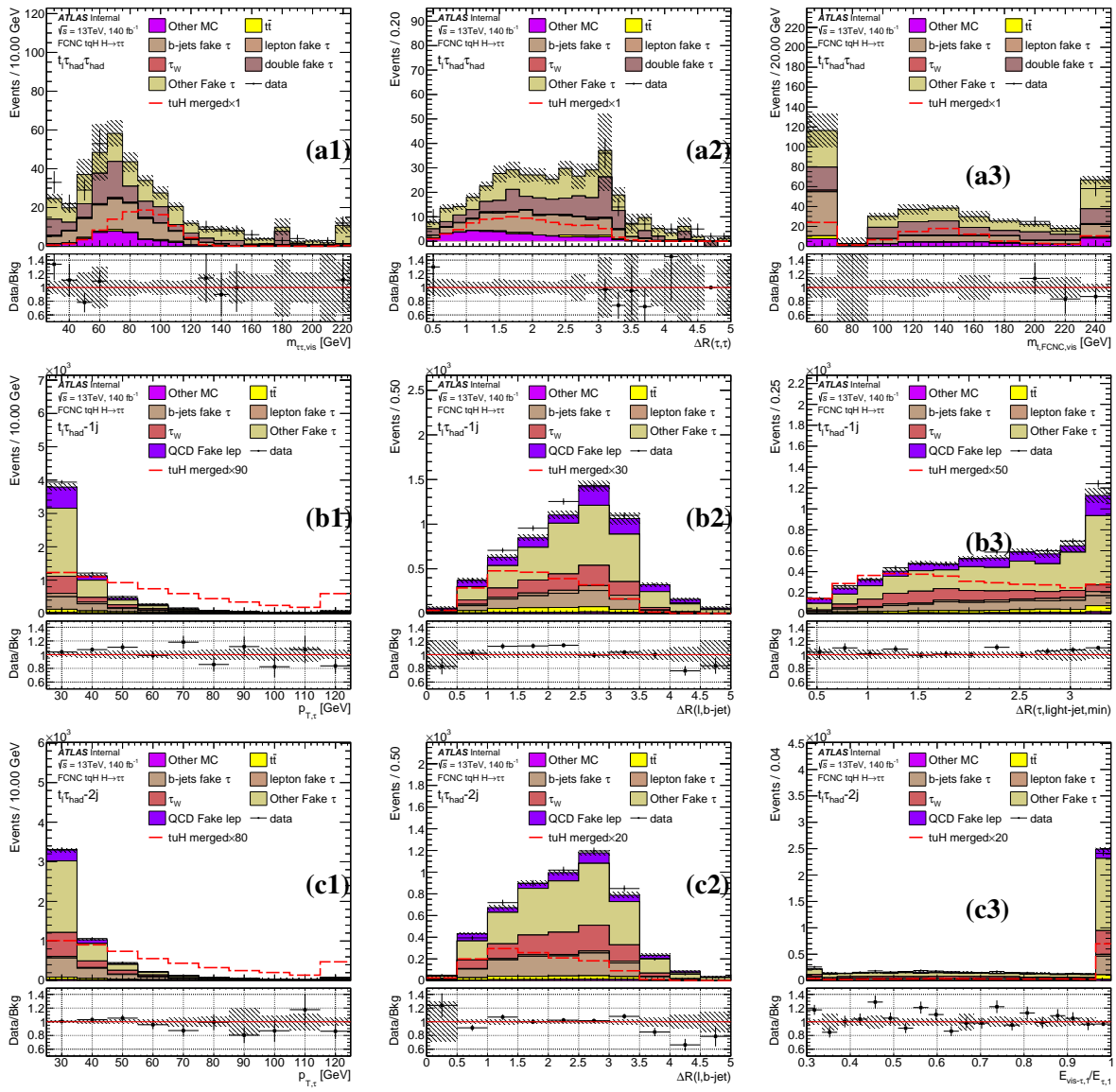
Figure 33: The BDT input distributions for the background and merged signal in the $t_h \tau_{\text{lep}} \tau_{\text{had-2j}}$ (a1-3), $t_h \tau_{\text{lep}} \tau_{\text{had-3j}}$ (b1-3).

Not reviewed, for internal circulation only

Table 23: The chosen nCuts and NTrees value for each channel.

	NCuts	NTrees
$t_h \tau_{\text{had}} \tau_{\text{had}} - 2j$	25.00	190.00
$t_h \tau_{\text{had}} \tau_{\text{had}} - 3j$	25.00	330.00

	NCuts	NTrees
$t_l \tau_{\text{had}} - 1j$	15.00	90.00
$t_h \tau_{\text{lep}} \tau_{\text{had}} - 2j$	20.00	380.00
$t_l \tau_{\text{had}} - 2j$	40.00	500.00
$t_h \tau_{\text{lep}} \tau_{\text{had}} - 3j$	55.00	460.00
$t_l \tau_{\text{had}} \tau_{\text{had}}$	10.00	100.00

Figure 34: The BDT input distributions for the background and merged signal in the $t_l \tau_{\text{had}} \tau_{\text{had}}$ (a1-3), $t_l \tau_{\text{had}} - 1j$ (b1-3), $t_l \tau_{\text{had}} \tau_{\text{had}} - 2j$ (c1-3) channels.

- 758 The importance factors¹ of different variables used in the training is listed in Table 21 and 22. The two
 759 numbers in each block represent the importance factor of the two models trained from even and odd parts.
 760 The consistency of these factors implies that the training models are stable. The variables with importance
 761 less than 1% are dropped from the training.
- 762 As a cross check, the comparisons between BDT distributions in testing samples, as well as the test even
 763 and test odd ROC curves, are shown in Figure 35 and 36.

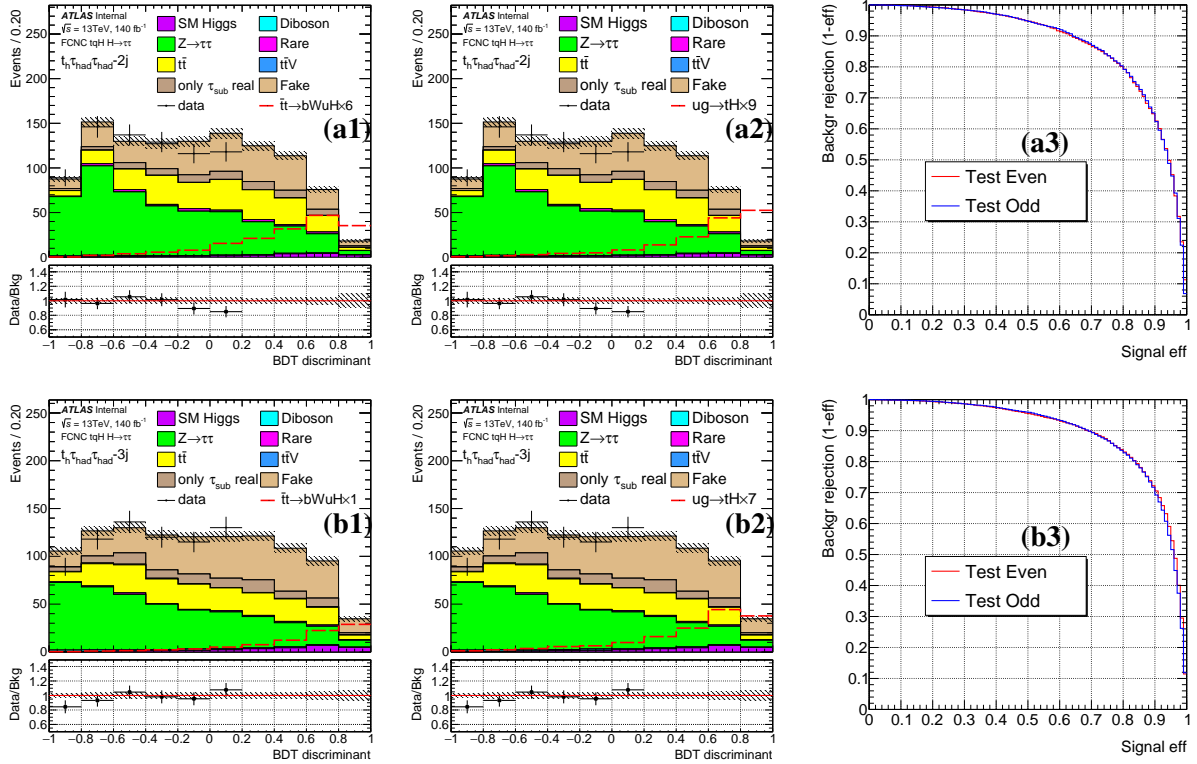


Figure 35: The BDT output distributions for the background and TT signal (a1, b1), background and ST signal (a2, b2) and ROC curves (a3, b3) in the $t_h \tau_{had} \tau_{had} - 2j$ (a1-3), $t_h \tau_{had} \tau_{had} - 3j$ (b1-3).

¹ The importance is evaluated as the total separation gain that this variable had in the decision trees (weighted by the number of events). It is normalized to all variables together, which have an importance of 1.

Not reviewed, for internal circulation only

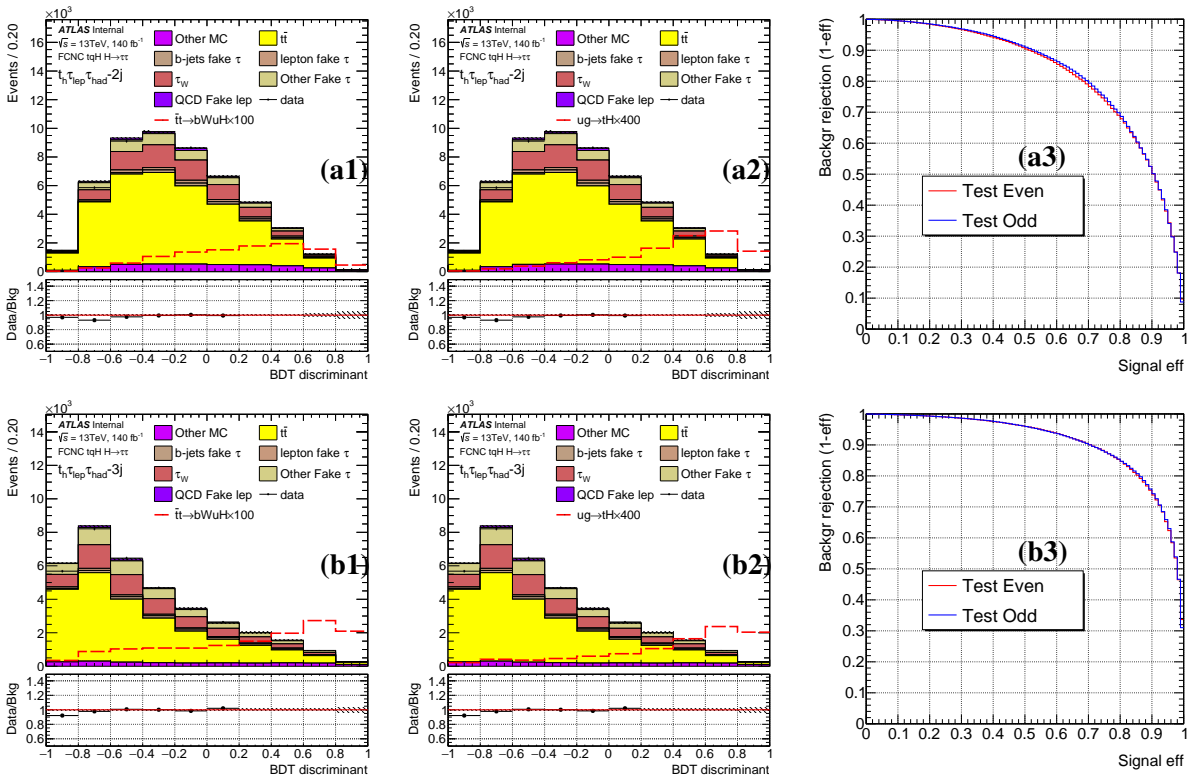


Figure 36: The BDT output distributions for the background and $t\bar{t}$ signal (a1, b1), background and ST signal (a2, b2) and ROC curves (a3, b3) in the $t_h \tau_{\text{lep}} \tau_{\text{had}} - 2j$ (a1-3), $t_h \tau_{\text{lep}} \tau_{\text{had}} - 3j$ (b1-3).

Not reviewed, for internal circulation only

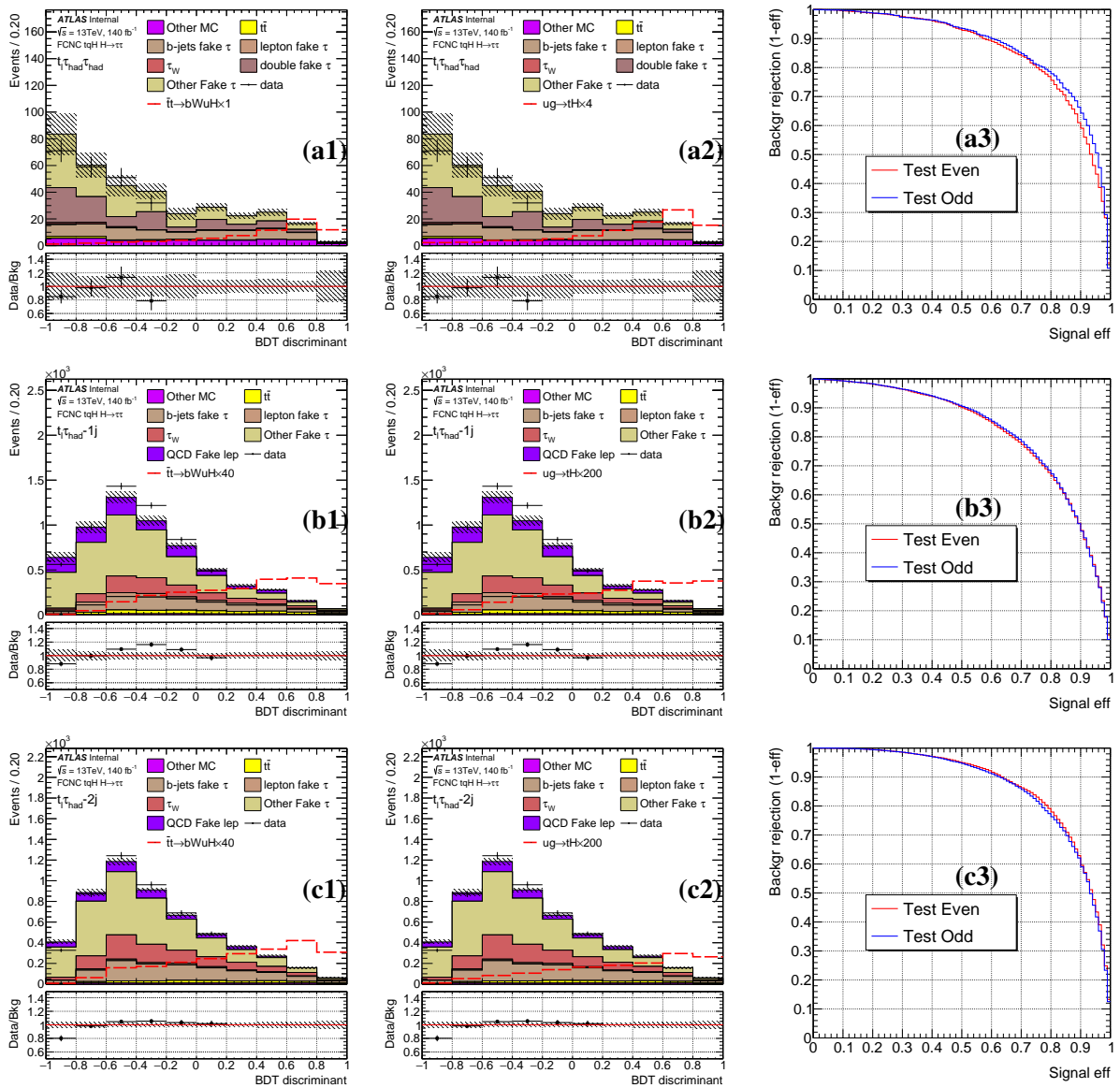


Figure 37: The BDT output distributions for the background and TT signal (a1, b1, c1), background and ST signal (a2, b2, c2) and ROC curves (a3, b3, c3) in the $t_l \tau_{had} \tau_{had}$ (a1-3), $t_l \tau_{had} - 1j$ (b1-3), $t_l \tau_{had} - 2j$ (c1-3) channels.

764 12 Systematic uncertainties

765 The signal efficiency and the background estimations are affected by uncertainties associated with the
 766 detector simulation, the signal modelling and the data-driven background determination. In the combined
 767 fit, these uncertainties recommended by the various ATLAS working groups are called Nuisance Para-
 768 meters (NP), as opposed to the parameter of interest, the signal strength, which is a scaling factor applied
 769 on the total signal events.

770 Any systematic effect on the the overall normalisation or shape of the final BDT distribution in the signal
 771 region is considered. In `TRExFitter` [62], the NP pruning is applied, which means that NPs whose
 772 impact are less than a certain threshold are discarded. The lower thresholds to remove a shape systematic
 773 and a normalisation systematic from the fit are both 1% in the fit.

774 12.1 Luminosity

775 The integrated luminosity measurement has an uncertainty of 1.7% for the combined Run-2 data, and it
 776 is applied to all simulated event samples including both signal and background.

777 12.2 Detector-related uncertainties

778 Uncertainties related to the detector are included for the signal and backgrounds that are estimated using
 779 simulation. These uncertainties are also taken into account for the simulated events that enter the data-
 780 driven background estimations. All instrumental systematic uncertainties arising from the reconstruction,
 781 identification and energy scale of electrons, muons, (b -)jets and the soft term of the E_T^{miss} measurement
 782 are considered. The effect of the energy scale uncertainties on the objects is propagated to the E_T^{miss}
 783 calculation. These systematics include uncertainty associated with:

- 784 • The electron and muon trigger, reconstruction, identification and isolation efficiencies. These are
 785 estimated with the tag-and-probe method on the $Z \rightarrow ll$, $J/\psi \rightarrow ll$ and $W \rightarrow l\nu$ events [63].
- 786 • Electron and muon momentum scales. They are estimated from the early 13 TeV $Z \rightarrow ll$ events.
- 787 • Jet energy scale (JES) and resolution (JER). The JES uncertainty is estimated by varying the jet
 788 energies according to the uncertainties derived from simulation and in-situ calibration measurements
 789 using a model with a reduced set of 39 orthogonal NPs [64] which has up to 30% correlation losses,
 790 which are assumed to be uncorrelated, and the induced changes can be added in quadrature. The
 791 individual scale variations on the jets are parameterised in p_T and η . The total JES uncertainty is
 792 below 5% for most jets and below 1% for central jets with pT between 300 GeV and 2 TeV. The

793 difference between the JER in data and MC is represented by one NP. It is applied on the MC by
 794 smearing the jet p_T within the prescribed uncertainty. JVT is applied in the analysis to select jets
 795 from hard-scattered vertices. It was found that different MC generators (and different fragmentation
 796 models) lead to efficiency differences of up to 1%, and the uncertainty on the efficiency measurement
 797 was found to be around 0.5%. Two NPs are assigned for the JVT efficiency, one for the central and
 798 the other for the forward jets.

- 799 • Calibration of the E_T^{miss} . The uncertainties on E_T^{miss} due to systematic shifts in the corrections for
 800 leptons and jets are accounted for in a fully correlated way in their evaluation for those physics
 801 objects, and are therefore not considered independently here. The systematic uncertainty assigned
 802 to the track-based soft term used in the E_T^{miss} definition quantifies the resolution and scale of the
 803 soft term measurement by using the balance between hard and soft contributions in $Z \rightarrow \mu\mu$
 804 events. These uncertainties are studied using the differences between Monte Carlo generators, using
 805 Powheg+Pythia8 as the nominal generator [65]. One NP is assigned for the soft-track scale, and
 806 two NPs for the soft-track resolution.
- 807 • Jet flavour tagging systematics. The uncertainties on the b -tagging are assessed independently for
 808 b , c and light-flavour quark jets[66]. The efficiencies are measured in data using the methods
 809 described in [67]-[68] with the 2015, 2016, 2017, and 2018 data set. There are 82 NPs assigned for
 810 the flavour tagging systematics with 19 NPs for light flavor, 19 for c , 44 for b .
- 811 • Pileup. The uncertainty on the pileup reweighting is evaluated by varying the pileup scale factors
 812 by 1σ based on the reweighting of the average interactions per bunch crossing. However, this
 813 uncertainty is highly correlated with the luminosity uncertainty and may be an overestimate.
- 814 • Tau object systematics. These include the τ_{had} reconstruction, identification and trigger efficiencies,
 815 the efficiency for tau-electron overlap removal of true τ_{had} and true electrons faking τ_{had} , and the
 816 efficiency for a “medium” BDT electron rejection. There are also three NPs that cover the tau energy
 817 scale (TES) systematics due to the modeling of the detector geometry (TAU_TES_DETECTOR), the
 818 measurement in the tag-and-probe analysis (TAU_TES_INSITU) and the Geant4 shower model
 819 (TAU_TES_MODEL). They are evaluated based on detailed MC variation study, as well as the Run-2
 820 $Z \rightarrow \tau\tau$ data for insitu calibrations of the tau TES and trigger efficiencies, as documented in [51]
 821 and the dedicated software tools [54] recommended by the Tau CP Woking Group [56].

822 12.3 Uncertainties on fake background estimations

823 Systematic uncertainties on the fake background as described in Sec. 10 are considered in the final fit.
 824 The uncertainties of the fake estimation are correlated among all the leptonic channels and among all the
 825 hadronic channels, respectively, but independent between them.

826 In the leptonic channels, they are named `fakeSFNP_Xp_ptY_*` ($X=1,3$ indicating the number of tracks.
 827 $Y=0,1,2$ indicating the p_T bins.) for tau fakes modelled by MC and `ABCD*` for QCD lepton fakes modelled
 828 by ABCD method.

829 In the hadronic channels, they are named `FFNP_Xprong_ptbinY_etabinZ` ($X=1,3$ indicating the number
 830 of tracks. $Y=0,1,2$ indicating the p_T bin. $Z=0,1$ indicating the central taus and forward taus.) for the
 831 statistical uncertainties of the FFs derived from the W+jets control region. `FFNP_OS_CR` and `FFNP_SS_CR`
 832 are one-sided NP for the systematic uncertainties of the FFs derived in the OS and SS control regions
 833 respectively. “Only τ_{sub} real modelling” is the uncertainty of the MC modelling of the events with
 834 leading tau fake but sub-leading tau real, which is varied by 50% to be conservative according to the study
 835 in the leptonic channels.

836 12.4 Theoretical uncertainties on the background

837 Theoretical uncertainties have been applied to the MC background in this analysis. The NNPDF3.0
 838 systematic set (which has 100 variations: PDFset=26001-26100) is used to get the variation envelope
 839 around the nominal PDF.

840 The α_s uncertainty is applied using weights PDFset=26600,26500. The impact is insignificant and pruned
 841 before the fit.

842 The renormalization and factorization scales are varied by a factor of 0.5 and 2.0 around the nominal
 843 values. There are eight such variations. In the final BDT distributions, the largest variations of the eight
 844 per bin are taken. The name of this theoretical NP is called “scale” in the final fit.

845 The ISR and FSR uncertainty are obtained by weights:

- 846 • FSR up: “`isr:muRfac=10_fsr:muRfac=05`”
- 847 • FSR down: “`isr:muRfac=10_fsr:muRfac=05`”
- 848 • ISR up: “`Var3cUp`”
- 849 • ISR down: “`Var3cDown`”

850 The theory uncertainty are applied with both shapes and normalisations hence no additional k-factor
 851 normalisation uncertainty is applied.

852 The default $t\bar{t}$ MC events are showered with Pythia8. A separate sample showered with Herwig7 is
 853 compared with the Pythia8 sample, and the difference is treated as fragmentation and hadronization
 854 systematics [69]. These two samples are both generated with ATLFast-II [36], and their difference is
 855 then applied to the default full-simulation $t\bar{t}$ sample, shown as “PS” in the ranking plots. (Currently the

856 Herwig7 generated with AFII is compared to the Full simulation powheg, the AFII powheg will be used
857 instead in the next version.)

858 The default $t\bar{t}$ sample is generated with full simulated Powheg. Separate AFII aMC and Powheg samples
859 are generated, and the difference between those two is treated as the hard scattering systematics [69],
860 shown as “ME” in the ranking plots.

861 **12.5 Uncertainties on the signal modelling**

862 An additional 1.6% uncertainty on $\text{BR}(H \rightarrow \tau\tau)$ (Named as HttBR in the Ranking plots.) is also assigned
863 [39] besides the theoretical uncertainties: PDF, α_s , ISR, FSR and scale.

864 In the leptonic channels, the fake tau calibration is also applied to the fake tau part of the signal the same
865 way as the background and treated correlatedly.

866 The ME and PS uncertainty of the decay mode signal is applied as a normalisation derived from the
867 relative yield difference between the $t\bar{t}$ samples, independently in each signal region. The yield variation
868 of the PS and ME before the event selection are all smaller than 10%. So in some regions with low $t\bar{t}$
869 yield, the normalisation is constrained to be between 0.9 to 1.1.

870 13 Fit model and signal extraction

871 The parameter of interest in this search is the signal strength of the FCNC interactions, $\text{BR}(t \rightarrow Hq)$
 872 and corresponding production mode cross section. The statistical analysis of the data employs a binned
 873 likelihood function constructed as the product of Poisson probability terms, in bins of the BDT output.

874 To take into account the systematic uncertainties associated with the MC estimation from different sources
 875 for both the signal and background samples, the fit model incorporates these systematics as extra Gaussian
 876 or Log-Normal constraint terms multiplied with the combined likelihood. The fitted central values and
 877 errors of the systematics parameters, or NPs, are expected to follow a normal distribution centered around 0
 878 with unit width, when the Asimov data is used. The fit model construction is obtained with the `RooFit` and
 879 `RooStats` software, and the model configuration and persistence files (as input to `RooStats`) are produced
 880 by `TRExFitter` [62], which is a software package interface with `HistFactory`. The `TRExFitter`
 881 includes additional features such as histogram smoothing, NP pruning and error symmetrization before
 882 the fits.

883 The correlated bin-by-bin histogram variation corresponds to the up and down variation of each NP.
 884 The independent bin-by-bin fluctuations in the combined MC templates are also treated as NPs. They are
 885 incorporated in the model as extra Poisson constraint terms, and are expected to have a fitted value of 1 and
 886 a fitted error reflecting the relative statistical error in each particular bin. There is one parameter of interest
 887 (POI) freely floating in the fit without any constraints, namely, the signal strength μ (`SigXsecOverSM`)
 888 which is a multiplicative factor on a presumed branching ratio of $\text{BR}(t \rightarrow Hq)=0.2\%$ in this analysis. The
 889 errors associated with the different systematics will be properly propagated to the fitted error of μ in a
 890 simultaneous fit of multiple regions via a profiled likelihood scan by the minimization program `MINUIT`.

891 The one-sided NPs in the analysis, namely, `fakeSFxprongXPtbin`, “`ttbar fragmentation`”, “`ttbar`
 892 `hard scattering`”, `JET_BJES_Response`, `JET_JER_DataVsMC_MC16`, `JET_SingleParticle_HighPt`,
 893 `JET_TILECORR_Uncertainty`, `MET_SoftTrk_ResoPara`, `MET_SoftTrk_ResoPerp` are symmetrized.
 894 This is done manually on the MC components of the background. By default, all the kinematic NPs (shape
 895 NPs due to, e.g., energy scales) are smoothed using the default smoothing parameters in `TRExFitter`.
 896 This helps removing the artificial NP constraints due to statistical fluctuations in the systematic variations,
 897 and makes the fit well behaved.

898 Figure 42 shows the ranking of the 30 top NPs along with their pull distributions, produced also with
 899 `TRExFitter`. The highest ranked NP is defined to have the largest impact on μ . The impact is evaluated by
 900 varying the NP under consideration by one σ (either pre or post-fit error) up and down, and afterwards
 901 looking at the relative change in μ under the conditional fit where the NP under consideration is fixed to
 902 its varied new value. Figure 41 shows the pull distributions of all NPs in asimov fit. Normalization and
 903 shape systematics whose impact is less than 1% are removed from the fit.

Figure 43 shows the correlation matrix for different NPs. Except for self-correlations, and the correlations between the normalization factors (including POI) and the others, all the NPs have relatively small correlations with each other, which justifies the fit models for independent systematics.

Not reviewed, for internal circulation only

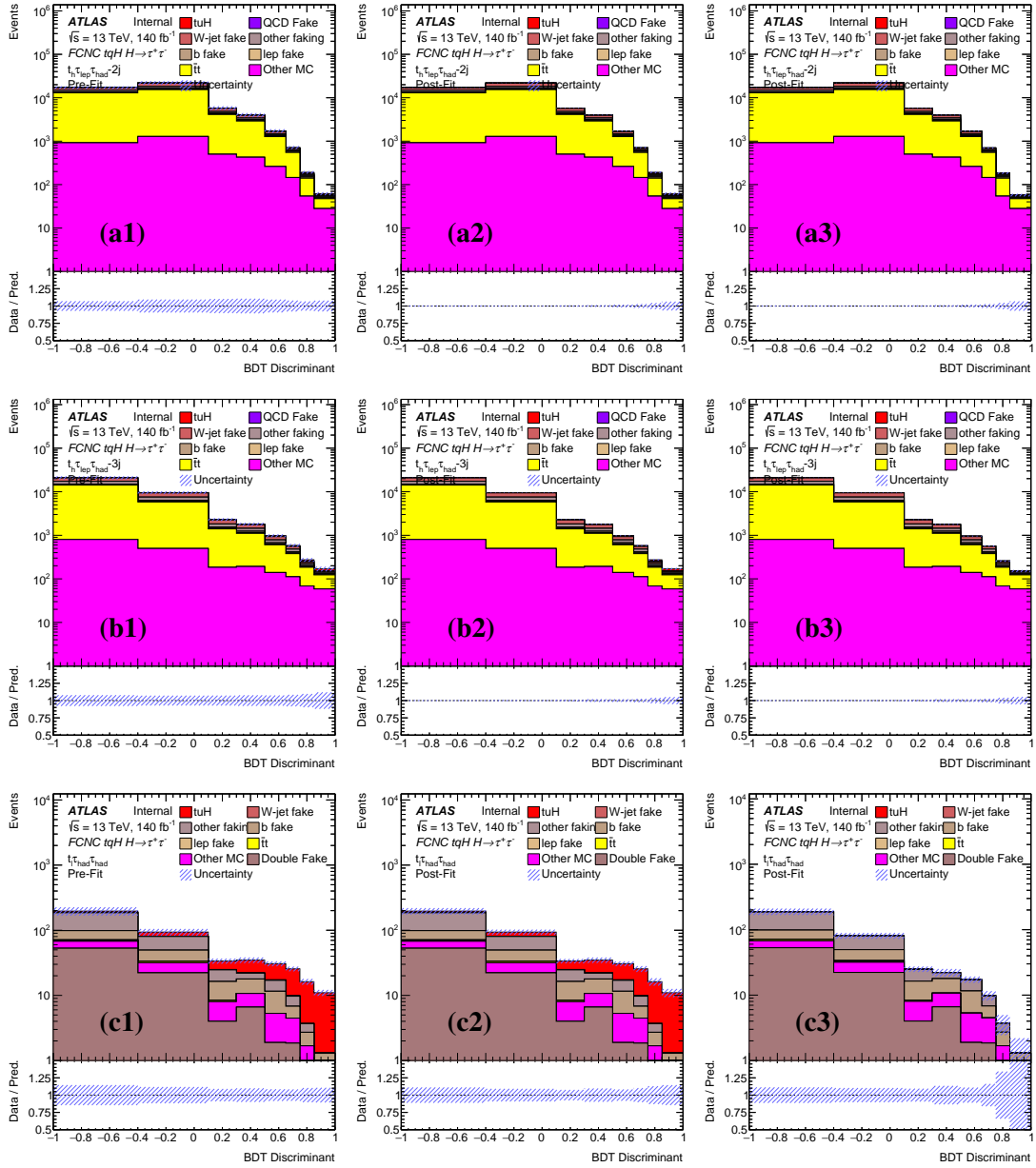


Figure 38: The asimov prefit (a-c1) and post-fit with $\mu=1$ (a-c2) and background only (a-c3) BDT distributions in the $t_h \tau_{\text{lep}} \tau_{\text{had}} - 2j$ (a1-3) and $t_h \tau_{\text{lep}} \tau_{\text{had}} - 3j$ (b1-3), $t_l \tau_{\text{had}} \tau_{\text{had}}$ (c1-3)

Not reviewed, for internal circulation only

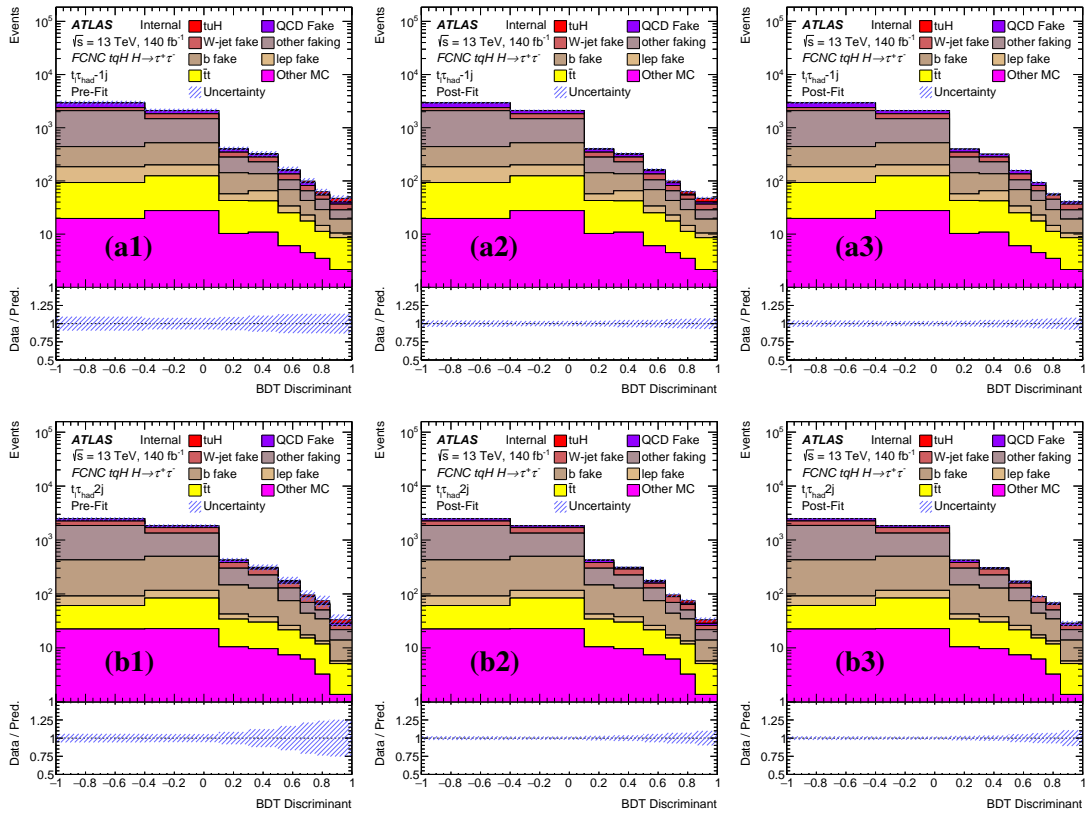


Figure 39: The asimov prefit (a1,b1) and post-fit with $\mu=1$ (a2,b2) and background only (a3,b3) BDT distributions in the $t_1\tau_{\text{had}-1j}$ (a1-3) and $t_1\tau_{\text{had}-2j}$ (b1-3)

Not reviewed, for internal circulation only

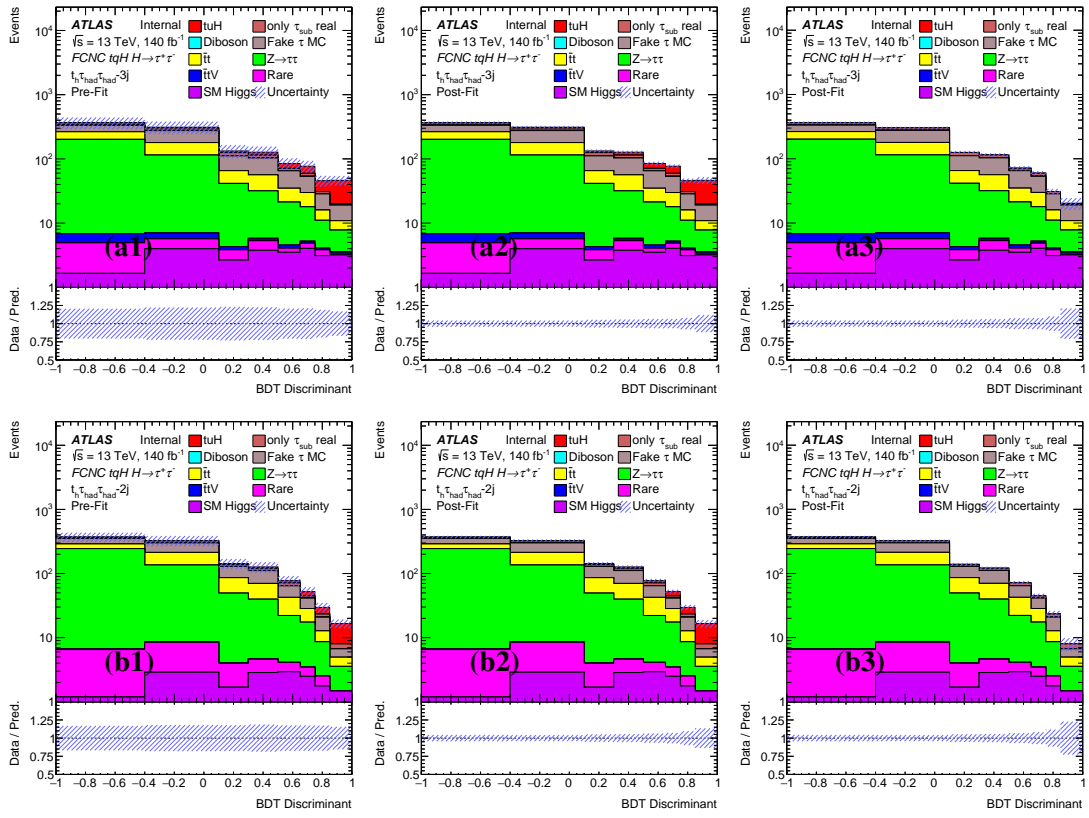


Figure 40: The asimov prefit (a-b1) and post-fit with $\mu=1$ (a-b2) and background only (a-b3) BDT distributions in the $t_h \tau_{\text{had}} \tau_{\text{had}} - 3j$ (a1-3) and $t_h \tau_{\text{had}} \tau_{\text{had}} - 2j$ (b1-3)

Not reviewed, for internal circulation only

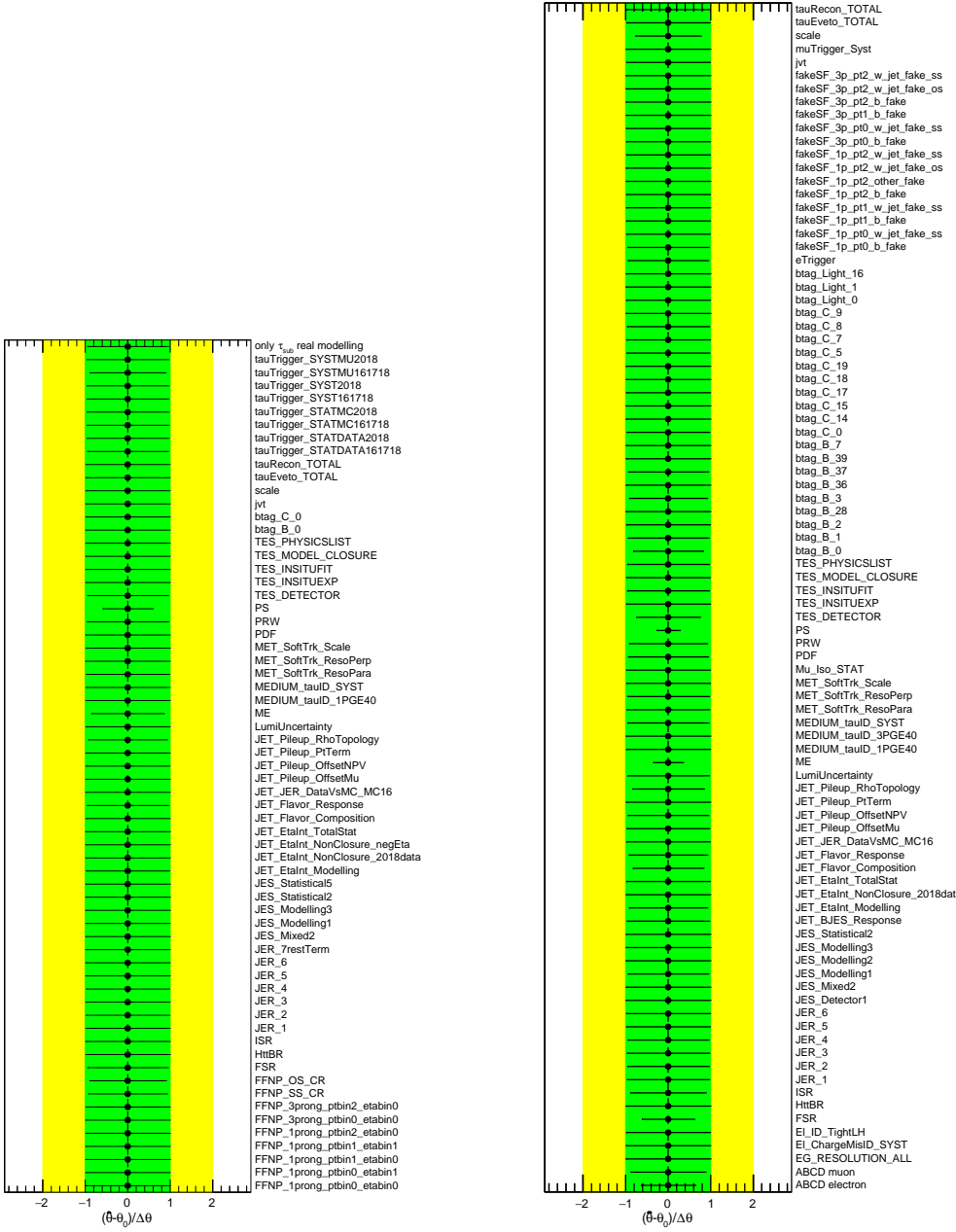


Figure 41: The pull distributions of asimov fit in $\tau_{\text{had}}\tau_{\text{had}}$ channels (left) combined and leptonic channels combined (right) in terms of tuH merged signal .

Not reviewed, for internal circulation only

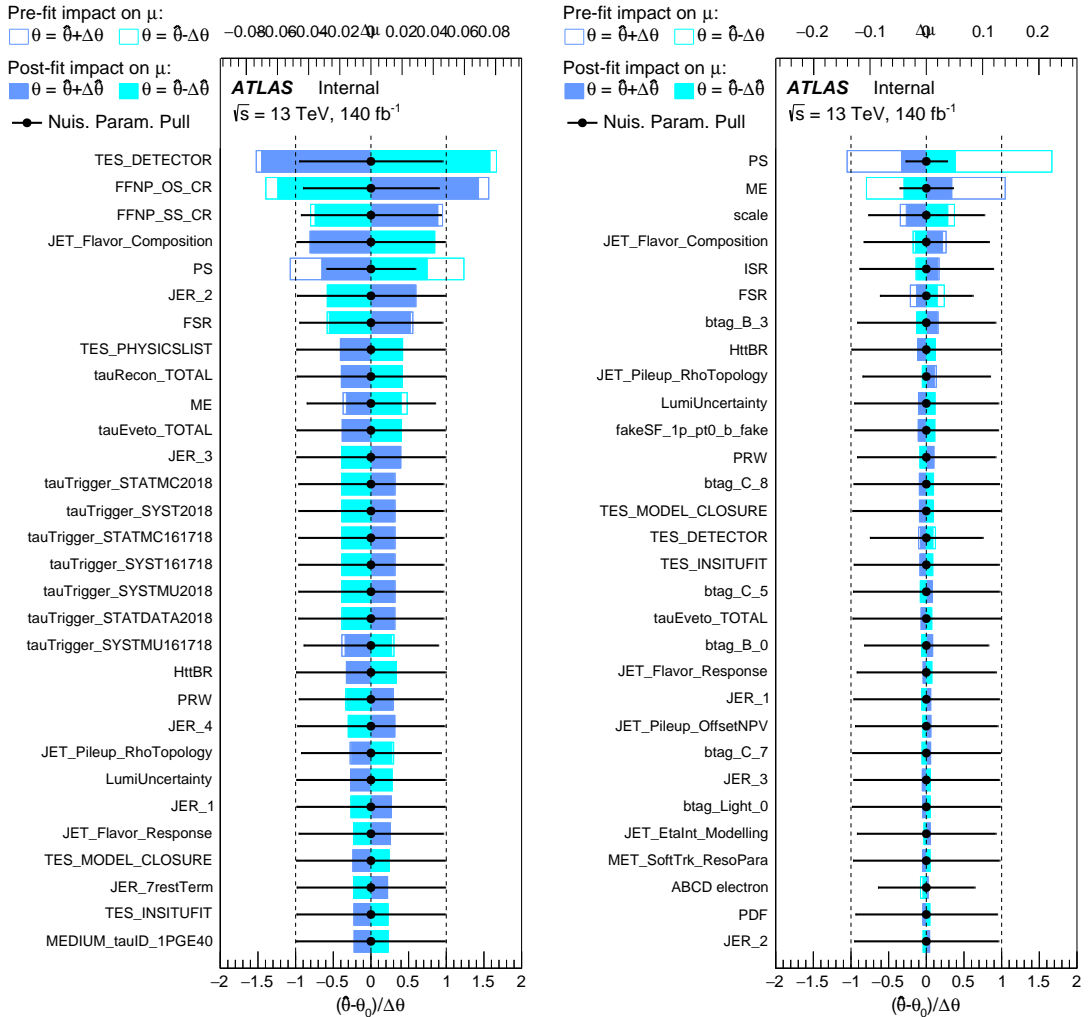


Figure 42: The asimov fit ranking of the top 30 NPs for $\tau_{\text{had}}\tau_{\text{had}}$ channels (left) and leptonic channels (right) in terms of tuH merged signal. The scale of the relative impact on μ (the pull) of the NPs is shown on the top (bottom) axis.

Not reviewed, for internal circulation only

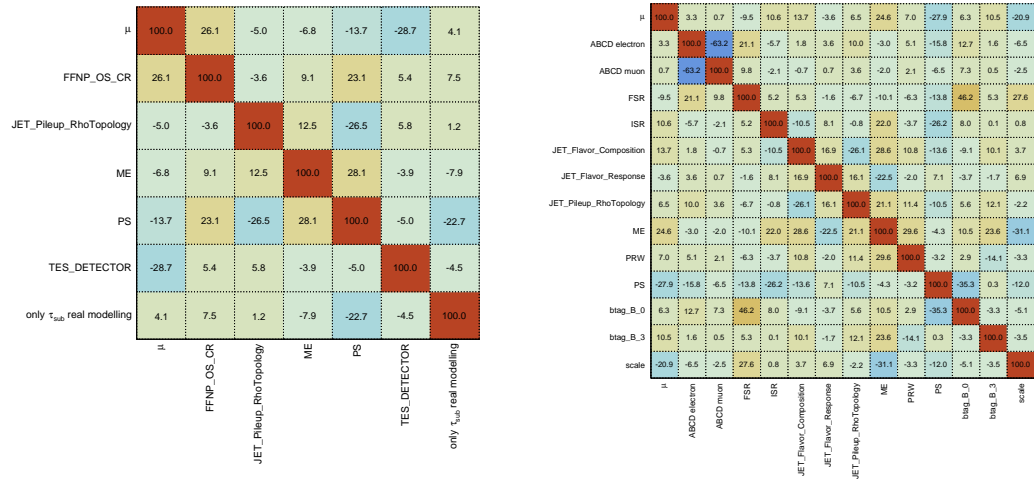


Figure 43: The asimov fit correlation matrix (%) of different NPs, with a threshold of 20% for $\tau_{had}\tau_{had}$ channels (left) combined and lepton channels combined (right).

Not reviewed, for internal circulation only

Table 24: The statistical only significance in leptonic channels based on BDT discriminant.

	$t_l \tau_{\text{had}-1j}$	$t_h \tau_{\text{lep}} \tau_{\text{had}-2j}$	$t_l \tau_{\text{had}-2j}$	$t_h \tau_{\text{lep}} \tau_{\text{had}-3j}$	$t_l \tau_{\text{had}} \tau_{\text{had}}$
$\bar{t}t \rightarrow bWcH$	1.45	0.77	1.37	1.59	6.76
$cg \rightarrow tH$	0.05	0.07	0.04	0.07	0.62
tcH merged	1.50	0.83	1.40	1.66	7.20
$\bar{t}t \rightarrow bWuH$	1.55	0.79	1.48	1.69	7.19
$ug \rightarrow tH$	0.31	0.40	0.23	0.39	2.74
tuH merged	1.84	1.16	1.69	2.07	9.19

Table 25: The statistical only significance in hadronic channels based on BDT discriminant.

	$t_h \tau_{\text{had}} \tau_{\text{had}-2j}$	$t_h \tau_{\text{had}} \tau_{\text{had}-3j}$
$\bar{t}t \rightarrow bWcH$	1.70	4.88
$cg \rightarrow tH$	0.25	0.24
tcH merged	1.92	5.08
$\bar{t}t \rightarrow bWuH$	1.71	5.12
$ug \rightarrow tH$	1.45	1.18
tuH merged	3.03	6.13

907 14 Results

908 The statistical only significance based on BDT discriminant is shown in Table 24, 25.

909 The significance of any small observed excess in data is evaluated by quoting the p -values to quantify the
910 level of consistency of the data with the BR=0 hypothesis. The asymptotic approximation in [70] is used.
911 The test statistic used for the exclusion limits derivation is the \tilde{q}_μ test statistic and for the p -values the q_0
912 test statistic² [70].

913 The 95% CL upper limits on tqH interaction with $\text{BR}(t \rightarrow Hq) = 0.2\%$ as reference are given in Table 27
914 (26 for statistical only.) and 28 for leptonic and hadronic channels respectively. The expected limits

² The definition of the test statistics used in this search is the following:

$$\tilde{q}_\mu = \begin{cases} -2 \ln(\mathcal{L}(\mu, \hat{\theta}) / \mathcal{L}(0, \hat{\theta})) & \text{if } \hat{\mu} < 0 \\ -2 \ln(\mathcal{L}(\mu, \hat{\theta}) / \mathcal{L}(\hat{\mu}, \hat{\theta})) & \text{if } 0 \leq \hat{\mu} \leq \mu \\ 0 & \text{if } \hat{\mu} > \mu \end{cases}$$

and

$$q_0 = \begin{cases} -2 \ln(\mathcal{L}(0, \hat{\theta}) / \mathcal{L}(\hat{\mu}, \hat{\theta})) & \text{if } \hat{\mu} \geq 0 \\ 0 & \text{if } \hat{\mu} < 0 \end{cases}$$

where $\mathcal{L}(\mu, \theta)$ denotes the binned likelihood function, μ is the parameter of interest (i.e. the signal strength parameter), and θ denotes the nuisance parameters. The pair $(\hat{\mu}, \hat{\theta})$ corresponds to the global maximum of the likelihood, whereas $(x, \hat{\theta})$ corresponds to a conditional maximum in which μ is fixed to a given value x .

Not reviewed, for internal circulation only

915 combining all channels are given in Table 29 and Figure 44. The sensitivity is significantly improved
 916 compared to the published results 4.

Table 26: The expected statistical only 95% CL exclusion upper limits on $\text{BR}(t \rightarrow Hc)$ and $\text{BR}(t \rightarrow Hu)$ (0.2%) with the Asimov (B-only) in the leptonic channels.

	$t_l \tau_{\text{had}-2j}$	$t_l \tau_{\text{had}-1j}$	$t_h \tau_{\text{lep}} \tau_{\text{had}-2j}$
$\bar{t}t \rightarrow bWcH$	$1.85^{+0.73}_{-0.52}$	$1.74^{+0.69}_{-0.48}$	$3.07^{+1.20}_{-0.86}$
$cg \rightarrow tH$	$67.32^{+26.76}_{-18.81}$	$48.10^{+19.10}_{-13.44}$	$33.39^{+13.23}_{-9.33}$
tcH merged	$1.80^{+0.71}_{-0.50}$	$1.68^{+0.67}_{-0.47}$	$2.83^{+1.11}_{-0.79}$
$\bar{t}t \rightarrow bWuH$	$1.69^{+0.67}_{-0.47}$	$1.63^{+0.65}_{-0.45}$	$3.00^{+1.17}_{-0.84}$
$ug \rightarrow tH$	$11.04^{+4.40}_{-3.08}$	$8.12^{+3.24}_{-2.27}$	$5.58^{+2.22}_{-1.56}$
tuH merged	$1.46^{+0.58}_{-0.41}$	$1.36^{+0.54}_{-0.38}$	$2.00^{+0.79}_{-0.56}$
	$t_h \tau_{\text{lep}} \tau_{\text{had}-3j}$	$t_l \tau_{\text{had}}$	Combined
$\bar{t}t \rightarrow bWcH$	$1.38^{+0.55}_{-0.39}$	$0.28^{+0.12}_{-0.08}$	$0.27^{+0.12}_{-0.08}$
$cg \rightarrow tH$	$31.40^{+12.46}_{-8.78}$	$3.73^{+1.60}_{-1.04}$	$3.66^{+1.57}_{-1.02}$
tcH merged	$1.33^{+0.52}_{-0.37}$	$0.26^{+0.11}_{-0.07}$	$0.25^{+0.11}_{-0.07}$
$\bar{t}t \rightarrow bWuH$	$1.31^{+0.52}_{-0.37}$	$0.26^{+0.11}_{-0.07}$	$0.25^{+0.11}_{-0.07}$
$ug \rightarrow tH$	$5.66^{+2.25}_{-1.58}$	$0.78^{+0.34}_{-0.22}$	$0.76^{+0.32}_{-0.21}$
tuH merged	$1.06^{+0.42}_{-0.30}$	$0.20^{+0.08}_{-0.05}$	$0.19^{+0.08}_{-0.05}$

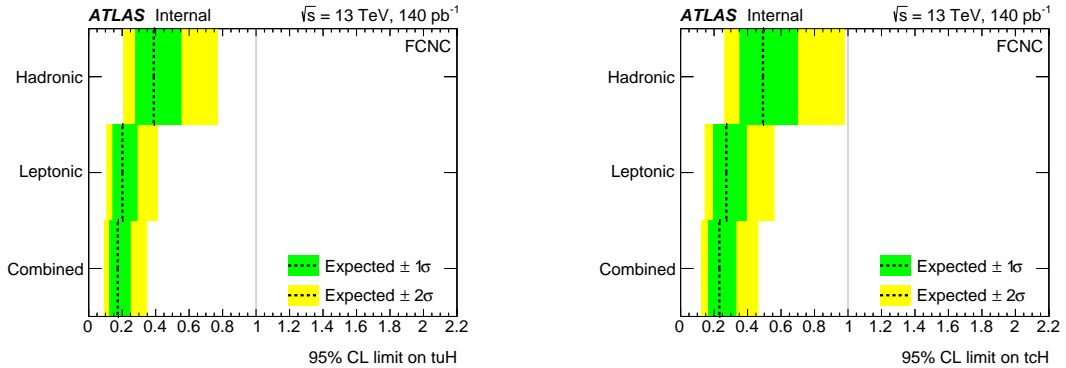


Figure 44: The combined limits for tuH (left) and tcH (right) signal.

917 The search for the FCNC decay $t \rightarrow Hq, H \rightarrow \tau\tau$ with the ATLAS detector at the LHC using 13 TeV
 918 data was presented in this note. The best-fit values for $\text{BR}(t \rightarrow Hc)$ and $\text{BR}(t \rightarrow Hu)$ are found to be
 919 $X.XX^{+X.XX}_{-X.XX}\%$ and $X.XX^{+X.XX}_{-X.XX}\%$ respectively, based on 140 fb^{-1} of data collected from 2015 to 2018.
 920 The observed (expected) 95% CL upper limits on $\text{BR}(t \rightarrow Hc)$ and $\text{BR}(t \rightarrow Hu)$ are found to be $X.XX\%$
 921 ($0.046^{+0.020}_{-0.012}\%$) and $X.XX\%$ ($0.034^{+0.014}_{-0.012}\%$), respectively.

Not reviewed, for internal circulation only

Table 27: The expected 95% CL exclusion upper limits on $\text{BR}(t \rightarrow Hc)$ and $\text{BR}(t \rightarrow Hu)$ (0.2%) with the Asimov (B-only) in the leptonic channels.

	$t_l \tau_{\text{had}-2j}$	$t_l \tau_{\text{had}-1j}$	$t_h \tau_{\text{lep}} \tau_{\text{had}-2j}$
$\bar{t}t \rightarrow bWcH$	$5.34^{+2.54}_{-1.49}$	$3.01^{+1.37}_{-0.84}$	$5.47^{+2.24}_{-1.53}$
$cg \rightarrow tH$	$88.39^{+34.38}_{-24.70}$	$80.08^{+32.47}_{-22.38}$	$47.34^{+19.27}_{-13.23}$
tcH merged	$5.15^{+2.44}_{-1.44}$	$2.91^{+1.32}_{-0.81}$	$4.91^{+2.00}_{-1.37}$
$\bar{t}t \rightarrow bWuH$	$4.44^{+2.06}_{-1.24}$	$2.88^{+1.32}_{-0.81}$	$5.44^{+2.28}_{-1.52}$
$ug \rightarrow tH$	$21.80^{+8.36}_{-6.09}$	$12.15^{+4.88}_{-3.39}$	$7.36^{+3.05}_{-2.06}$
tuH merged	$3.69^{+1.64}_{-1.03}$	$2.33^{+1.04}_{-0.65}$	$3.09^{+1.24}_{-0.86}$
	$t_h \tau_{\text{lep}} \tau_{\text{had}-3j}$	$t_l \tau_{\text{had}}$	Combined
$\bar{t}t \rightarrow bWcH$	$1.96^{+0.80}_{-0.55}$	$0.31^{+0.15}_{-0.09}$	$0.29^{+0.13}_{-0.08}$
$cg \rightarrow tH$	$43.64^{+18.05}_{-12.20}$	$3.91^{+1.69}_{-1.09}$	$3.84^{+1.66}_{-1.07}$
tcH merged	$1.87^{+0.77}_{-0.52}$	$0.29^{+0.14}_{-0.08}$	$0.27^{+0.12}_{-0.08}$
$\bar{t}t \rightarrow bWuH$	$1.84^{+0.75}_{-0.51}$	$0.28^{+0.14}_{-0.08}$	$0.27^{+0.12}_{-0.07}$
$ug \rightarrow tH$	$7.67^{+3.06}_{-2.14}$	$0.82^{+0.36}_{-0.23}$	$0.80^{+0.35}_{-0.22}$
tuH merged	$1.49^{+0.61}_{-0.42}$	$0.21^{+0.10}_{-0.06}$	$0.20^{+0.09}_{-0.06}$

Table 28: The expected 95% CL exclusion upper limits on $\text{BR}(t \rightarrow Hc)$ and $\text{BR}(t \rightarrow Hu)$ (0.2%) with the Asimov (B-only) in the hadronic channels.

	$t_h \tau_{\text{had}} \tau_{\text{had}-2j}$	$t_h \tau_{\text{had}} \tau_{\text{had}-3j}$	Combined
$\bar{t}t \rightarrow bWcH$	$1.63^{+0.76}_{-0.46}$	$0.54^{+0.23}_{-0.15}$	$0.51^{+0.22}_{-0.14}$
$cg \rightarrow tH$	$10.22^{+4.55}_{-2.86}$	$14.48^{+6.15}_{-4.05}$	$8.65^{+3.77}_{-2.42}$
tcH merged	$1.41^{+0.64}_{-0.39}$	$0.52^{+0.22}_{-0.15}$	$0.49^{+0.21}_{-0.14}$
$\bar{t}t \rightarrow bWuH$	$1.62^{+0.76}_{-0.45}$	$0.52^{+0.22}_{-0.14}$	$0.50^{+0.21}_{-0.14}$
$ug \rightarrow tH$	$1.59^{+0.71}_{-0.45}$	$2.83^{+1.23}_{-0.79}$	$1.42^{+0.63}_{-0.40}$
tuH merged	$0.80^{+0.36}_{-0.22}$	$0.44^{+0.18}_{-0.12}$	$0.39^{+0.16}_{-0.11}$

Table 29: The combined expected 95% CL exclusion upper limits on $\text{BR}(t \rightarrow Hc)$ and $\text{BR}(t \rightarrow Hu)$ (0.2%) with the Asimov (B-only).

	tcH merged	tuH merged
Combined Limit	$0.23^{+0.10}_{-0.06}$	$0.17^{+0.07}_{-0.05}$

922 Appendix

923 A Sample DSID list

- 924 $t\bar{t} \rightarrow bWcH, W \rightarrow lv, H \rightarrow \tau^+\tau^-$: 411172 411173
- 925 $t\bar{t} \rightarrow bWcH$ 1 lepton filter: 410694 410695
- 926 $t\bar{t} \rightarrow bWcH, W \rightarrow q\bar{q}, H \rightarrow \tau^+\tau^-$: 411170 411171
- 927 $cg \rightarrow tH, H \rightarrow \tau^+\tau^-$: 412104 412105 412100 412101
- 928 $t\bar{t} \rightarrow bWuH, W \rightarrow lv, H \rightarrow \tau^+\tau^-$: 411176 411177
- 929 $t\bar{t} \rightarrow bWuH$ 1 lepton filter: 410692 410693
- 930 $t\bar{t} \rightarrow bWuH, W \rightarrow q\bar{q}, H \rightarrow \tau^+\tau^-$: 411174 411175
- 931 $ug \rightarrow tH, H \rightarrow \tau^+\tau^-$: 412098 412099 412102 412103
- 932 Diboson: 364250 363355 363356 363357 363358 363359 363360 363489 345708 345716 364253 364254
- 933 364255
- 934 Rare: 410080 410081 304014 341998 342004 343267 343270 410408 410560 345716 345708 410644
- 935 410645 410646 410647
- 936 SM Higgs: 342001 342282 342283 342284 342285 343273 345873 345874 345875
- 937 $t\bar{t}$: 410470 410471
- 938 $t\bar{t}V$: 410155 410156 410157 410218 410219 410220 410276 410277 410278 410397 410398 410399
- 939 $W+$ jets: 364156 364157 364158 364159 364160 364161 364162 364163 364164 364165 364166 364167
- 940 364168 364169 364170 364171 364172 364173 364174 364175 364176 364177 364178 364179 364180
- 941 364181 364182 364183 364184 364185 364186 364187 364188 364189 364190 364191 364192 364193
- 942 364194 364195 364196 364197
- 943 $Z \rightarrow l^+l^-$: 364100 364101 364102 364103 364104 364105 364106 364107 364108 364109 364110
- 944 364111 364112 364113 364114 364115 364116 364117 364118 364119 364120 364121 364122 364123
- 945 364124 364125 364126 364127 364198 364199 364200 364201 364202 364203 364204 364205 364206
- 946 364207 364208 364209
- 947 $Z \rightarrow \tau^+\tau^-$: 364128 364129 364130 364131 364132 364133 364134 364135 364136 364137 364138
- 948 364139 364140 364141 364210 364211 364212 364213 364214 364215

949 B Derivation and framework level cuts

950 A number of event cuts are applied before getting to the signal enhanced regions with the back-
 951 ground suppressed. Then the DAOD_HIGG8D1 (DAOD_HIGG4D3) derivation is feed to ttHMultiAna
 952 (`xTauFramework`) to produce n-tuples for leptonic (hadronic) channels, where ttHMultiAna is AnalysisTop
 953 [71] based. The list of event-level selection criteria is as follows:

- 954 1. DAOD_HIGG8D1 (leptonic) and DAOD_HIGG4D3 (hadronic) derivations are used for this ana-
 955 lysis. At the derivation level, the following cuts are applied:
 - 956 • In DAOD_HIGG8D1, trigger skimming: all electron, muon, tau triggers; Offline skimming:
 957 at least 2 light leptons or at least 1 lepton plus 1 tau.
 - 958 • In DAOD_HIGG4D3, no trigger skimming. Offline skimming: 2taus
- 959 2. At the ttHMultiAna level, skim cuts in [58] are applied , then only the events passing either of the
 960 following cut are saved for the n-tuples:
 - 961 • At least two light leptons passing loose identification criteria with leading lepton $p_T > 15$
 962 GeV and subleading lepton $p_T > 5$ GeV within $|\eta| < 2.6$.
 - 963 • At least one light lepton passing loose identification criterua with $p_T > 15$ GeV and $|\eta| < 2.5$,
 964 and at least one hadronic tau. The tau lepton has to pass RNN loose requirement with $p_T > 15$
 965 GeV and $|\eta| < 2.5$.
- 966 3. If the tau candidate overlaps with a muon or fails Loose electron-BDT cut, the event is removed.
- 967 4. If the event neither fires single lepton nor dilepton trigger, the event is removed.
- 968 5. If the lepton fails tight lepton selection, the event is removed.
- 969 6. If the leading or sub-leading tau candidate has p_T less than 25GeV or fails RNN medium criteria,
 970 the event is removed.
- 971 7. If the event has two same-charged lepton, the electrons are required to pass Loose charge BDT. (Not
 972 affecting this analysis.)
- 973 8. If the tau is tagged as b -jet by 70% WP, the event is removed.
- 974 9. At the `xTauFramework` level, skim cuts are applied to reduce the ntuple size:
 - 975 • No leptons.
 - 976 • At least 1 RNN Loose tau.

- 977 • At least 3 jets with $p_T > 30$ GeV, $|\eta| < 4.5$ and passing either central or forward JVT cuts,
 978 with at least 1 b-tagged. (The jets are further required to have $|\eta| < 2.5$ at n-tuple level to be
 979 consistent with leptonic channels.)

- 980 • Taus trigger matched.

- 981 • LooseBad Event Cleaning.

- 982 • Leading tau $p_T > 40$ GeV, sub-leading tau $p_T > 30$ GeV, two taus comes from a single vertex.

- 983 • Leading jet $p_T > 70$ GeV, $|\eta| < 3.2$

- 984 • $E_T^{\text{miss}} > 15$ GeV.

- 985 • In the case of data, GRL cut as defined in Sec. 6.2 is also applied.

986 10. At least one primary vertex exists in the event. The primary vertex is defined as the vertex that has
 987 the largest sum of track p_T^2 associated to it, and has at least 4 tracks with $|z_0| < 100$ mm.

988 The corresponding cutflow for the n-tuple level selection and each channel are given in Table 30 - 38.

Table 30: The cutflow tables for the preselection in the hadronic channels.

	SM Higgs	W+jets	Diboson	$Z \rightarrow ll$
n-tuple	676.49 ± 1.91	11732.85 ± 124.96	1051.56 ± 11.87	1167.56 ± 48.10
pass trigger	543.51 ± 1.76	7305.26 ± 97.16	755.24 ± 9.61	905.30 ± 31.11
ntrack = 1,3	374.81 ± 1.55	3483.97 ± 85.34	449.69 ± 7.17	542.26 ± 25.31
ele veto	264.27 ± 1.32	2084.24 ± 49.96	299.13 ± 5.82	4.33 ± 0.93
jet num \geq 3	206.40 ± 1.07	1385.84 ± 44.66	229.60 ± 5.05	3.49 ± 0.76
tau rnn score \geq 0.01	187.70 ± 1.05	1014.28 ± 23.94	202.37 ± 4.67	2.04 ± 0.29
	$Z \rightarrow \tau\tau$	Rare	$t\bar{t}$	$t\bar{t}V$
n-tuple	14879.46 ± 55.73	14329.96 ± 52.89	189864.11 ± 210.84	491.85 ± 2.19
pass trigger	13065.11 ± 51.01	9324.55 ± 42.29	125670.32 ± 171.27	359.85 ± 1.88
ntrack = 1,3	10361.59 ± 45.91	4732.10 ± 30.15	63031.31 ± 119.31	207.39 ± 1.45
ele veto	7616.84 ± 39.97	2867.35 ± 22.85	38450.70 ± 92.64	133.91 ± 1.15
jet num \geq 3	4832.42 ± 24.29	2148.52 ± 19.55	34673.13 ± 88.63	131.86 ± 1.14
tau rnn score \geq 0.01	4708.25 ± 24.00	1578.54 ± 16.26	25495.22 ± 74.67	112.96 ± 1.06
	$t\bar{t} \rightarrow bWcH$	$cg \rightarrow tH$	tcH merged	$t\bar{t} \rightarrow bWuH$
n-tuple	3480.44 ± 15.20	186.55 ± 1.12	3666.99 ± 15.25	3428.60 ± 15.37
pass trigger	2883.81 ± 13.82	163.69 ± 1.06	3047.50 ± 13.86	2858.57 ± 14.04
ntrack = 1,3	2197.02 ± 12.05	134.00 ± 0.96	2331.02 ± 12.09	2176.08 ± 12.21
ele veto	1666.34 ± 10.51	102.97 ± 0.84	1769.31 ± 10.54	1654.36 ± 10.67
jet num \geq 3	1560.37 ± 10.22	87.29 ± 0.79	1647.66 ± 10.25	1548.51 ± 10.38
tau rnn score \geq 0.01	1499.72 ± 10.01	86.12 ± 0.78	1585.84 ± 10.04	1491.69 ± 10.18
	$ug \rightarrow tH$	tuH merged	Data	total background
n-tuple	1025.81 ± 5.76	4454.41 ± 16.41	1460658.00 ± 1208.58	234193.83 ± 261.60
pass trigger	889.85 ± 5.40	3748.41 ± 15.04	975476.00 ± 987.66	157929.14 ± 210.31
ntrack = 1,3	700.77 ± 4.80	2876.85 ± 13.12	383804.00 ± 619.52	83183.11 ± 158.85
ele veto	533.50 ± 4.19	2187.86 ± 11.46	276245.00 ± 525.59	51720.77 ± 115.05
jet num \geq 3	448.86 ± 3.90	1997.37 ± 11.09	187734.00 ± 433.28	43611.26 ± 104.17
tau rnn score \geq 0.01	443.20 ± 3.88	1934.89 ± 10.89	123625.00 ± 351.60	33301.36 ± 83.74

Not reviewed, for internal circulation only

Table 31: The cutflow tables in the $t_h\tau_{\text{had}}\tau_{\text{had}}\text{-}2j$ signal region.

	SM Higgs	W+jets	Diboson	$Z \rightarrow \tau\tau$
this region	20.48 ± 0.46	37.90 ± 5.19	25.03 ± 1.17	1018.56 ± 10.82
$\Delta R(\tau, \tau) < 3.4$	20.46 ± 0.46	36.91 ± 5.16	25.05 ± 1.17	1018.55 ± 10.82
$m_{\tau\tau,\text{vis}} > 60$	18.70 ± 0.44	10.85 ± 2.07	16.40 ± 0.92	691.81 ± 9.56
$m_{\tau\tau,\text{vis}} < 120$	18.25 ± 0.44	8.39 ± 1.64	15.03 ± 0.90	674.61 ± 9.46
$100\text{GeV} < m_{\tau\tau} < 150\text{GeV}$	17.66 ± 0.44	5.91 ± 1.29	10.56 ± 0.71	511.13 ± 8.77
$m_{t,\text{FCNC}} > 140\text{GeV}$	17.31 ± 0.43	5.67 ± 1.28	10.05 ± 0.68	487.59 ± 8.63
	Rare	$t\bar{t}$	$t\bar{t}V$	$\bar{t}t \rightarrow bWcH$
this region	91.67 ± 3.76	909.52 ± 12.50	2.69 ± 0.15	171.88 ± 3.29
$\Delta R(\tau, \tau) < 3.4$	89.97 ± 3.72	887.25 ± 12.36	2.67 ± 0.15	171.25 ± 3.28
$m_{\tau\tau,\text{vis}} > 60$	57.30 ± 2.90	633.30 ± 10.46	1.73 ± 0.12	159.03 ± 3.16
$m_{\tau\tau,\text{vis}} < 120$	34.07 ± 2.21	397.24 ± 8.29	1.25 ± 0.10	151.80 ± 3.11
$100\text{GeV} < m_{\tau\tau} < 150\text{GeV}$	24.98 ± 1.88	296.73 ± 7.17	0.80 ± 0.08	142.94 ± 3.05
$m_{t,\text{FCNC}} > 140\text{GeV}$	24.04 ± 1.84	290.64 ± 7.10	0.78 ± 0.08	140.65 ± 3.03
	$cg \rightarrow tH$	tcH merged	$\bar{t}t \rightarrow bWuH$	$ug \rightarrow tH$
this region	19.84 ± 0.37	191.71 ± 3.31	176.50 ± 3.42	106.32 ± 1.85
$\Delta R(\tau, \tau) < 3.4$	19.81 ± 0.37	191.06 ± 3.30	175.98 ± 3.41	106.13 ± 1.84
$m_{\tau\tau,\text{vis}} > 60$	18.33 ± 0.35	177.36 ± 3.18	163.46 ± 3.28	94.35 ± 1.75
$m_{\tau\tau,\text{vis}} < 120$	17.67 ± 0.35	169.47 ± 3.12	154.47 ± 3.21	91.33 ± 1.72
$100\text{GeV} < m_{\tau\tau} < 150\text{GeV}$	16.97 ± 0.34	159.91 ± 3.07	144.58 ± 3.14	87.62 ± 1.69
$m_{t,\text{FCNC}} > 140\text{GeV}$	16.75 ± 0.34	157.40 ± 3.05	141.87 ± 3.11	86.43 ± 1.68
	tuH merged	Data	total background	
this region	282.82 ± 3.88	2383.00 ± 48.82	2105.86 ± 17.77	
$\Delta R(\tau, \tau) < 3.4$	282.11 ± 3.88	2337.00 ± 48.34	2080.88 ± 17.66	
$m_{\tau\tau,\text{vis}} > 60$	257.80 ± 3.71	1695.00 ± 41.17	1430.08 ± 14.65	
$m_{\tau\tau,\text{vis}} < 120$	245.79 ± 3.64	1364.00 ± 36.93	1148.84 ± 12.92	
$100\text{GeV} < m_{\tau\tau} < 150\text{GeV}$	232.20 ± 3.57	1073.00 ± 32.76	867.77 ± 11.59	
$m_{t,\text{FCNC}} > 140\text{GeV}$	228.30 ± 3.54	1033.00 ± 32.14	836.08 ± 11.43	

Not reviewed, for internal circulation only

Table 32: The cutflow tables in the $t_h\tau_{\text{had}}\tau_{\text{had}}\text{-}3j$ signal region.

	SM Higgs	W+jets	Diboson	$Z \rightarrow \tau\tau$
this region	34.09 ± 0.48	31.31 ± 3.23	37.59 ± 1.47	928.27 ± 9.67
$\Delta R(\tau, \tau) < 3.4$	34.02 ± 0.48	30.45 ± 3.19	37.00 ± 1.36	927.72 ± 9.67
$m_{\tau\tau,\text{vis}} > 60$	30.22 ± 0.45	8.94 ± 1.40	22.82 ± 0.93	604.96 ± 8.57
$m_{\tau\tau,\text{vis}} < 120$	28.55 ± 0.44	5.29 ± 1.17	20.59 ± 0.90	586.09 ± 8.49
$100\text{GeV} < m_{\tau\tau} < 150\text{GeV}$	26.81 ± 0.44	4.81 ± 1.14	14.38 ± 0.75	438.47 ± 7.78
$m_{t,\text{FCNC}} > 140\text{GeV}$	26.00 ± 0.43	4.81 ± 1.14	13.23 ± 0.71	406.88 ± 7.65
	Rare	$t\bar{t}$	$t\bar{t}V$	$t\bar{t} \rightarrow bWcH$
this region	75.24 ± 3.37	1171.73 ± 14.33	19.93 ± 0.46	482.85 ± 5.65
$\Delta R(\tau, \tau) < 3.4$	73.61 ± 3.33	1143.72 ± 14.17	19.84 ± 0.46	482.33 ± 5.65
$m_{\tau\tau,\text{vis}} > 60$	47.43 ± 2.67	739.25 ± 11.49	12.27 ± 0.36	446.73 ± 5.44
$m_{\tau\tau,\text{vis}} < 120$	26.24 ± 2.02	453.75 ± 9.04	10.21 ± 0.33	430.37 ± 5.36
$100\text{GeV} < m_{\tau\tau} < 150\text{GeV}$	16.97 ± 1.67	331.16 ± 7.77	6.04 ± 0.26	414.14 ± 5.28
$m_{t,\text{FCNC}} > 140\text{GeV}$	16.97 ± 1.67	320.21 ± 7.65	5.63 ± 0.25	400.68 ± 5.20
	$cg \rightarrow tH$	tcH merged	$\bar{t}t \rightarrow bWuH$	$ug \rightarrow tH$
this region	25.75 ± 0.44	508.60 ± 5.67	501.98 ± 5.97	133.64 ± 2.23
$\Delta R(\tau, \tau) < 3.4$	25.70 ± 0.44	508.03 ± 5.67	501.07 ± 5.97	133.47 ± 2.23
$m_{\tau\tau,\text{vis}} > 60$	23.34 ± 0.42	470.07 ± 5.46	464.52 ± 5.75	118.27 ± 2.09
$m_{\tau\tau,\text{vis}} < 120$	22.80 ± 0.42	453.16 ± 5.38	445.37 ± 5.65	115.18 ± 2.07
$100\text{GeV} < m_{\tau\tau} < 150\text{GeV}$	22.16 ± 0.41	436.30 ± 5.30	429.87 ± 5.59	111.04 ± 2.04
$m_{t,\text{FCNC}} > 140\text{GeV}$	21.51 ± 0.41	422.19 ± 5.21	418.73 ± 5.52	108.17 ± 2.01
	tuH merged	Data	total background	
this region	635.62 ± 6.37	2554.00 ± 50.54	2298.16 ± 17.98	
$\Delta R(\tau, \tau) < 3.4$	634.53 ± 6.37	2506.00 ± 50.06	2266.37 ± 17.83	
$m_{\tau\tau,\text{vis}} > 60$	582.79 ± 6.11	1865.00 ± 43.19	1465.89 ± 14.69	
$m_{\tau\tau,\text{vis}} < 120$	560.55 ± 6.02	1451.00 ± 38.09	1130.73 ± 12.66	
$100\text{GeV} < m_{\tau\tau} < 150\text{GeV}$	540.90 ± 5.95	1124.00 ± 33.53	838.64 ± 11.21	
$m_{t,\text{FCNC}} > 140\text{GeV}$	526.90 ± 5.87	1052.00 ± 32.43	793.73 ± 11.03	

Not reviewed, for internal circulation only

Table 33: The cutflow tables for the preselection in the leptonic channels.

	SM Higgs	W+jets	Diboson	$Z \rightarrow ll$
n-tuple	9605.63 ± 52.35	2666001.33 ± 9855.34	260983.68 ± 341.31	5075872.99 ± 9314.17
pass trigger	9119.19 ± 51.06	2634692.81 ± 9800.60	250112.16 ± 339.81	4703869.40 ± 8977.21
leadtauOLR	8941.03 ± 50.51	2531478.93 ± 9687.84	241499.86 ± 331.44	4415725.55 ± 8703.29
subtauOLR	8934.70 ± 50.50	2531094.58 ± 9687.42	241402.36 ± 331.33	4414900.65 ± 8702.67
trigger match	8888.07 ± 50.42	2518974.10 ± 9662.49	240512.01 ± 330.61	4406612.41 ± 8697.04
tight lepton	8188.67 ± 48.53	2433607.57 ± 9502.79	227059.64 ± 325.00	3600064.57 ± 7200.66
Medium,25GeV leadtau	7188.59 ± 44.99	742346.21 ± 4891.76	149780.07 ± 204.27	2774412.81 ± 5529.53
Medium,25GeV subtau	7132.86 ± 44.80	738787.27 ± 4882.13	149134.54 ± 203.64	2772021.52 ± 5526.54
2ISS chargeBDT	6964.05 ± 44.26	734717.56 ± 4867.44	144456.99 ± 202.87	2410482.28 ± 5186.45
SR+CR	526.87 ± 7.21	9369.17 ± 248.82	1509.55 ± 24.72	3660.21 ± 118.03

	$Z \rightarrow \tau\tau$	Rare	$t\bar{t}$	$t\bar{t}V$
n-tuple	562961.80 ± 2569.58	278704.72 ± 187.24	3566937.50 ± 696.84	7012.99 ± 6.37
pass trigger	552556.20 ± 2551.56	266961.94 ± 183.46	3392547.79 ± 680.41	6712.14 ± 6.19
leadtauOLR	540477.68 ± 2525.97	261076.79 ± 181.46	3320024.94 ± 673.13	6601.03 ± 6.14
subtauOLR	540382.95 ± 2525.82	261017.54 ± 181.44	3319089.44 ± 673.04	6597.39 ± 6.14
trigger match	533599.82 ± 2507.35	259963.53 ± 181.08	3300798.05 ± 671.24	6561.67 ± 6.12
tight lepton	509108.93 ± 2455.42	239879.88 ± 174.06	3024804.51 ± 642.96	6080.89 ± 5.89
Medium,25GeV leadtau	329372.98 ± 1937.70	206437.94 ± 161.45	2637223.73 ± 600.12	5411.57 ± 5.55
Medium,25GeV subtau	328066.63 ± 1934.44	206215.52 ± 161.36	2634096.13 ± 599.76	5394.78 ± 5.54
2ISS chargeBDT	326074.04 ± 1930.46	201690.62 ± 159.65	2575318.87 ± 593.28	5261.80 ± 5.47
SR+CR	3633.31 ± 55.18	8324.04 ± 32.21	160957.07 ± 147.94	574.85 ± 1.84

	$\bar{t}t \rightarrow bWcH$	$cg \rightarrow tH$	tcH merged	$\bar{t}t \rightarrow bWuH$
n-tuple	3063.06 ± 4.99	139.78 ± 0.36	3202.84 ± 5.00	3070.72 ± 4.94
pass trigger	2936.51 ± 4.89	133.89 ± 0.36	3070.40 ± 4.91	2945.93 ± 4.84
leadtauOLR	2899.38 ± 4.86	132.41 ± 0.36	3031.80 ± 4.87	2912.82 ± 4.81
subtauOLR	2892.68 ± 4.86	132.06 ± 0.35	3024.74 ± 4.87	2907.42 ± 4.81
trigger match	2875.03 ± 4.84	131.25 ± 0.35	3006.28 ± 4.85	2889.73 ± 4.80
tight lepton	2636.75 ± 4.63	120.42 ± 0.34	2757.17 ± 4.64	2651.58 ± 4.59
Medium,25GeV leadtau	2168.49 ± 4.17	100.95 ± 0.31	2269.44 ± 4.18	2176.91 ± 4.13
Medium,25GeV subtau	2098.47 ± 4.11	97.09 ± 0.30	2195.56 ± 4.12	2102.53 ± 4.07
2ISS chargeBDT	2065.19 ± 4.08	95.65 ± 0.30	2160.85 ± 4.09	2069.38 ± 4.04
SR+CR	652.48 ± 2.35	30.09 ± 0.17	682.57 ± 2.36	653.70 ± 2.31

Not reviewed, for internal circulation only

Table 34: The cutflow tables in the $t_l\tau_{\text{had}}\text{-1j}$ signal region.

	SM Higgs	W+jets	Diboson	$Z \rightarrow ll$
this region	9.57 ± 1.08	1966.00 ± 100.19	132.17 ± 10.68	531.68 ± 44.56
	$Z \rightarrow \tau\tau$	Rare	$t\bar{t}$	$t\bar{t}V$
this region	56.04 ± 15.61	466.66 ± 7.56	4161.47 ± 24.10	19.33 ± 0.27
	$\bar{t}t \rightarrow bWcH$	$cg \rightarrow tH$	tcH merged	$\bar{t}t \rightarrow bWuH$
this region	65.56 ± 0.65	2.53 ± 0.04	68.10 ± 0.65	66.79 ± 0.66
	$ug \rightarrow tH$	tuH merged	Data	total background
this region	12.81 ± 0.22	79.60 ± 0.69	8411.00 ± 91.71	7342.92 ± 114.11

Table 35: The cutflow tables in the $t_h\tau_{\text{lep}}\tau_{\text{had}}\text{-2j}$ signal region.

	SM Higgs	W+jets	Diboson	$Z \rightarrow ll$
this region	41.41 ± 2.42	1636.25 ± 77.55	281.73 ± 10.75	744.82 ± 37.49
	$Z \rightarrow \tau\tau$	Rare	$t\bar{t}$	$t\bar{t}V$
this region	1636.93 ± 37.14	3546.49 ± 21.22	54238.80 ± 86.30	73.02 ± 0.57
	$\bar{t}t \rightarrow bWcH$	$cg \rightarrow tH$	tcH merged	$\bar{t}t \rightarrow bWuH$
this region	119.13 ± 1.06	6.53 ± 0.09	125.66 ± 1.06	122.69 ± 1.04
	$ug \rightarrow tH$	tuH merged	Data	total background
this region	32.79 ± 0.43	155.48 ± 1.13	57347.00 ± 239.47	62199.44 ± 129.69

Table 36: The cutflow tables in the $t_l\tau_{\text{had}}\text{-2j}$ signal region.

	SM Higgs	W+jets	Diboson	$Z \rightarrow ll$
this region	18.35 ± 1.39	949.60 ± 41.19	108.36 ± 8.99	257.72 ± 25.63
	$Z \rightarrow \tau\tau$	Rare	$t\bar{t}$	$t\bar{t}V$
this region	25.47 ± 3.95	356.42 ± 6.59	5391.85 ± 27.28	37.13 ± 0.40
	$\bar{t}t \rightarrow bWcH$	$cg \rightarrow tH$	tcH merged	$\bar{t}t \rightarrow bWuH$
this region	59.88 ± 0.62	1.54 ± 0.04	61.42 ± 0.62	62.66 ± 0.64
	$ug \rightarrow tH$	tuH merged	Data	total background
this region	8.48 ± 0.19	71.13 ± 0.66	7083.00 ± 84.16	7144.90 ± 56.92

Not reviewed, for internal circulation only

Table 37: The cutflow tables in the $t_h \tau_{\text{lep}} \tau_{\text{had}}\text{-}3j$ region.

	SM Higgs	W+jets	Diboson	$Z \rightarrow ll$
this region	107.92 ± 2.27	978.23 ± 23.03	272.50 ± 11.56	378.79 ± 13.62
	$Z \rightarrow \tau\tau$	Rare	$t\bar{t}$	$t\bar{t}V$
this region	989.21 ± 15.25	1742.75 ± 14.80	39933.94 ± 73.85	142.93 ± 1.00
	$\bar{t}t \rightarrow bWcH$	$cg \rightarrow tH$	tcH merged	$\bar{t}t \rightarrow bWuH$
this region	153.93 ± 1.29	5.03 ± 0.08	158.96 ± 1.29	161.90 ± 1.28
	$ug \rightarrow tH$	tuH merged	Data	total background
this region	27.49 ± 0.42	189.39 ± 1.35	40426.00 ± 201.06	44546.27 ± 82.22

Table 38: The cutflow tables in the $t_l \tau_{\text{had}} \tau_{\text{had}}$ signal region.

	SM Higgs	W+jets	Diboson	$Z \rightarrow ll$
this region	18.46 ± 0.61	12.79 ± 13.02	17.97 ± 1.56	14.99 ± 7.16
	$Z \rightarrow \tau\tau$	Rare	$t\bar{t}$	$t\bar{t}V$
this region	21.52 ± 5.19	25.26 ± 1.53	356.05 ± 6.97	4.81 ± 0.16
	$\bar{t}t \rightarrow bWcH$	$cg \rightarrow tH$	tcH merged	$\bar{t}t \rightarrow bWuH$
this region	71.01 ± 0.67	5.44 ± 0.06	76.44 ± 0.68	73.51 ± 0.69
	$ug \rightarrow tH$	tuH merged	Data	total background
this region	25.42 ± 0.31	98.93 ± 0.76	442.00 ± 21.02	471.85 ± 17.36

Not reviewed, for internal circulation only

989 C BDT Optimisation steps

- 990 The calculated optimisation factor defined as $L = S_{\text{avg}} - xS_{\text{diff}}$ for each step taken during the BDT nCuts
 991 and nTrees optimisation in each signal region are shown below. The L value is in 1%.

Table 39: The BDT optimisation steps for $t_l\tau_{\text{had}}\text{-}1j$ region.

	NCuts=5	NCuts=10	NCuts=15	NCuts=20
NTrees=10	72.87	79.68	79.58	/
NTrees=20	74.53	80.06	80.35	80.28
NTrees=30	/	80.09	80.71	80.67
NTrees=40	/	/	81.05	80.98
NTrees=50	/	/	81.20	81.25
NTrees=60	/	/	81.33	81.33
NTrees=70	/	/	81.42	81.39
NTrees=80	/	/	81.52	81.47
NTrees=90	/	/	81.53	81.53
NTrees=100	/	/	81.52	/

Table 40: The BDT optimisation steps for $t_l\tau_{\text{had}}\text{-}2j$ region.

	NCuts=5	NCuts=10	NCuts=15	NCuts=20	NCuts=25
NTrees=10	67.23	76.76	76.72	/	/
NTrees=20	75.18	77.99	78.19	/	/
NTrees=30	/	78.66	78.95	78.39	/
NTrees=40	/	78.72	79.21	79.15	/
NTrees=50	/	/	79.93	79.66	/
NTrees=60	/	/	80.33	80.16	/
NTrees=70	/	/	81.01	80.99	/
NTrees=80	/	/	81.34	81.06	/
NTrees=90	/	/	81.74	81.44	/
NTrees=100	/	/	82.01	82.01	/
NTrees=110	/	/	82.16	82.15	/
NTrees=120	/	/	82.49	82.39	/
NTrees=130	/	/	82.56	82.67	/
NTrees=140	/	/	82.88	82.90	/
NTrees=150	/	/	82.91	83.09	/
NTrees=160	/	/	83.16	83.22	/

Not reviewed, for internal circulation only

Table 40: The BDT optimisation steps for $t_l\tau_{had}-2j$ region.

	NCuts=5	NCuts=10	NCuts=15	NCuts=20	NCuts=25
NTrees=170	/	/	83.22	83.45	/
NTrees=180	/	/	83.52	83.54	/
NTrees=190	/	/	83.75	83.70	/
NTrees=200	/	/	83.97	83.81	/
NTrees=210	/	/	84.07	83.99	/
NTrees=220	/	/	84.16	84.06	/
NTrees=230	/	/	84.25	84.14	/
NTrees=240	/	/	84.36	84.26	/
NTrees=250	/	/	84.46	84.42	/
NTrees=260	/	/	84.50	84.57	84.62
NTrees=270	/	/	84.56	84.65	84.76
NTrees=280	/	/	/	84.73	84.83
NTrees=290	/	/	/	/	84.99
NTrees=300	/	/	/	/	85.03
NTrees=310	/	/	/	/	85.08
NTrees=320	/	/	/	/	85.14
NTrees=330	/	/	/	/	85.25
NTrees=340	/	/	/	/	85.28
NTrees=350	/	/	/	/	85.34
NTrees=360	/	/	/	/	85.38
NTrees=370	/	/	/	/	85.42
NTrees=380	/	/	/	/	85.51
NTrees=390	/	/	/	/	85.54
NTrees=400	/	/	/	/	85.55
NTrees=410	/	/	/	/	85.61
NTrees=420	/	/	/	/	85.64
NTrees=430	/	/	/	/	85.73
NTrees=440	/	/	/	/	85.78
NTrees=450	/	/	/	/	85.85
NTrees=460	/	/	/	/	85.91
NTrees=470	/	/	/	/	85.95
NTrees=480	/	/	/	/	86.02
NTrees=490	/	/	/	/	86.05
NTrees=500	/	/	/	/	86.10
NTrees=510	/	/	/	/	86.11

Not reviewed, for internal circulation only

Table 41: The BDT optimisation steps for $t_l\tau_{had}-2j$ region.

	NCuts=30	NCuts=35	NCuts=40	NCuts=45
NTrees=270	84.82	/	/	/
NTrees=280	84.90	/	/	/
NTrees=290	84.98	/	/	/
NTrees=300	85.01	/	/	/
NTrees=310	85.03	/	/	/
NTrees=320	85.06	/	/	/
NTrees=330	85.21	/	/	/
NTrees=340	85.25	/	/	/
NTrees=350	85.29	/	/	/
NTrees=360	85.40	/	/	/
NTrees=370	85.47	/	/	/
NTrees=380	85.52	/	/	/
NTrees=390	85.49	/	/	/
NTrees=400	85.55	/	/	/
NTrees=410	85.62	/	/	/
NTrees=420	85.65	/	/	/
NTrees=430	85.76	/	/	/
NTrees=440	85.81	/	/	/
NTrees=450	85.85	/	/	/
NTrees=460	85.91	/	/	/
NTrees=470	85.95	/	/	/
NTrees=480	86.01	/	/	/
NTrees=490	86.08	/	/	/
NTrees=500	86.18	86.47	86.48	86.42
NTrees=510	86.20	86.47	86.48	/

Table 42: The BDT optimisation steps for $t_h\tau_{lep}\tau_{had}-2j$ region.

	NCuts=5	NCuts=10	NCuts=15	NCuts=20	NCuts=25
NTrees=10	65.62	72.06	71.79	/	/
NTrees=20	70.49	73.45	73.83	/	/
NTrees=30	/	74.18	74.77	/	/
NTrees=40	/	74.78	75.55	75.60	/
NTrees=50	/	75.53	76.10	76.04	/
NTrees=60	/	/	76.71	76.32	/

Not reviewed, for internal circulation only

Table 42: The BDT optimisation steps for $t_h\tau_{lep}\tau_{had}$ -2j region.

	NCuts=5	NCuts=10	NCuts=15	NCuts=20	NCuts=25
NTrees=70	/	/	76.91	76.40	/
NTrees=80	/	/	77.09	77.06	/
NTrees=90	/	/	77.62	77.50	/
NTrees=100	/	/	77.77	77.95	77.82
NTrees=110	/	/	77.74	78.23	77.77
NTrees=120	/	/	/	78.36	78.32
NTrees=130	/	/	/	78.75	78.53
NTrees=140	/	/	/	78.93	78.58
NTrees=150	/	/	/	79.09	78.87
NTrees=160	/	/	/	79.37	79.15
NTrees=170	/	/	/	79.67	79.37
NTrees=180	/	/	/	79.92	79.53
NTrees=190	/	/	/	80.05	79.59
NTrees=200	/	/	/	80.29	79.74
NTrees=210	/	/	/	80.36	79.91
NTrees=220	/	/	/	80.48	80.13
NTrees=230	/	/	/	80.68	80.18
NTrees=240	/	/	/	80.80	80.28
NTrees=250	/	/	/	80.89	80.53
NTrees=260	/	/	/	81.04	80.68
NTrees=270	/	/	/	81.20	80.83
NTrees=280	/	/	/	81.30	80.96
NTrees=290	/	/	/	81.41	81.08
NTrees=300	/	/	/	81.46	81.18
NTrees=310	/	/	/	81.58	81.30
NTrees=320	/	/	/	81.66	81.35
NTrees=330	/	/	/	81.69	81.42
NTrees=340	/	/	/	81.81	81.54
NTrees=350	/	/	/	81.90	81.69
NTrees=360	/	/	/	82.01	81.82
NTrees=370	/	/	/	82.10	81.97
NTrees=380	/	/	/	82.18	82.04
NTrees=390	/	/	/	82.17	/

Not reviewed, for internal circulation only

Table 43: The BDT optimisation steps for $t_h\tau_{lep}\tau_{had}$ -3j region.

	NCuts=5	NCuts=10	NCuts=15	NCuts=20	NCuts=25	NCuts=30
NTrees=10	70.98	71.72	75.45	75.44	/	/
NTrees=20	71.65	75.29	78.54	78.81	/	/
NTrees=30	/	/	79.98	80.46	80.62	/
NTrees=40	/	/	80.36	81.09	81.32	81.17
NTrees=50	/	/	/	81.29	81.82	81.56
NTrees=60	/	/	/	/	82.33	81.85
NTrees=70	/	/	/	/	82.78	81.96
NTrees=80	/	/	/	/	82.98	82.16
NTrees=90	/	/	/	/	83.16	82.32
NTrees=100	/	/	/	/	83.35	82.43
NTrees=110	/	/	/	/	83.49	83.01
NTrees=120	/	/	/	/	83.61	83.50
NTrees=130	/	/	/	/	83.75	83.88
NTrees=140	/	/	/	/	84.10	84.06
NTrees=150	/	/	/	/	84.50	84.54
NTrees=160	/	/	/	/	84.54	84.69
NTrees=170	/	/	/	/	84.48	84.99

Table 44: The BDT optimisation steps for $t_h\tau_{lep}\tau_{had}$ -3j region.

	NCuts=35	NCuts=40	NCuts=45	NCuts=50	NCuts=55	NCuts=60
NTrees=160	85.81	85.81	/	/	/	/
NTrees=170	86.03	86.15	/	/	/	/
NTrees=180	86.32	86.27	/	/	/	/
NTrees=190	86.47	86.65	86.88	/	/	/
NTrees=200	86.46	86.93	87.09	/	/	/
NTrees=210	/	87.13	87.35	87.23	/	/
NTrees=220	/	87.27	87.64	87.46	/	/
NTrees=230	/	/	87.75	87.43	/	/
NTrees=240	/	/	87.89	87.59	/	/
NTrees=250	/	/	87.97	87.70	/	/
NTrees=260	/	/	88.10	87.88	/	/
NTrees=270	/	/	88.18	87.91	/	/
NTrees=280	/	/	88.39	88.16	/	/
NTrees=290	/	/	88.59	88.36	/	/

Not reviewed, for internal circulation only

Table 44: The BDT optimisation steps for $t_h \tau_{\text{lep}} \tau_{\text{had}}\text{-}3j$ region.

	NCuts=35	NCuts=40	NCuts=45	NCuts=50	NCuts=55	NCuts=60
NTrees=300	/	/	88.78	88.64	/	/
NTrees=310	/	/	89.04	88.83	/	/
NTrees=320	/	/	89.06	88.94	/	/
NTrees=330	/	/	89.13	89.10	/	/
NTrees=340	/	/	89.24	89.26	/	/
NTrees=350	/	/	89.41	89.36	/	/
NTrees=360	/	/	89.46	89.41	/	/
NTrees=370	/	/	89.58	89.60	/	/
NTrees=380	/	/	89.69	89.78	/	/
NTrees=390	/	/	89.86	89.87	/	/
NTrees=400	/	/	89.94	90.03	90.23	90.10
NTrees=410	/	/	90.02	90.11	90.33	90.15
NTrees=420	/	/	/	/	90.38	90.32
NTrees=430	/	/	/	/	90.52	90.32
NTrees=440	/	/	/	/	90.68	90.43
NTrees=450	/	/	/	/	90.76	90.51
NTrees=460	/	/	/	/	90.90	90.65
NTrees=470	/	/	/	/	90.89	/

Table 45: The BDT optimisation steps for $t_l \tau_{\text{had}} \tau_{\text{had}}$ region.

	NCuts=5	NCuts=10	NCuts=15
NTrees=10	79.59	79.51	/
NTrees=20	79.93	81.68	82.08
NTrees=30	80.85	82.68	83.21
NTrees=40	/	83.30	83.79
NTrees=50	/	83.88	83.99
NTrees=60	/	84.27	84.49
NTrees=70	/	84.65	84.72
NTrees=80	/	84.86	85.05
NTrees=90	/	85.16	85.18
NTrees=100	/	85.32	85.29
NTrees=110	/	85.26	/

Not reviewed, for internal circulation only

Not reviewed, for internal circulation only

Table 46: The BDT optimisation steps for $t_h \tau_{\text{had}} \tau_{\text{had}} - 2j$ region.

	NCuts=5	NCuts=10	NCuts=15	NCuts=20	NCuts=25	NCuts=30
NTrees=10	79.60	80.74	/	/	/	/
NTrees=20	82.66	82.79	/	/	/	/
NTrees=30	83.09	83.82	84.18	85.45	85.39	/
NTrees=40	83.68	84.17	84.66	85.82	85.58	/
NTrees=50	/	/	/	86.05	85.95	/
NTrees=60	/	/	/	86.17	86.15	/
NTrees=70	/	/	/	86.27	86.26	/
NTrees=80	/	/	/	86.33	86.46	/
NTrees=90	/	/	/	86.47	86.52	/
NTrees=100	/	/	/	86.65	86.69	/
NTrees=110	/	/	/	86.75	86.85	86.93
NTrees=120	/	/	/	86.77	86.99	86.96
NTrees=130	/	/	/	/	87.12	87.02
NTrees=140	/	/	/	/	87.20	87.12
NTrees=150	/	/	/	/	87.24	87.16
NTrees=160	/	/	/	/	87.26	87.24
NTrees=170	/	/	/	/	87.32	87.24
NTrees=180	/	/	/	/	87.36	87.32
NTrees=190	/	/	/	/	87.42	87.32
NTrees=200	/	/	/	/	87.36	/

Table 47: The BDT optimisation steps for $t_h \tau_{\text{had}} \tau_{\text{had}} - 3j$ region.

	NCuts=5	NCuts=10	NCuts=15	NCuts=20	NCuts=25	NCuts=30
NTrees=10	81.14	74.67	/	/	/	/
NTrees=20	83.99	84.86	/	/	/	/
NTrees=30	85.08	86.16	86.81	86.86	/	/
NTrees=40	86.02	86.67	87.31	87.15	/	/
NTrees=50	/	/	87.57	87.49	/	/
NTrees=60	/	/	87.71	87.89	87.80	/
NTrees=70	/	/	87.86	88.06	88.02	/
NTrees=80	/	/	/	88.25	88.14	/
NTrees=90	/	/	/	88.30	88.11	/
NTrees=100	/	/	/	88.38	88.18	/
NTrees=110	/	/	/	88.51	88.36	/

Table 47: The BDT optimisation steps for $t_h\tau_{had}\tau_{had}$ -3j region.

	NCuts=5	NCuts=10	NCuts=15	NCuts=20	NCuts=25	NCuts=30
NTrees=120	/	/	/	88.57	88.45	/
NTrees=130	/	/	/	88.60	88.55	/
NTrees=140	/	/	/	88.67	88.64	/
NTrees=150	/	/	/	88.73	88.71	/
NTrees=160	/	/	/	88.77	88.74	/
NTrees=170	/	/	/	88.81	88.80	/
NTrees=180	/	/	/	88.82	88.83	/
NTrees=190	/	/	/	88.88	88.90	88.91
NTrees=200	/	/	/	88.88	88.95	88.95
NTrees=210	/	/	/	/	88.98	88.98
NTrees=220	/	/	/	/	89.06	88.99
NTrees=230	/	/	/	/	89.08	89.02
NTrees=240	/	/	/	/	89.10	89.00
NTrees=250	/	/	/	/	89.11	89.02
NTrees=260	/	/	/	/	89.12	89.03
NTrees=270	/	/	/	/	89.14	89.04
NTrees=280	/	/	/	/	89.15	89.07
NTrees=290	/	/	/	/	89.17	89.09
NTrees=300	/	/	/	/	89.18	89.11
NTrees=310	/	/	/	/	89.20	89.10
NTrees=320	/	/	/	/	89.20	89.12
NTrees=330	/	/	/	/	89.26	89.13
NTrees=340	/	/	/	/	89.24	/

Not reviewed, for internal circulation only

992 References

- 993 [1] ATLAS Collaboration,
 Combined Measurement of the Higgs Boson Mass in pp Collisions at $\sqrt{s}=7$ and 8 TeV with the ATLAS and CM
 994 Phys. Rev. Lett. **114** (2015) 191803, arXiv: [1503.07589 \[hep-ex\]](#).
- 995 [2] S. Glashow, J. Iliopoulos and L. Maiani, Weak Interactions with Lepton-Hadron Symmetry,
 996 Phys. Rev. D **2** (1970) 1285.
- 997 [3] J. Aguilar-Saavedra,
 Top flavor-changing neutral interactions: Theoretical expectations and experimental detection,
 999 Acta Phys. Polon. B **35** (2004) 2695, arXiv: [0409342 \[hep-ph\]](#).
- 1000 [4] F. del Aguila, J. A. Aguilar-Saavedra, and R. Miquel,
 Constraints on top couplings in models with exotic quarks, Phys. Rev. Lett. **82** (1999) 1628,
 1001 arXiv: [9808400 \[hep-ph\]](#).
- 1002 [5] J. Aguilar-Saavedra, Effects of mixing with quark singlets, Phys. Rev. D **67** (2003) 035003,
 1003 arXiv: [0210112 \[hep-ph\]](#).
- 1004 [6] S. Bejar, J. Guasch and J. Sola,
 Loop induced flavor changing neutral decays of the top quark in a general two Higgs doublet model,
 1007 Nucl. Phys. B **600** (2001) 21, arXiv: [0011091 \[hep-ph\]](#).
- 1008 [7] I. Baum, G. Eilam and S. Bar-Shalom,
 Scalar flavor changing neutral currents and rare top quark decays in a two Higgs doublet model 'for the top quark'
 1009 Phys. Rev. D **77** (2008) 113008, arXiv: [0802.2622 \[hep-ph\]](#).
- 1010 [8] J. J. Cao et al., SUSY-induced FCNC top-quark processes at the large hadron collider,
 1011 Phys. Rev. D **75** (2007) 075021, arXiv: [0702264 \[hep-ph\]](#).
- 1012 [9] G. Eilam et al., Top quark rare decay $t \rightarrow ch$ in R-parity violating SUSY,
 1013 Phys. Lett. B **510** (2001) 227, arXiv: [0102037 \[hep-ph\]](#).
- 1014 [10] G. Lu et al., The rare top quark decays $t \rightarrow cV$ in the topcolor-assisted technicolor model,
 1015 Phys. Rev. D **68** (2003) 015002, arXiv: [0303122 \[hep-ph\]](#).
- 1016 [11] K. Agashe, G. Perez and A. Soni,
 Collider signals of top quark flavor violation from a warped extra dimension,
 1017 Phys. Rev. D **75** (2007) 015002, arXiv: [0606293 \[hep-ph\]](#).
- 1018 [12] B. Yang, N. Liu and J. Han,
 Top quark flavor-changing neutral-current decay to a 125 GeV Higgs boson in the littlest Higgs model with T par
 1019 , Phys. Rev. D **89** (2014) 034020, arXiv: [1308.4852 \[hep-ph\]](#).
- 1020 [13] K. Agashe and R. Contino, Composite Higgs-mediated flavor-changing neutral current,
 1021 Phys. Rev. D **80** (2009) 075016, arXiv: [0906.1542 \[hep-ph\]](#).

- 1026 [14] T. P. Cheng and Marc Sher,
 1027 Mass Matrix Ansatz and Flavor Nonconservation in Models with Multiple Higgs Doublets,
 1028 Phys. Rev. D **35** (1987) 3484.
- 1029 [15] Wei-Shu Hou, Tree level $t \rightarrow ch$ or $h \rightarrow t\bar{c}$ decays, Phys. Lett. B **296** (1992) 179.
- 1030 [16] Federico Demartin, Fabio Maltoni, Kentarou Mawatari, Marco Zaro,
 1031 Higgs production in association with a single top quark at the LHC, (2015),
 1032 arXiv: [1504.00611 \[hep-ph\]](https://arxiv.org/abs/1504.00611).
- 1033 [17] ATLAS Collaboration,
 1034 Search for top quark decays $t \rightarrow qH$, with $H \rightarrow \gamma\gamma$, in $\sqrt{s} = 13$ TeV pp collisions using the ATLAS detector,
 1035 JHEP (2017) **129**, arXiv: [1707.01404 \[hep-ex\]](https://arxiv.org/abs/1707.01404).
- 1036 [18] ATLAS Collaboration,
 1037 Search for flavor-changing neutral currents in top quark decays $t \rightarrow Hc$ and $t \rightarrow Hu$ in multilepton final states in
 1038 Phys. Rev. D (2018) **36**, arXiv: [1805.03483 \[hep-ex\]](https://arxiv.org/abs/1805.03483).
- 1039 [19] ATLAS Collaboration,
 1040 Search for top-quark decays $t \rightarrow qH$ with 36 fb-1 of pp collision data at $\sqrt{s}=13$ TeV with the ATLAS detector,
 1041 (), arXiv: [1812.11568 \[hep-ex\]](https://arxiv.org/abs/1812.11568).
- 1042 [20] CMS Collaboration,
 1043 Search for the flavor-changing neutral current interactions of the top quark and the Higgs boson which decays into
 1044 JHEP **06** (2018) **102**, arXiv: [1712.02399 \[hep-ex\]](https://arxiv.org/abs/1712.02399).
- 1045 [21] Celine Degrande, Fabio Maltoni, Jian Wang, Cen Zhang,
 1046 Automatic computations at next-to-leading order in QCD for top-quark flavor-changing neutral processes,
 1047 Phys. Rev. D (2015) **6**, arXiv: [1412.5594 \[hep-ex\]](https://arxiv.org/abs/1412.5594).
- 1048 [22] ATLAS Collaboration, The ATLAS Experiment at the CERN Large Hadron Collider,
 1049 JINST **3** (2008) S08003.
- 1050 [23] ATLAS Collaboration, ATLAS Insertable B-Layer Technical Design Report,
 1051 CERN-LHCC-2010-013; ATLAS-TDR-19, 2010,
 1052 URL: <https://cds.cern.ch/record/1291633>.
- 1053 [24] ATLAS Collaboration,
 1054 Luminosity determination in pp collisions at $\sqrt{s} = 8$ TeV using the ATLAS detector at the LHC,
 1055 (2016), arXiv: [1608.03953 \[hep-ex\]](https://arxiv.org/abs/1608.03953).
- 1056 [25] Celine Degrande et al.,
 1057 Automatic computations at next-to-leading order in QCD for top-quark flavor-changing neutral processes,
 1058 Phys. Rev. D **91** (2015) 034024, arXiv: [1412.5594 \[hep-ph\]](https://arxiv.org/abs/1412.5594).
- 1059 [26] Celine Degrande et al., Effective theory for top flavor changing interactions, 2016,
 1060 URL: <https://feynrules.irmp.ucl.ac.be/wiki/TopFCNC>.

- [27] J. Alwall et al.,
The automated computation of tree-level and next-to-leading order differential cross sections, and their matching
JHEP **07** (2014) 079, arXiv: [1405.0301 \[hep-ph\]](#).
- [28] T. Sjostrand et al., An introduction to PYTHIA 8.2, Comp. Phys. Commun. **191** (2015) 159,
arXiv: [1410.3012 \[hep-ph\]](#).
- [29] ATLAS Collaboration, ATLAS Pythia 8 tunes to 7 TeV data, ATL-PHYS-PUB-2014-021, 2014,
URL: <https://cdsweb.cern.ch/record/196641>.
- [30] R. D. Ball et al., Parton distributions for the LHC Run II, JHEP **04** (2015) 040,
arXiv: [1410.8849 \[hep-ph\]](#).
- [31] C. Oleari, The POWHEG-BOX, Nucl. Phys. Proc. Suppl. **205-206** (2010) 36–41,
arXiv: [1007.3893 \[hep-ph\]](#).
- [32] T. Gleisberg et al., Event generation with Sherpa 1.1, JHEP **02** (2009) 007,
arXiv: [0811.4622 \[hep-ph\]](#).
- [33] N. Davidson et al., Universal interface of TAUOLA: Technical and physics documentation,
Comp. Phys. Commun. **183** (2012) 821.
- [34] S. Agostinelli et al., GEANT4 - A simulation toolkit, Nucl. Instrum. Meth. A **506** (2003) 250.
- [35] J. Bellm et al., Herwig 7.0/Herwig++ 3.0 release note, Eur. Phys. J. C **76** (2016) 196.
- [36] ATLAS Collaboration,
The simulation principle and performance of the ATLAS fast calorimeter simulation FastCaloSim,
ATL-PHYS-PUB-2010-013, 2010, URL: <http://cds.cern.ch/record/1300517>.
- [37] J Butterworth et al.,
Single Boson and Diboson Production Cross Sections in pp Collisions at $\sqrt{s}=7$ TeV,
ATL-COM-PHYS-2010-695, 2010, URL: <http://cds.cern.ch/record/1287902>.
- [38] M. Czakon and A. Mitov,
Top++: a program for the calculation of the top-pair cross-section at hadron colliders,
Comput. Phys. Commun. **185** (2014) 2930, arXiv: [1112.5675 \[hep-ph\]](#).
- [39] D. de Florian et al.,
Handbook of LHC Higgs Cross Sections: 4. Deciphering the Nature of the Higgs Sector,
CERN-2017-002-M (2017), arXiv: [1610.07922 \[hep-ph\]](#),
URL: <https://cds.cern.ch/record/2227475>.
- [40] J. Alwall et al.,
The automated computation of tree-level and next-to-leading order differential cross sections, and their matching
JHEP **07** (2014) 079, arXiv: [1405.0301 \[hep-ph\]](#).
- [41] M. Aliiev et al., HATHOR - HAdrionic Top and Heavy quarks crOss section calculatoR,
Comput. Phys. Commun. **182** (2011) 1034, arXiv: [1007.1327 \[hep-ph\]](#).

- 1096 [42] P. Kant et al.,
1097 HATHOR for single top-quark production: Updated predictions and uncertainty estimates for single top-quark p
1098 Comput. Phys. Commun **191** (2015) 74, arXiv: [1406.4403 \[hep-ph\]](https://arxiv.org/abs/1406.4403).
- 1099 [43] N. Kidonakis,
1100 Two-loop soft anomalous dimensions for single top quark associated production with a W^- or H^- ,
1101 Phys. Rev. D **82** (2010) 054018, arXiv: [1005.4451 \[hep-ph\]](https://arxiv.org/abs/1005.4451).
- 1102 [44] J. Pumplin et al.,
1103 New Generation of Parton Distributions with Uncertainties from Global QCD Analysis,
1104 JHEP **07** (2002) 012, arXiv: [0201195 \[hep-ph\]](https://arxiv.org/abs/0201195).
- 1105 [45] M. Cacciari, G. P. Salam, and G. Soyez, The Anti-k(t) jet clustering algorithm,
1106 JHEP **04** (2008) 063, arXiv: [0802.1189 \[hep-ph\]](https://arxiv.org/abs/0802.1189).
- 1107 [46] ATLAS Collaboration, Tagging and suppression of pileup jets with the ATLAS detector,
1108 ATLAS-CONF-2014-018, 2014, URL: <http://cds.cern.ch/record/1700870>.
- 1109 [47] ATLAS Collaboration,
1110 Optimisation of the ATLAS b-tagging performance for the 2016 LHC Run,
1111 ATL-PHYS-PUB-2016-012, 2016, URL: <https://cds.cern.ch/record/2160731>.
- 1112 [48] Electron and Photon Selection and Identification for Run2, Accessible on 2021-1-3, URL: <https://twiki.cern.ch/twiki/bin/view/AtlasProtected/EGammaIdentificationRun2>.
- 1113 [49] Official Isolation Working Points, Accessible on 2021-1-3, URL: <https://twiki.cern.ch/twiki/bin/viewauth/AtlasProtected/IsolationSelectionTool#Leptons>.
- 1114 [50] MuonSelectionTool, Accessible on 2021-1-3,
1115 URL: <https://twiki.cern.ch/twiki/bin/view/Atlas/MuonSelectionTool>.
- 1116 [51] ATLAS Collaboration,
1117 Reconstruction, Energy Calibration, and Identification of Hadronically Decaying Tau Leptons in the ATLAS Ex
1118 ATL-PHYS-PUB-2015-045, 2015, URL: <https://cds.cern.ch/record/2064383>.
- 1119 [52] ATLAS Collaboration,
1120 Jet energy measurement with the ATLAS detector in proton-proton collisions at $\sqrt{s} = 7$ TeV,
1121 Eur. Phys. J. C **73** (2013) 2304, arXiv: [1112.6426 \[hep-ex\]](https://arxiv.org/abs/1112.6426).
- 1122 [53]
1123 Measurement of the Higgs boson coupling properties in the $H \rightarrow \tau\tau$ decay channel at $\sqrt{s}=13$ TeV with the ATLA
1124 2020, URL: <https://cds.cern.ch/record/2741326>.
- 1125 [54] TauAnalysisTools, Accessible on 2021-1-3,
1126 URL: <https://twiki.cern.ch/twiki/bin/view/AtlasProtected/TauAnalysisTools>.

- 1129 [55] Measurement of the total and differential production cross-sections of $t\bar{t}W$ production at 13 TeV in 139 fb^{-1} of da
 1130 2021,
 1131 URL: <https://atlas-glance.cern.ch/atlas/analysis/analyses/details?id=3390>.
- 1133 [56] Tau Recommendations, Accessible on 2021-1-3, URL:
 1134 <https://twiki.cern.ch/twiki/bin/view/AtlasProtected/TauRecommendationsR21>.
- 1135 [57] Usage of Missing ET in analyses: rebuilding and systematics, Accessible on 2021-1-3,
 1136 URL: <https://twiki.cern.ch/twiki/bin/viewauth/AtlasProtected/METUtilities>.
- 1137 [58] ATLAS Collaboration,
 1138 Search for the Associated Production of a Higgs Boson and a Top Quark Pair in multilepton final states in 80 fb^{-1}
 1139 ATL-COM-PHYS-2018-410, 2018, URL: <https://cds.cern.ch/record/2314122>.
- 1140 [59] ATLAS Collaboration,
 1141 Measurement of the $H \rightarrow \tau^+\tau^-$ cross-section in 13TeV Collisions with the ATLAS Detector,
 1142 ATL-COM-PHYS-2017-446, 2017, URL: <https://cds.cern.ch/record/2261605>.
- 1143 [60] J. Friedman, Stochastic gradient boosting, Comput. Stat. Data Anal. **38** (2002) 367.
- 1144 [61] A. Hoecker et al., TMVA - Toolkit for Multivariate Data Analysis, PoS A CAT **040** (2007),
 1145 arXiv: [0703039 \[physics\]](https://arxiv.org/abs/0703039).
- 1146 [62] TRExFitter, Accessible on 2021-1-3,
 1147 URL: <https://gitlab.cern.ch/TRExStats/TRExFitter>.
- 1148 [63] ATLAS Collaboration,
 1149 Electron efficiency measurements with the ATLAS detector using the 2015 LHC proton–proton collision data,
 1150 ATLAS-CONF-2016-024, 2016, URL: <https://cds.cern.ch/record/2157687>.
- 1151 [64] ATLAS Collaboration,
 1152 Jet Calibration and Systematic Uncertainties for Jets Reconstructed in the ATLAS Detector at $\sqrt{s} = 13 \text{ TeV}$,
 1153 ATL-PHYS-PUB-2015-015, 2015, URL: <https://cds.cern.ch/record/2037613>.
- 1154 [65] ATLAS Collaboration,
 1155 Performance of missing transverse momentum reconstruction for the ATLAS detector in the first proton-proton c
 1156 ATL-PHYS-PUB-2015-027, 2015, URL: <https://cds.cern.ch/record/2037904>.
- 1157 [66] ATLAS Collaboration, Expected performance of the ATLAS b-tagging algorithms in Run-2,
 1158 ATL-PHYS-PUB-2015-022, 2015, URL: <https://cds.cern.ch/record/2037697>.
- 1159 [67] ATLAS Collaboration,
 1160 Calibration of the performance of b-tagging for c and light-flavour jets in the 2012 ATLAS data,
 1161 ATLAS-CONF-2014-046, 2014, URL: <https://cds.cern.ch/record/1741020>.
- 1162 [68] ATLAS Collaboration,
 1163 Calibration of b-tagging using dileptonic top pair events in a combinatorial likelihood approach with the ATLAS
 1164 ATLAS-CONF-2014-004, 2014, URL: <https://cds.cern.ch/record/1664335>.

- 1165 [69] ATLAS Collaboration,
1166 Studies on top-quark Monte Carlo modelling with Sherpa and MG5_aMC@NLO,
1167 ATL-PHYS-PUB-2017-007, 2017, URL: <https://cds.cern.ch/record/2261938>.
- 1168 [70] G. Cowan, K. Cranmer, E. Gross and O. Vitells,
1169 Asymptotic formulae for likelihood-based tests of new physics, Eur. Phys. J. C **71** (2011) 1554,
1170 arXiv: [1007.1727 \[physics.data-an\]](https://arxiv.org/abs/1007.1727).
- 1171 [71] AnalysisTop, Accessible on 2021-1-3,
1172 URL: <https://twiki.cern.ch/twiki/bin/view/AtlasProtected/AnalysisTop21>.

Not reviewed, for internal circulation only

1173 List of contributions

1174

- 1175 • Boyang Li: main analyser, analysis code maintainer; signal generation; derivation, ntuple produc-
1176 tion; fake tau estimation; BDT analysis; systematics; fit; support note.
- 1177 • Weiming Yao: main analyser, `ttHML` ntuple skimming and support; fake tau estimation; BDT
1178 analysis; cross check; support note.
- 1179 • MingMing Xia: main analyser, `xTauFramework` n-tuple production; production validation; fake
1180 tau estimation in hadronic channels.
- 1181 • Xin Chen: Supervisor of Boyang Li and MingMing Xia

Not reviewed, for internal circulation only